Joint Time-Frequency Analysis and Filtering of Single Trial Event-Related Potentials

Christopher Gibson

A thesis submitted in partial fulfilment of the requirements of
Sheffield Hallam University
for the degree of Doctor of Philosophy

March 2000

Abstract

The ongoing electrical activity of the brain is known as the electroencephalograph (EEG). Event related potentials (ERPs) are voltage deviations in the EEG elicited in association with stimuli. Their elicitation require cognitive processes such as response to a recognised stimulus. ERPs therefore provide clinical information by allowing an insight into neurological processes. The amplitude of an event-related potential is typically several times less than the background EEG. The background EEG has the effect of obscuring the ERP and therefore appropriate signal processing is required for its recovery. Traditionally ERPs are estimated using the synchronised averaging of several single trials or sweeps. This inhibits investigation of any trial-to-trial variation, which can prove valuable in understanding cognitive processes. An aim of this study was to develop wavelet-based techniques for the recovery of single trial ERPs from background EEG.

A novel wavelet-based adaptive digital filtering method for ERPs has been developed. The method provides the ability to effectively estimate or recover single ERPs. The effectiveness of the method has been quantitatively evaluated and compared with other methods of ERP estimation.

The ability to recover single sweep ERPs allowed the investigation of characteristics that are not possible using the conventional averaged estimation. The development of features of a cognitive ERP known as the contingent negative variation over a number of trials was investigated. The trend in variation enabled the identification of schizophrenic subjects using artificial intelligence methods.

A new technique to investigate the phase dynamics of ERPs was developed. This was successfully applied, along with other techniques, to the investigation of independent component analysis (ICA) component activations in a visual spatial attention task. Two components with scalp projections that suggested that they may be sources within the visual cortex were investigated. The study showed that the two components were visual field selective and that their activation was both amplitude and phase modulated.

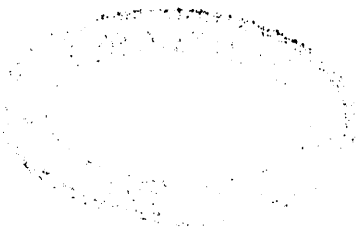

Acknowledgements

I would like to express my gratitude to Dr Reza Saatchi, for his considerable support, energy and ideas. Without his guidance, this study would not have been possible.

During my time with the Electronics Research Group at Sheffield Hallam University, I have benefited greatly from interactions with other researchers. In particular I would like thank Professor Ray for introducing me to Reza and providing financial assistance for my visit to San Diego, Professor Ghassemlooy for his support as a supervisor and to other members of the group for our discussions. I greatly appreciate the help Dr Hugh Porteous provided in my understanding of the mathematics behind the techniques used in this study.

Without the Dr Last travel grant, from the British Society for Clinical Neurophysiology, I would not have been able to visit the Dr Terry Sejnowski's computational neurobiology laboratory in San Diego. This visit provided me with a greater understanding of neuroscience and the clinical importance of this area of research. I would particularly like to thank Dr Scott Makeig for providing inspiration, supervision and the opportunity to work at the cutting edge with the team in the San Diego area. Thanks also to Dr Terry Sejnowski and everyone at the Salk institute, for providing a warm welcome to their wonderful research environment.

Contents

List of Figures

List of Tables

List of Publications

Saatchi, M.R., Gibson, C. Rowe, J.W.K. and Allen, E.M.:
Adaptive multiresolution analysis based evoked potential filtering,
IEE Proceedings Science, Measurement and Technology,
144 (1997) 149-155.

Gibson, C., Saatchi, M.R. and Allen, E.M.:
A comparative investigation of wavelet based EP estimation,
Proceedings of the first international symposium on communication systems and digital signal processing,
Sheffield, UK, (1998) 524-528.

Saatchi, R. Gibson, C, Allen, E.M. and Ghassemlooy, Z.:
Application of Kohonen artificial network for identification of schizophrenic subjects based on the CNV waveforms trial-to-trial- variation trends,
Proceedings of Fourth Annual International CSI Computer Conference,
Tehran, Iran, (1999) 65-68

Chapter 1

Introduction

1.1 Chapter Summary

In this chapter a brief introduction to the background of this study is provided. The aims and objectives of the research are stated. An outline of the thesis is provided.

1.2 Introduction

The recorded, ongoing electrical activity of the brain is known as the electroencephalograph (EEG) [1]. Evoked potentials (EPs) are voltage deviations in the EEG elicited in association with stimuli [2]. For example, a light flashed into the eye would produce a visual evoked potential. EPs are classified with respect to their stimuli and include, for example, auditory and somatosensory evoked potentials. Event-related potentials (ERPs) are voltage deviations in the EEG produced by a cognitive response to a stimulus [3]. For example a subject may be asked to recognise an event or respond to a specific stimulus.

ERPs provide clinical information by allowing an insight into neurological processes [4]. ERPs, such as the contingent negative variation (CNV), are used to investigate abnormal brain processes and disorders, for example schizophrenia [5].

The magnitude of an event-related potential is typically several times less than the background EEG. The background EEG has the effect of obscuring the ERP and therefore appropriate signal processing is required for its recovery and analysis [6].

Traditionally ERPs are estimated using the synchronised averaging of several single trials. A number of single sweeps (or trials) are combined to produce a single averaged waveform that is an estimate of the underlying ERP. This however loses important clinical information on trial-to-trial variation and attenuates signal components not phase-locked to stimulus [7].

ERPs are transient, non-stationary signals. Therefore their signal characteristics vary with time. The signal processing techniques employed for both filtering and analysis of ERPs must cater for these properties. As a result, more advanced signal processing techniques have been applied to the analysis and estimation (filtering) of ERPs [8] [9].

The processing of neurophysiological signals relies on assumptions based on the characteristics of the signal in question. Recently developed wavelet based signal processing methods allow a multiresolution analysis of waveforms in the time-scale domain [10][11]. Wavelets have been successfully applied to a range of biomedical signals [12][13] including ERPs [14].

In this study, state of the art digital signal processing techniques were applied to improve the analysis of ERPs. ERPs are transient waveforms that warrant the utilisation of joint time-frequency analysis techniques. The recently developed family of wavelet transforms [15] provides the basis for the techniques developed in this study.

A novel adaptive wavelet-based filtering technique was developed to recover single trial ERPs. The technique was carefully evaluated and optimised. This method was then used in the investigation of the trial-to-trial variation of a particular type of ERP, known as the contingent negative variation (CNV).

The trial-to-trial differences between schizophrenic and matched normal control subjects were used to automatically differentiate subject categories based on this variation.

A new technique to investigate the phase dynamics of ERPs was developed. The results obtained when combined with existing joint time-frequency analysis methods revealed new information concerning the functioning of the brain.

1.3 Aims and Objectives of the Study

The aim of the study was to develop and apply novel signal processing techniques to improve the estimation, analysis and interpretation of event-related potentials. The objectives of the study were as follows.

1. **Development of novel wavelet-based filtering techniques for the recovery of single trial event-related potentials.**

   Traditionally evoked and event-related potentials have been estimated using the synchronised averaging of several single trials. This however loses valuable clinical information on trial-to-trial variation. An ideal filter would improve the signal to noise ratio (SNR) of a given trial whilst maintaining essential trial specific details. The amount of improvement in signal SNR as a result of filtering is largely dependent on the amount of spectral overlap between signal and noise. Due to the characteristics of ERPs, the use of a deterministic filter will either attenuate signal detail or fail to sufficiently attenuate the background EEG.

   The family of wavelet transforms facilitates the representation of a waveform in the time-scale domain [16]. Develop a wavelet-based filter that is suited to ERP characteristics.

2. **Evaluation of the developed filtering techniques and their comparison with other approaches.**

   Develop a method to evaluate and compare the performance of a range of filtering techniques and make a quantitative comparison between the methods.

   Compare a number of conventional and wavelet-based filtering approaches with the filter developed in this study.

3. **Investigation of the contingent negative variation trial-to-trial variation trend in normal and schizophrenic subjects.**

   The magnitude of the averaged CNV is reduced in schizophrenic subjects when compared with matched normal control subjects [5]. Possible causes are that all individual

trials are reduced in magnitude or that there is a considerable peak latency variation (jitter) between trials resulting in the attenuation of averaged trials.

Using recovered single trials from schizophrenic and matched normal control subjects, investigate the trial-to-trial variation of the CNV. Investigate trends in variation within subject categories and examine the feasibility of classification based on these trends.

4. **Investigation of alpha phase resetting in visual event-related potentials.**

   Investigate the development of the early components of a visual P300 ERP [19](a positive peak observed around 300 ms post-stimulus). In particular consider the genesis of the N100 peak (a negative peak observed between 100 and 200 ms post-stimulus) in a visual spatial attention task. Consideration was given to the two hypotheses concerning ERP genesis, i.e. the additive model and phase reordering [17].

   Employ the spatial filtering technique of independent component analysis [18] to estimate signal sources within the visual cortex. Investigate the characteristics of these components.

1.4 Organisation of Thesis

An overview of the aims and objectives of this study and an outline of the thesis is provided in this chapter.

Chapter 2 covers information on ERPs including the recording method and analysis by conventional techniques such as synchronised averaging of several single trials or sweeps and peak analysis. The two ERPs, the CNV and visual P300, investigated in this study are described. A brief description of their clinical and other applications is provided.

In chapter 3 background information on the digital signal processing techniques used in this study is provided. The discussion leads to the time-scale approach facilitated by 'wavelets'. Other techniques employed including independent component analysis and artificial neural networks are briefly described.

In chapter 4 the filtering of event-related potentials is discussed. Synchronised averaging inhibits investigation of trial-to-trial variation, which can prove valuable in understanding

cognitive processes. An objective of this study was to develop wavelet-based techniques for the estimation of single trial ERPs. Estimation can be regarded as the filtering or removal of unwanted EEG thus leaving the enhanced underlying ERP. A comparison of wavelet-based filtering approaches for single trial recovery is made. A novel wavelet-based method for the adaptive digital filtering of event-related potentials has been developed in this study. The development of the adaptive filtering approach is presented. The effectiveness of the method was quantitatively evaluated and compared with the conventional and other methods of ERP estimation. The developed adaptive filtering method provides the ability to effectively estimate or recover single ERPs.

In chapter 5 the investigation of the trend in trial-to-trial variation of the CNV in normal and schizophrenic subjects is discussed. The the filter developed in this study and detailed in chapter 4 was applied to recover single sweep CNVs from 20 schizophrenic and 20 age and sex matched normal control subjects. This enabled the investigation of characteristics that are not possible using conventional averaged ERPs. In particular, the development of the CNV features over a number of trials was investigated. The observed subject specific trend in trial-to-trial variation was used as the input to a Kohonen self-organising artificial neural network. This analysis enabled the differences in the CNV trend for both subject categories to be investigated and the possibility of using this information for automatic subject classification to be explored.

In chapter 6 a fundamental investigation of the genesis of event-related potentials using novel phase analysis methods and joint time frequency techniques is provided. The methods developed for analysis of the phase of alpha component in the P300 recorded during visual spatial attention experiments show the importance of phase information in understanding the complex dynamics of cortical processes. The relationship of known active regions of the brain during a visual spatial attention task and the topographical distribution of the P300 was considered using the developed techniques following the application of independent component analysis.

Chapter 7 provides a conclusion to the study. This study lead to the development of novel techniques that facilitated an increased understanding of event-related potentials. A novel wavelet-based filter was developed to estimate single trial ERPs. The effectiveness of the

filter was evaluated in comparison with other techniques. The application of new analysis techniques was demonstrated in the differentiation of schizophrenic and matched normal subjects and in the understanding of the development of the P300 in a visual spatial attention task.

Chapter 2

EEG and Event-Related Potentials

2.1 Chapter Summary

This chapter provides an introduction to event-related potentials (ERPs). First an overview of the ERP recording method is provided. Some factors that need to be considered during recording are discussed. The conventional method of estimating an ERP from several recorded trials is introduced. The two event-related potentials used in this study are discussed. The applications of ERPs in clinical and other studies are outlined.

2.2 Introduction

The electrical activity of the brain was first reported by Caton [20]. The electroencephalograph (EEG) is the observed electrical signal at various sites on the scalp. Event-related potentials (ERPs) are electrical signals generated by the brain in a cognitive response to a stimulus [21]. They cause a voltage deviation from the ongoing electrical activity of the brain (EEG).

ERPs are time locked or synchronised to the stimuli that elicited the response. The functioning of the brain can therefore be investigated by considering event-related potentials (ERPs). The analysis of ERPs can reveal valuable clinical information about particular brain disorders.

2.3 ERP Characteristics

Event-related potentials are recorded from a number of sites on the scalp. A marked variation in ERP amplitude is generally observed at topographically distinct points [22]. ERPs are electrical signals generated by compound neural activity in a cognitive response to a stimulus. The magnitude of an ERP is typically several times smaller than the background EEG.

An ERP cannot usually be observed without appropriate signal processing due to the presence of larger amplitude background noise sources. The contaminating noise can be of an order of magnitude larger than the desired signal. For example the magnitude of a particular ERP known as the contingent negative variation (CNV) [23] is typically 20 μV. This signal is obscured by noise of typically 100 μV. The source of noise is both physiological e.g. ongoing electroencephalogram (EEG), electrooculargram (EOG), electromyogram (EMG) and non-physiological such as instrumentation noise, electromagnetically induced signals from mains electricity and radio broadcasts [7].

By inspecting gross deviations in the recorded waveforms, severely contaminated waveforms can be rejected from subsequent processing and analysis. Even after differential recording, ocular artefact removal and bandpass filtering, the ERP is still obscured by background EEG.

The conventional signal to noise ratio (SNR) improvement method employed in ERP analysis is synchronised or coherent averaging [7][6]. This approach assumes that the ERP is deterministic and appears coherently in successive trials whilst being uncorrelated with the ongoing background EEG. The improvement in SNR is proportional to the square root of the number of trials used [24].

Various factors such as age and sex are known to affect the characteristics of ERPs. When

using ERPs to investigate brain malfunction, the patients are usually matched with normal control subjects in terms of these contributing factors.

2.3.1 ERP Models

The electrical activity recorded on the surface of the scalp is widely assumed to be the summation of a number of signal sources within the cortex [25]. Functional imaging studies of the brain [26] show small distinct regions (of the order of a cubic centimetre) activated in response to a given task. The time course of these activations suggests the hypothesis that spatially independent groups of neurons are recruited to accomplish a given task. Furthermore, different regions of the brain are known to be responsible for given tasks, i.e. visual and motor cortex.

In trying to understand the functionality of the brain several models have been suggested [17]. Most models are based on grouping of a number of neurons into a single source or generator of electrical activity. The way in which the models differ is related to the constraints which are placed on the sources. In particular the types of signal or activity they produce.

Each signal source can be considered to be an oscillator which has analogies in both electrical and mechanical engineering [27]. An oscillator has a number of parameters which alter its characteristics. These are the amplitude, frequency and phase of the signal's oscillation.

2.4 ERP Analysis

An ERP is a combination of transient components. The latency of signal features from stimuli allows the electrical response to be separated into two sections. The evoked potential which lasts for typically 100ms following the stimulus and the event-related potential that reflects cognitive processing. The latter commences approximately 300ms after the onset of the stimulus and can last for several hundred milliseconds.

ERPs are time locked or synchronised to external stimuli. The standard signal-to-noise ratio

(SNR) improvement method of synchronised or coherent averaging relies on this idea [7][6]. The assumptions made are that successive signals contain a constant signal component (i.e. ERPs are deterministic) and an uncorrelated noise component (background EEG in this case)that is representative of a zero-mean Gaussian process.

Following SNR improvement techniques, ERPs are typically characterised using peak polarity, amplitude and latency measures. For example, the P300 is a positive peak occurring at around 300 milliseconds following the presentation of the stimulus.

2.5 ERPs Considered in this Study

The ERPs included in this study were the contingent negative variation and the visual P300.

2.5.1 The Contingent Negative Variation

A well known ERP is the contingent negative variation (CNV) first described by Walter *et al.* [28] in 1964. In this study subjects received two successive stimuli. The first was a click (known as the warning stimulus, S1) and this was followed by a continuous tone (imperative stimulus, S2) one second later. The subjects terminated the imperative stimulus by pressing a hand held push-button.

A typical CNV waveform in a normal subject is shown in Fig.2.1.

Immediately following the warning stimulus a negative voltage shift was observed in the background electroencephalogram (EEG). The negative potential returned to its original baseline after the imperative stimulus and the subjects' response to it.

In normal subjects the CNV magnitude is approximately 20 μV. CNV amplitude reaches its peak after a number of recordings (trials). This CNV development time can vary with the mental state of the subject and the particular experimental conditions. For example, in a study the CNV development time was reported to be about 10 trials [29].

The CNV amplitude depends on a number of cognitive processes. The focus was initially on the effect of expectancy [28]. Later studies emphasised conation or intention to act [30] and

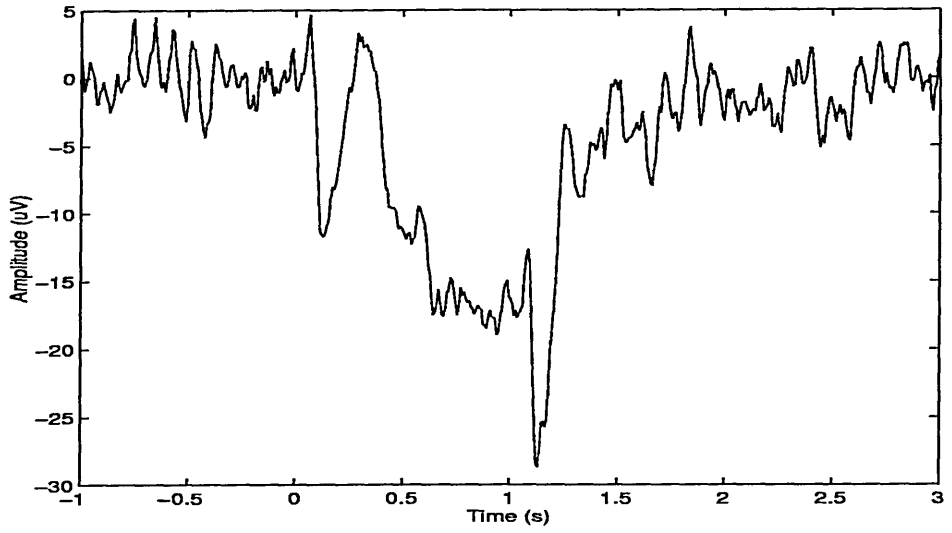

Figure 2.1: A CNV produced as an average of 32 single trials recorded from a normal subject. The stimuli are presented at 0 and 1 seconds

motivation [31] to explain their findings. Level of attention is believed to be important in CNV development. In a study designed to investigate this, letters were presented to normal subjects during the interstimulus interval of randomly selected CNV trials and randomly omitted during others [32]. It was observed that CNV amplitude increased for the trials in which no letters were shown. This was considered to reflect the state of undivided attention in the no-letter trials. Factors which might increase attention (such as experiments requiring a faster motor response to S2 or providing an S2 that is harder to detect) increase CNV amplitude [33]. Distraction is believed to be one of the most significant factors that can affect CNV amplitude development [23].

2.5.2 Late Positive Event-Related Potential (P300)

The P300, or late positive complex, was first reported by Sutton *et al.* in 1965 [19]. The P300 can be elicited in both auditory and visual tasks [4], however in this study only a visual spatial attention paradigm was selected.

The P300 is most commonly recorded using an oddball paradigm [36]. In such a paradigm,

the target stimulus occurs infrequently in a random sequence of a number of different stimuli. For example, in this study, each subject received a psuedorandom sequence of visual stimuli presented in one of number of spatial locations. The subjects were asked to respond to targets (stimuli appearing at a given position) by pressing a button.

A typical P300 waveform in a normal subject is shown in Fig 2.2.

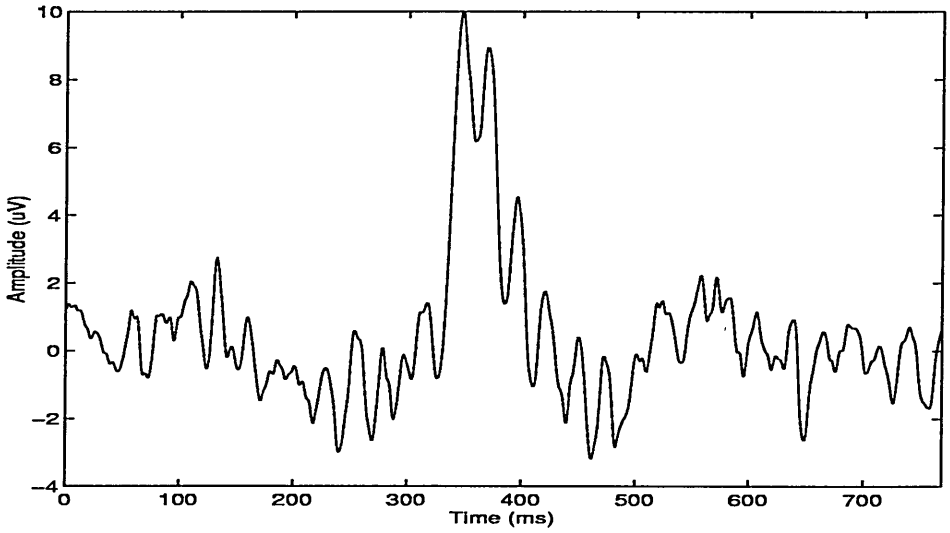

Figure 2.2: A P300 produced as an average of 100 single trials recorded from a normal subject. The visual stimulus is presented at time 0

From Fig.2.2 it can be seen that a relatively large positive peak is evoked approximately 300 ms post-stimulus. In normal subjects the P300 magnitude is approximately 10 μV

Late positive responses are evoked in response to relevant but infrequent visual, auditory and somatosensory stimuli (pertaining to the electrical stimulation of peripheral nerves) [36]. The fact that the P300 is typically present only in target trials suggests that it reflects information processing [37]. The cognitive nature of the P300 has been exploited in the investigation of brain disorders [38]. The peak amplitude and latency vary with several task-related variables including attention and novelty [39].

2.6 Clinical and Other Applications of ERPs

An understanding of the genesis and workings of ERP's leads to increased knowledge of the complex system associated with the brain. This knowledge has application in a number of areas. Most importantly, in understanding the workings of the brain, mental disorders including schizophrenia and epilepsy can be better understood and perhaps treated more efficiently. This knowledge also allows modeling of the brain and hence the ability to produce improved artificially intelligent systems. The application of such systems is widespread and is likely to change the way in which computers operate. The intermediate ground is in the area of human computer interfacing. Thought control used to be a figment of science fiction. Recent reports [40] show that control of computers by severely disabled people will be possible in the near future.

2.7 Conclusion

Cognitive event-related potentials lend themselves to studies in brain disorders, for example the CNV in schizophrenia. Conventional synchronised averaging produces a single ERP from many trials. One severely contaminated trial can have a large effect on the averaged waveform. An effective single trial ERP recovery method would extract more information from the recorded waveform data. This increase in information will allow a more detailed analysis of ERPs to be possible. Currently, the ability to investigate the development of an ERP over a number of trials (habituation) is inhibited. This trial-to-trial variation is important in understanding the functioning of the brain. Similarly the opportunity for real time monitoring of brain processes may become viable.

An effective single trial recovery method would improve the signal to noise ratio of the ERP whilst maintaining trial specific detail.

Chapter 3

Signal Processing and Interpretation Techniques Used in this Study

3.1 Chapter Summary

An overview of a number of signal expansion techniques used in this study is provided in this chapter. A general introduction to discrete signal expansions is initially presented. The Fourier transform and its time varying derivative are covered. The family of wavelet transforms are then introduced from a filter bank perspective. The other analysis techniques employed are briefly discussed. These are the Hilbert transform, independent component analysis and the Kohonen artificial neural network.

3.2 Introduction

Signal processing uses mathematical techniques to perform operations on data. The use of signal expansions provides alternative representations of the same data. By considering the

characteristics of the signal and the aim of the signal processing, the correct representation, or view, of the data can be identified. The chosen view should facilitate the subsequent data processing in a more efficient manner.

The signals considered in this study were discrete. During the recording process the continuous electrical activity was sampled at discrete time intervals and quantised to discrete amplitude values. All subsequent processes can thus be considered as digital signal processing [41] [42].

3.3 Discrete Signal Expansions

The signal of interest x can be expressed as a linear combination of a set of elementary functions, i.e.

$$\mathrm{x} = \sum_i \alpha_i \varphi_i \tag{3.1}$$

where α_i are the expansion coefficients and φ_i are the basis functions [16].

The expansion coefficients in (3.1) can be computed by (3.2).

$$\alpha_i = \sum_n \tilde{\varphi}_i[n]\mathrm{x}[n] \tag{3.2}$$

Where $\tilde{\varphi}_i$ is the dual of the basis functions φ_i.

The expansion coefficients are a measure of similarity between the signal and elementary function. The larger the similarity, the larger the coefficient. Equation (3.2) is the inner product of two vectors i.e. the elementary or basis function and the signal. This can be denoted as $< \tilde{\varphi}_i, x >$.

The set $\{\varphi_i\}$ is complete for the space S if all signals $x \in S$ can be expanded as in (3.1).

If the set $\{\varphi_i\}$ is complete and orthonormal then we have an orthonormal basis for S. The basis and its dual are the same i.e. $\varphi_i = \tilde{\varphi}_i$.

A set is orthonormal if $< \varphi_i, \varphi_j >= \delta_{ij}$ where $\delta_{ij} = 1$ if $i = j$, and 0 otherwise.

If the set is complete and the elementary functions are linearly independent but not orthonormal, then we have a biorthogonal basis. The basis and it's dual satisfy $< \varphi_i, \tilde{\varphi}_i >= \delta_{ij}$ [43].

If the set is complete but not linearly independent then we have an overcomplete representation called a frame and not a basis [11]. An overcomplete representation may contain a number of bases.

3.4 Fourier Transforms

the Fourier transform use harmonically related sinusoids as elementary functions (the complex exponential in (3.3) and (3.4)) [44]. The Fourier transform may be expressed as

$$F(\omega) = \int_{-\infty}^{\infty} f(t) e^{-j\omega t} dt \tag{3.3}$$

$$F(\omega) =< f(t), e^{j\omega t} > \tag{3.4}$$

where $F(\omega)$ are the Fourier transform coefficients for function $f(t)$ at angular frequency ω.

The discrete Fourier transform, for a signal of length N, is given by (3.5).

$$F(k) = \sum_{n=0}^{N-1} f[n] W_N^{nk} \quad \text{where} \quad W_N = e^{\frac{-j2\pi}{N}} \tag{3.5}$$

The discrete Fourier transform provides a view of the signal purely in the frequency domain. Any transient features and discontinuities are not well represented.

3.5 Inter-Trial Coherence

Coherence provides a measure of the similarity of phase angle between two or more signals at a given frequency [41]. For two signal vectors x and y of length n, the coherence is a

function of the power spectra of x and y and the cross spectrum of x and y [45] and may be denoted by

$$C_{xy}(\omega) = \frac{G_{xy}(\omega)}{\sqrt{G_{xx}(\omega)G_{yy}(\omega)}} \tag{3.6}$$

where $G_{xy}(\omega)$ is the cross spectrum of x and y at frequency ω. For a vector of length N where $X_n(\omega)$ and $Y_n(\omega)$ are the complex FFTs then $G_{xy}(\omega)$ is given by,

$$G_{xy}(\omega) = \frac{1}{N}\sum_{n=1}^{N} X_n(\omega)Y_n(\omega) \tag{3.7}$$

and $G_{xx}(\omega)$ and $G_{yy}(\omega)$ are the power spectra of x and y denoted by

$$G_{xx}(\omega) = \frac{1}{N}\sum_{n=1}^{N} |X_n(\omega)|^2 \tag{3.8}$$

$$G_{yy}(\omega) = \frac{1}{N}\sum_{n=1}^{N} |Y_n(\omega)|^2 \tag{3.9}$$

respectively. The algorithm used in this study provides an estimate of the magnitude squared coherence [48] denoted by,

$$|C_{xy}(\omega)|^2 = \frac{|G_{xy}(\omega)|^2}{G_{xx}(\omega)G_{yy}(\omega)} \tag{3.10}$$

An application of coherence to the analysis of visual evoked potentials is provided by Challis and Kitney [45].

3.6 Deterministic and Adaptive Filters

Ideal deterministic filters (finite impulse response (FIR) or infinite impulse response (IIR)) allow or pass a section of the spectrum of a signal whilst rejecting or stopping the remainder. For example applying a lowpass filter with a cutoff frequency of 10 Hz to a signal would

allow all frequencies below 10 Hz to remain unaffected whilst attenuating all frequencies higher than 10 Hz.

An example of the application of deterministic filters to EEG analysis is in mains line removal.

5assumed to be stationary. The characteristics of event-related potentials

The characteristics of deterministic filters do not reflect the nature of single-trial ERPs in which the ongoing EEG is considered to be the additive noise. ERPs have non stationary spectral characteristics which completely lie within the frequency spectrum of the background EEG. In the general ERP case, a deterministic filter cannot separate desired signal from noise.

3.6.1 Conventional Adaptive Filters

Adaptive filters automatically adjust their coefficients (hence frequency response) to optimise the SNR of the desired underlying signal [46]. A separate channel is employed that provides a time series estimate of the additive noise. Ifeachor *et al.* [47], applied an adaptive filter to the problem of ocular artifact removal from EEG. An estimate of the noise (the ocular artefacts) was obtained from the electrooculogram recorded from a number of electrodes located around the eyes. This noise estimate was subtracted from each EEG channel to produce an 'artefact free' EEG.

The application of conventional adaptive filters to the reduction of background EEG (noise in this case) is not suitable due to a number of limitations. The primary concern being that they require a good model of the 'noise'. That is no noise channel exists for EEG and since EEG is non-stationary the method usually does not provide satisfactory results.

3.7 Discrete Hilbert Transform

The instantaneous frequency characteristics of a real signal can be obtained from its Hilbert transform [48]. The Fourier transform of the original signal is calculated. The negative

frequencies are set to zero and the inverse Fourier transform is computed. To compensate for removing half of the signal energy (by setting negative frequencies to zero), the calculated signal is then multiplied by two. The resulting complex signal is called the analytic signal [49].

The real part of the analytic signal is the original time series and the imaginary part is a 90 degree phase shifted version of the original time series [42]. From this, estimates of the instantaneous frequency and phase can be obtained [41]. The discrete analytic signal is complex and can be expressed in terms of its magnitude and phase by

$$s(n) = A(n)e^{j\phi(n)} \tag{3.11}$$

where the magnitude of the signal $A(n)$ in terms of its real (s_r) and imaginary (s_i) parts is given by,

$$A(n) = \sqrt{s_r^2(n) + s_i^2(n)} \tag{3.12}$$

and the instantaneous phase $\phi(n)$ is expressed as,

$$\phi(n) = arctan\frac{s_i(n)}{s_r(n)} \tag{3.13}$$

The technique has been used to obtain the amplitude envelope of single harmonics for the analysis of the dynamics of EPs [55]. In this study the Hilbert transform was used to estimate the instantaneous phase of the alpha band activity in a visual P300 ERP. This facilitated the investigation of event-related phase dynamics [50][51].

3.8 Short-Time Fourier Transform

In order to obtain some temporal localisation of the Fourier transform, the short-time Fourier transform was developed [52][53]. The STFT is obtained by computing the Fourier transform of several temporal sections of the signal. The sectioning of the signal is implemented using

window functions which also decrease the edge effects incurred when processing a finite length signal. The window for a given transformation is fixed in size. The choice of the window size is a compromise between time and frequency localisation.

The window function $v(t)$ can act on either the signal or basis functions (complex exponentials). Some examples of windowed basis functions are shown in 3.1.

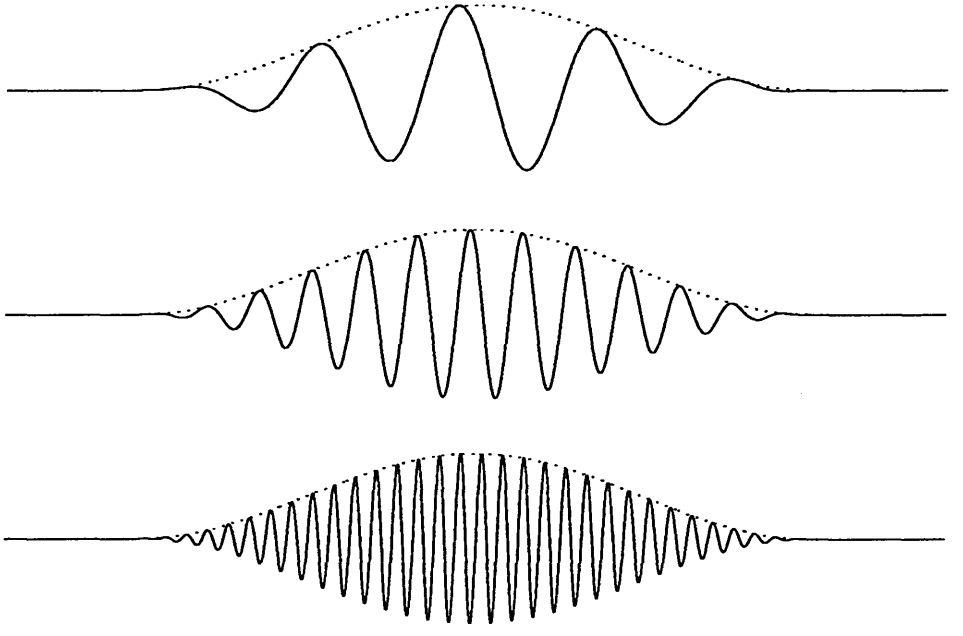

Figure 3.1: Basis functions used in the STFT. The horizontal axis shows time. The fixed length and amplitude window function is shown as a dotted line.

The short-time Fourier transform of a signal $f(t)$ can be expressed as,

$$STFT(\omega,\tau) = \int_{-\infty}^{\infty} f(t)v(t-\tau)e^{-j\omega t}dt \tag{3.14}$$

or alternatively,

$$STFT(\omega,\tau) = < g_{\omega,\tau}(t), f(t) > \tag{3.15}$$

where

$$g_{\omega,\tau} = v(t-\tau)e^{j\omega t} \tag{3.16}$$

and τ is the time shift between successive transformations.

The transformed signal can be viewed on a time-frequency plane as shown in Fig.3.2.

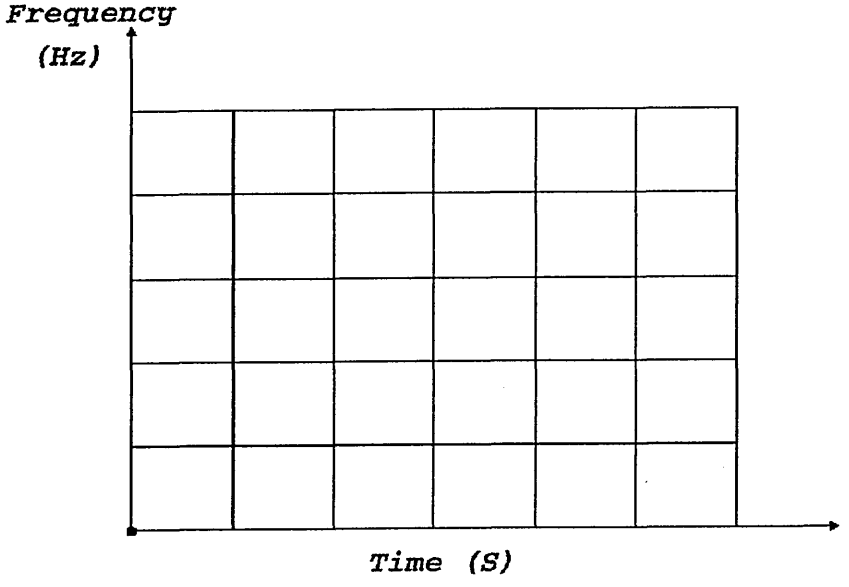

Figure 3.2: The time-frequency plane produced by the STFT

The type or size of window function is chosen based on the signal characteristics and the aim of subsequent processing. From Fig.3.2, it can be seen that the size of the window, and hence time-frequency bins, remains constant during transformation. The optimal window for good time and frequency resolution is Gaussian shaped.

Due to the basis functions used, the STFT is well suited to localised oscillations, i.e periodic signals of short time duration, but is less well suited to pulses or spikes, i.e. transient components.

3.9 Event-Related Spectral Perturbation

The event-related spectral perturbation (ERSP) [54] is a method of averaging normalised time-frequency transforms. Pfurtschellers method of event-related desynchronisation (ERD) and event-related synchronisation (ERS) [55] [56] provide a measure of event-related changes in single frequencies. The ERSP extends this ideas by generalising them to be broadband. The ERSP is a tool for the analysis of ERPs. It focuses in particular on their dynamics. The technique is applicable to all joint time-frequency transforms and to data sets that consist of several epochs with similar underlying responses.

The methodology employed is as follows. For each single sweep recorded from a single channel, the joint time-frequency (STFT in this case) is calculated. This includes a section of pre-stimulus baseline EEG. The spectral distribution is normalised using the mean baseline spectrum (calculated by taking bootstrap [57] samples from the recorded pre-stimulus signal). The scale is converted to be logarithmic. The ERSP is obtained by repeating the above procedure for several trials then calculating the average time frequency distribution. A subsequent processing step using bootstrap data is to set significance levels which are then used to threshold the data. All non-significant values are set to a central value (zero). This enables the regions of significance to be more easily observed from the plots.

The application of the technique to auditory event-related potentials [54] shows the effectiveness of such a joint time-frequency technique. The dynamics of the EEG spectrum in response to a stimulus is revealed. The ERSP has also been applied to magneto-encephalogram

(MEG) recordings of an auditory ERP [58].

Makeig [54] discussed a problem in the ERSP as proposed in that the time resolution is not fine enough to reveal a relatively high frequency Gamma burst (a transient period of EEG activity in the 30-80 Hz range). He suggested that a future ERSP method may use a finer or variable time resolution method. Wavelets provide a solution to this problem. They inherently provide higher temporal resolution at higher frequencies.

The ERSP however does not reveal the amplitude and latency variability of individual single trials. This is best investigated using single trial analysis methods (Chapter 6) and visualised using techniques such as Jung *et al.*'s erpimage [59] (see also phase analysis chapter 6).

3.10 Wavelet Transforms

A family of wavelet transforms was developed recently from research in the different disciplines of mathematics and signal processing [60] [61]. The time-scale representation promises improved performance in a wide range of signal processing applications [62]. In particular, wavelets may be applied to biomedical applications [12]. Their application to the analysis of EEG is currently an active area of research [63][64][65]. Wavelets are also emerging as an ideal tool for modeling the dynamics of the brain [66].

Wavelets can be considered a natural development of the short-time Fourier transform [67]. In the STFT, the basis functions are time shifted and modulated versions of the primary basis function. The time shift and scaling of a prototype basis function provides a constant relative bandwidth analysis known as the wavelet transform (WT). The WT can offer a better compromise in terms of time and frequency. At low frequencies, the frequency (or more correctly scale) resolution is increased at the expense of temporal resolution. Conversely at higher frequencies temporal resolution is increased to the detriment of scale resolution.

The term wavelets covers a family of transforms. In this chapter, wavelet transforms applicable to discrete signals are discussed.

3.10.1 Continuous Wavelet Transform

The continuous wavelet transform (CWT) [68] provides a representation of a signal on a time-scale plane. The CWT of a signal $f(t)$ can be expressed as 3.17 [69]

$$CWT(\omega,\tau) = \frac{1}{\sqrt{\omega}} \int_{\Re} \Psi(\frac{t-\tau}{\omega}) f(t) dt \tag{3.17}$$

Where $\omega \in \Re^{+}$ is the scale factor, $\tau \in \Re$ is the time shift and Ψ is the prototype basis function.

The CWT can also be expressed mathematically as an inner product as in 3.18

$$CWT(\omega,\tau) = < \Psi_{\omega,\tau}(t), f(t) > \tag{3.18}$$

Where the basis functions $\Psi_{\omega,\tau}$ are given by

$$\Psi_{\omega,\tau} = \frac{1}{\sqrt{\omega}} \Psi(\frac{t-\tau}{\omega}) \tag{3.19}$$

That is we measure the similarity between the signal and shifts and scales of an elementary function. Some scaled and translate (shifts) of a wavelet are depicted in Fig.3.3 [70].

A popular basic wavelet is Morlet function [70], expressed as 3.20

$$\Psi(t) = e^{j\omega_0 t} e^{\frac{-t^2}{2}} \tag{3.20}$$

Its corresponding Fourier transform is 3.21

$$\Psi(\omega) = \sqrt{2\pi} e^{\frac{-(\omega-\omega_0)^2}{2}} \tag{3.21}$$

By setting the centre frequency $\omega_0 = 5.3$, Morlet function closely approximates the necessary properties for a basic wavelet [71]. The approximation of both the basis functions and the transform allows the application to digital signal processing.

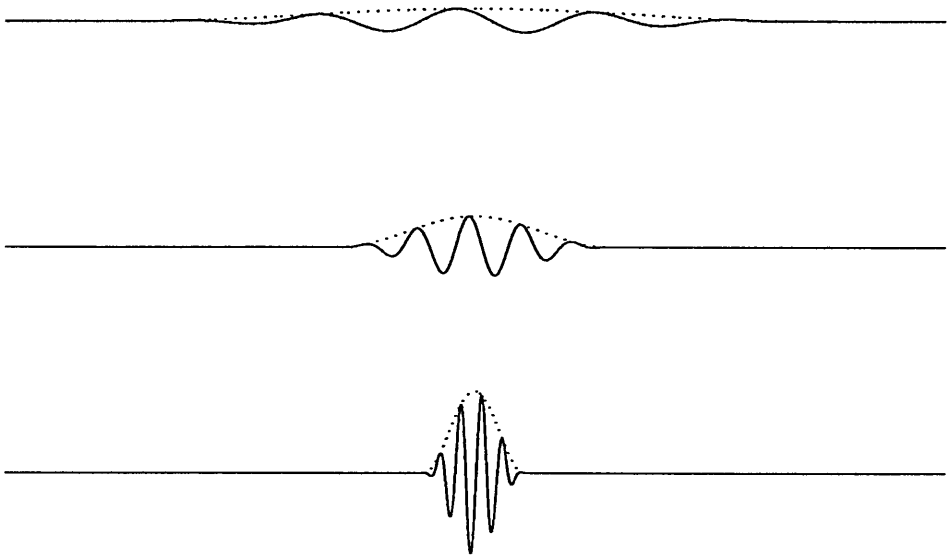

Figure 3.3: Wavelet basis functions produced by scaling a single prototype. The horizontal axis shows time. The variable length and amplitude window function is shown as a dotted line.

3.10.2 Discrete Wavelet Transform

The discrete wavelet transform represents a signal $x(t)$ by the relationship

$$x(t) = \sum_{j,k} < x, \Psi_{j,k} > \Psi_{j,k}(t) \tag{3.22}$$

Where the DWT coefficients $< x, \Psi_{j,k} >$ are a measure of the energy of the signal components located at $(2^{-j}k, 2^j)$ on the time-frequency plane [43].

If the basis functions are implemented as filters, the discrete wavelet transform can be implemented by as a tree structured filter bank [61].

From a filter bank perspective, the discrete wavelet transform processing element can be considered to be a two channel filter bank [72]. As the name implies, the filter bank separates the signal into two channels, or subbands. This is achieved through the use of a complementary pair of high and low pass filters for analysis and a similar pair for synthesis.

The two subbands have the same sampling rate as the original signal and hence contain reduntant information (there are two full length signals where previously there was one). The bandwidth of each subband is half of that of the original signal so the sampling rate can be downsampled, or decimated, by a factor of two. That is, every other sample may be thrown away. For an N band filter bank, each subband can be decimated by a factor of up to N. When the factor by which each subband is downsampled is equal to the number of bands in the filter bank, the filter bank is said to be maximally decimated.

The process of downsampling or decimation is usually depicted by a down arrow followed by the decimation factor. The corresponding upsampling operation in the synthesis bank, denoted by an up arrow follwed by the upsampling factor, introduces zero valued samples into each subband. The effect is to increase the sampling rate.

Fig.3.4 shows a two channel, maximally decimated, orthogonal filter bank. The low and highpass filters in the analysis section are represented by H_0 and H_1 respectively. The corresponding filters in the synthesis section are F_0 and F_1.

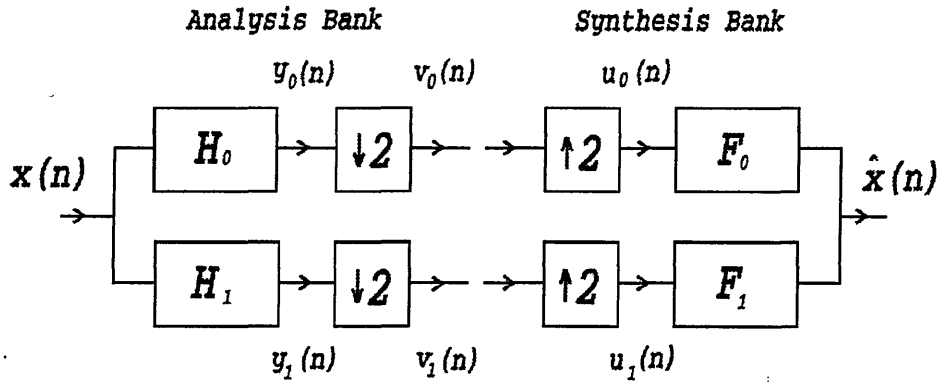

Figure 3.4: A two channel, maximally decimated filter bank (QMF)

It can be seen in Fig.3.4 that the analysis filter comprises a high pass / low pass filter pair followed by a decimator. The frequency response of the analysis filters is shown in Fig.3.5.

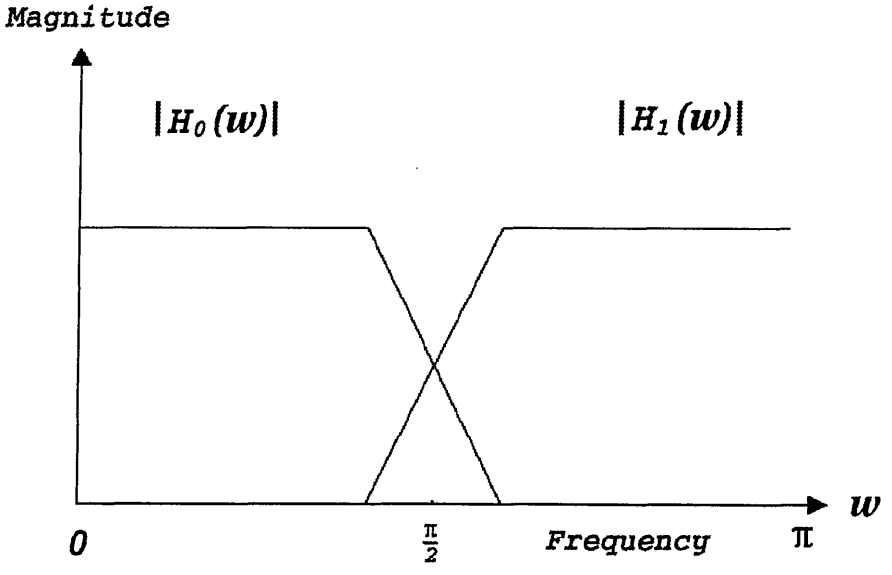

Figure 3.5: The frequency response of a QMF

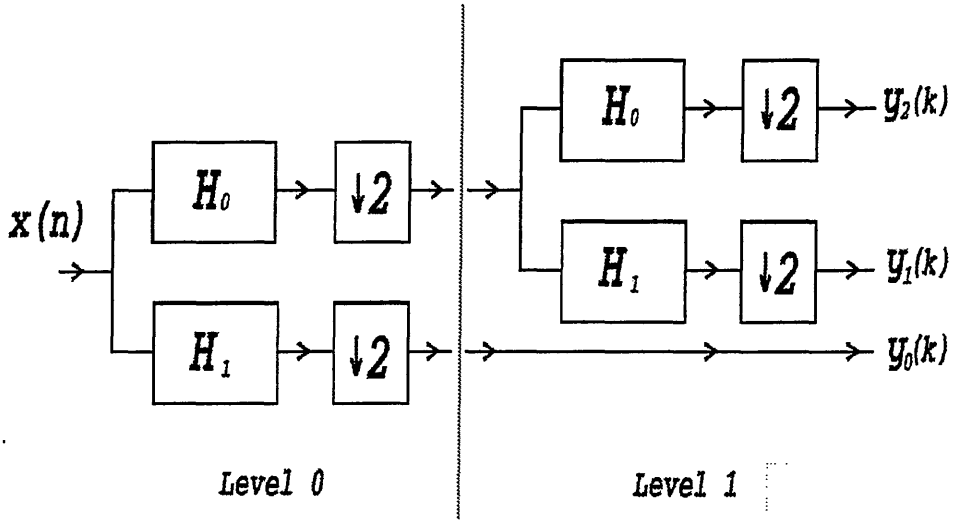

Figure 3.6: A two level tree structured filter bank

The analysis filter decomposes a signal into two subbands or channels. The lowpass channel is the trend of the signal, the highpass is its detail. Each channel is then down sampled by a factor of two. The synthesis filter is comprised of an interpolator (upsampler) and a high pass / low pass filter pair (matched or mirrored with the analysis filter). The aliasing, or the error caused by a spectral overlap, introduced by the analysis filters is cancelled by the correct design of the synthesis filters [73]. The repeated application of the analysis filter to the lowpass channel leads to a tree structured filter bank as shown in Fig.3.6.

The highpass channel, which contains the details of the signal at a given level in the tree, is not further processed. The analysis filter is then applied to the lowpass channel. The subsequent splitting of the lowpass channel is carried out until the signal has been decomposed to a pre-determined number of levels or the length of the signal has been downsampled to 1.

The discrete wavelet transform (DWT) produces a proportional bandwidth filter bank, each filter has a bandwidth proportional to its centre frequency as shown in Fig.3.7. This arrangement provides, respectively, the spectral/temporal resolution trade-off at lower/higher

frequencies.

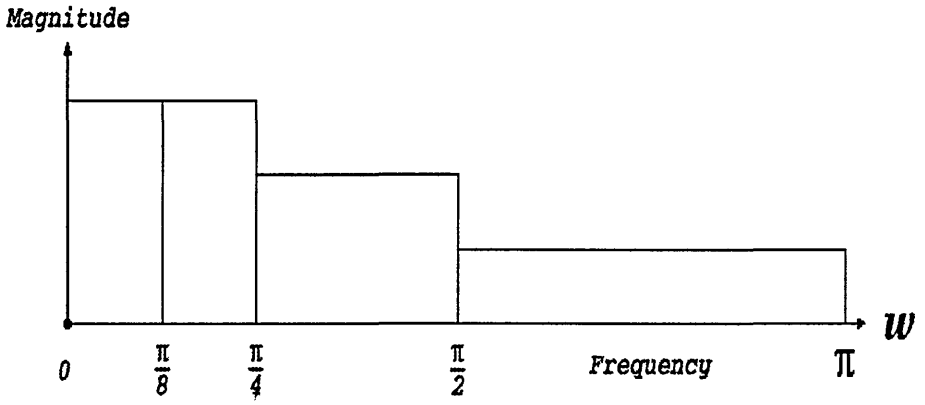

Figure 3.7: The frequency response of two level tree structured filter bank

The application of the filter bank results in the signal being separated into frequency bands. The lowest frequency band represents the trend of the signal. Each subsequent addition of higher frequency bands results in more details being added to the signal. Hence the idea of multiresolution [74]. The signal can be viewed at different levels of resolution simply by adding or removing detail as necessary. Each channel or subband can be processed independently. The signal is synthesised by the repeated application of the synthesis filter starting with the lowest frequency channels.

3.10.3 Wavelet Packet Transform

The wavelet packet transform (WPT) [75] is a superset of the discrete wavelet transform [76]. Instead of applying the analysis filter solely to the lowpass channel as in the case of the wavelet transform, in the wavelet packet transform the filter is applied to the highpass channel as well [78]. As with the discrete wavelet transform the WPT can be implemented by the repeated application of a maximally decimated, two channel filter bank [73], i.e. recursively splitting a signal into two sub-bands which are then decimated by a factor of two. The time-scale plane produced is shown in Fig.3.8, the vertical axis represents scale,

while the horizontal axis is time. Each bin or rectangle in the table has the same area resulting from constant Q filters. The trade-off between time and scale resolution can be seen in Fig.3.8.

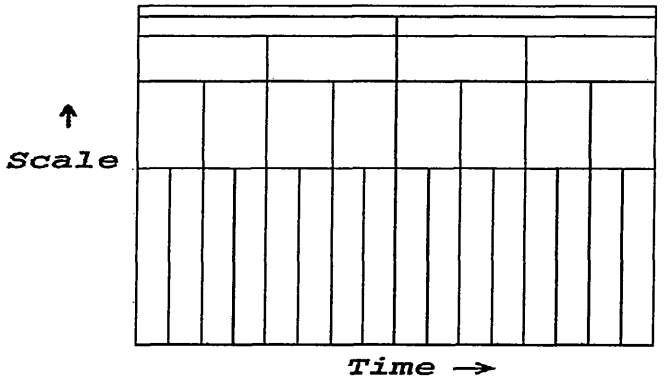

Figure 3.8: The time-scale plane (or wavelet packet table) the vertical axis is scale, horizontal is time

The resulting transform is overcomplete allowing a basis to be chosen that best matches the processing task. For example Wickerhauser's best basis search algorithm selects the best basis in terms of the minimisation of an information cost function [77]. As such Wickerhauser's best basis is ideally suited to signal compression. Another basis that spans the wavelet packet table is the wavelet basis. Which is, in fact, the discrete wavelet transform. The transform can be 'adaptive' since the basis can be chosen from a set of bases to meet the needs of the application.

3.11 Independent Component Analysis (ICA)

Independent component analysis (ICA) performs a blind signal source separation on a linear mixture of unknown signals [18]. Significant progress has been made recently in the area of separating independent components from signal mixtures. An number of information theoretic based approaches are reviewed by Lee [79]. The aim of a signal source separation method is to minimise the mutual information between the separated components thus making them statistically independent. The goal of ICA is therefore to perform a linear transform which makes the resulting variables as statistically independent from each other as possible [79].

ICA uses an unsupervised learning algorithm based on information theory [18] to obtain an unmixing matrix that maximises the mutual entropy of the input and output vectors. The algorithm is outlined in the following steps.

The unmixing matrix W is initialised to the identity matrix.

The signal sources are estimated by $U = WX$ where U contains the unmixed components and X contains the original mixed signals.

The estimated signal sources U are transformed by a non-linear transfer function such as a sigmoid function. The output Y of a sigmoid transfer function is denoted by 3.23.

$$Y = \frac{1}{1 + e^{-(U+\omega_0)}} \tag{3.23}$$

where ω_0 is a weight vector whose elements are initialised to zero.

A learning rule is used to determine the change of the weights in the unmixing matrix W. The learnig rule is expressed in 3.24.

$$\Delta W = [W^T]^{-1} + (1 - 2Y)X^T \tag{3.24}$$

The symbols T and -1 denote matrix transpose and inversion respectively. The change in the bias weigth vector is given by 3.25.

$$\Delta\omega_0 = 1 - 2Y \tag{3.25}$$

The algorthim repeats the above steps, updating the unmixing matrix and bias vector each iteration. The algorithm stops when the magnitude of change of the unmixing matrix falls below a predefined small value. The magnitude of change of matrix is calculated using the mean squared difference between the corresponding elements in the matrix obtained before and after each iteration.

In the analysis of cortical electrical activity, ICA aims to spatially filter the recorded EEG from multiple electrodes into a number of temporally independent components or signal sources [80]. Consideration of the projected location of signal sources along with existing knowledge of regions of the brain active during a given task enhances the investigation of cortical dynamics. Sources producing specific signal components for a given experiment can be identified considering the scalp distribution of components. Ocular artefacts for example can be greatly attenuated by identifying and removing components that represent electroocculargram (EOG) components [59]. A quantitative comparison of ICA and other signal source separation techniques was reported by Vigon *et.al.* [81]. Where it was shown that ICA was more effective than decorrelation methods.

3.12 Kohonen Artificial Neural Network

Artificial neural networks (ANNs) are parallel processing structures which attempt to simulate the learning behaviour of the brain. They consist of interconnected neurons capable of storing and processing information. Their applications included pattern recognition, process control, forecasting, modelling and optimisation [82]. Compared to statistical methods of data analysis, ANNs are more effective for analysing noisy signals and less sensitive to the distribution of their input data. The process of learning in an ANN can be supervised or unsupervised. In applications requiring pattern recognition, a supervised learning algorithm involves presenting known patterns and their corresponding classification categories to an ANN. The ANN can then adjust its parameters to become capable of recognising the patterns from those categories. In the unsupervised learning however, the pattern categories

are not presented to the ANN. The learning algorithm is therefore a form of clustering in which the patterns are grouped on the basis of their similarities.

The self organising feature map (SOFM) developed by Kohonen [83] typically performs a transformation of patterns from a high dimensional feature space into a two dimensional, topologically ordered map shown in Fig.3.9.

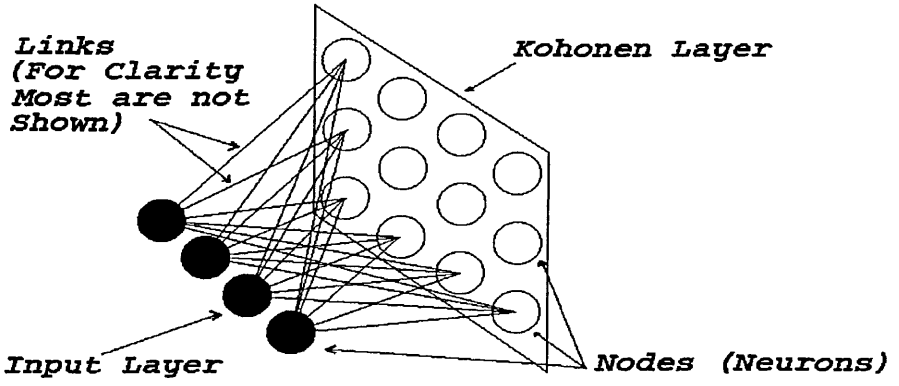

Figure 3.9: The Kohonen self-organising feature map

The network has a two layers of neurons (processing elements). An input layer which provides connections to the Kohonen layer or map [84]. Typically each neuron in this map is connected to all the inputs to the network. Associated with each connection there is a weight. For clarity, only the connections of some of the neurons are shown in Fig.3.9. The Kohonen map can be arranged in various topologies, including rectangular and hexagonal.

The network employs an unsupervised competitive learning algorithm and hence self organises [85]. The network is initialised by setting the connection weights to small random values between 0 and 1 [84]. Data is presented to the network via the input layer. The input vector which represents a set of input patterns is denoted by,

$$X = [x_1, x_2, ..., x_p]^T \tag{3.26}$$

where p is the number of elements in a given input pattern.

The resulting effect on each neuron in the Kohonen layer is calculated by determining the Euclidean distance between an input pattern and the connection weights for each neuron. The weight vector for node j in the Kohonen layer is denoted by,

$$W_j = [w_{j1}, w_{j2}, ..., w_{jp}]^T \; for \; j = 1, 2, ..., N \tag{3.27}$$

where w_{ji} is the weight of the link connecting input node i to Kohonen node j and N is the number of nodes in the Kohonen Layer. Since each node in the Kohonen layer is usually connected to every input node, the nodes weight vector comprises p weights. The winning neuron j for an input vector X is said to be the neuron which has the smallest Euclidean distance d between it's weights and the input vector calculated using,

$$d(X) = \sqrt{\sum_{k=1}^{p}(x_k - w_{jk})^2} \quad for \; j = 1, 2, ..., N \tag{3.28}$$

The weights associated with winning neuron are then updated in such a way that gradually the winning neuron becomes representative of a specific pattern category using,

$$W_j' = W_j + \alpha(x_i - W_j) \tag{3.29}$$

where W_j' is the the updated weight, W_j the weight prior to updating, α is the learning rate and $(x_i - W_j)$ provides a measure of the error between the winning node and the input pattern x_i. The group of neurons around the winning neuron are known as a neighbourhood. The weights associated with neurons in the neighbourhood around the winning neuron are also updated. Generally the learning rate for a given node is decreased with increasing topological distance from the winning node. This enables specific regions of the Kohonen map to be associated with different pattern categories. The value of the learning rate α for all nodes is generally scaled using a neighbourhood function centred on the winning node. A typical choice [82] of neighbourhood function β is a gaussian-type function such as,

$$\beta_{p,q} = e^{-\frac{d_{p,q}^2}{2\sigma^2}} \tag{3.30}$$

where the amplitude of β_{pq} for node q centred on winning node p is maximal when node q is the winning node (i.e. $p = q$) and decreases with increases topological distance d. σ represents the size of the neighbourhood. The learning rate and neighbourhood size are reduced gradually during the many training iterations (presentations of input patterns). This allows the network to self organise and cluster similar patterns in topographically distinct regions whilst gradually increasing the separation between dissimilar patterns.

The discrete time (n) algorithm for network training [82] of Kohonen node j can be expressed as,

$$W_j(n+1) = W_j(n) + \alpha(n)\beta_{j,i}(n)[X(n) - W_j(n)] \tag{3.31}$$

The trained network maps similar features in feature space to similar areas in the output layer of the network. Since the learning process is unsupervised, the network clusters the input data based on patterns that it discovers. The Kohonen SOFM is commonly used as an investigative classification tool when the output categories are unknown.

3.13 Conclusion

A brief overview of the signal analysis techniques used in this study has been presented. Generic discrete signal expansions have been introduced along with the corresponding terminology. The Fourier transform was briefly discussed. The improvement on temporal localisation provided by the time-varying short-time Fourier transform was introduced. The natural successors (and recently developed) wavelet transforms have improved time-scale characteristics.

Chapter 4

Development of a Wavelet-Based Single Trial ERP Recovery Technique

4.1 Chapter Summary

In this chapter, a comparative investigation of wavelet-based filtering is carried out [104]. The methodology and results obtained are discussed. An adaptive multiresolution analysis filter has been developed [105]. The implementation details are provided. Plots of simulated CNVs and the estimated single trials produced by the different filtering approaches are provided and the results are compared.

4.2 Introduction

The conventional method of recovering event-related potentials (ERPs) from the background electroencephalogram (EEG) is synchronised averaging. The assumption is that the background EEG tends to be random while the ERP is consistent both in amplitude and latency.

The process of synchronised averaging therefore enhances the ERP while attenuating the background EEG. A shortcoming of the method is that it inhibits measurement of the trial-to-trial variations which can develop as a result of factors such learning, changes in the level of attention, fatigue etc.

The aim of filtering is to enhance the desired signal by attenuating unwanted 'noise' components. This is usually achieved in the transform domain. Transform domain filtering is a three stage process. Transform the signal, leave out the coefficients that best represent the noise and then reconstruct the now filtered signal. The resulting signal has an improved signal-to-noise ratio (SNR). Deterministic filtering can be considered as filtering in the frequency domain. Filtering is achieved through the maintenance of selected frequency bands whilst attenuating the remainder. This method works well when there is a separation of the signal spectrum from the noise spectrum. Unfortunately in the case of ERPs, there is a large spectral overlap between the desired signal and the unwanted noise. The transformation of the recorded waveform into the frequency domain does not separate the desired ERP from the unwanted background EEG. A more suitable form of digital filtering can be achieved by transforming the signal into a domain that provides a better separation of signal components from noise.

ERPs recorded during a given task is severely obscured by background EEG and therefore their SNR is very low. Typical magnitudes are 5-20 μV for the desired signal (ERP) and 100 μV for the noise (background EEG in this case). Single trial recovery is the removal of unwanted noise from a single sweep ERP recorded from a single scalp electrode. The ideal recovered signal component would contain only stimulus related brain activity. The on-going background EEG would be removed along with any ocular, motor and other unwanted electrical activity. Currently ERPs are analysed following the synchronised averaging of many trials to improve the SNR. The application of time domain averaging attenuates all signal components not time and phase locked to the stimulus.

The validity of synchronised averaging has been challenged for many years. [86]. The assumption made for averaging, that the ongoing EEG is random and uncorrelated with the ERP has been questioned [87]. Similarly averaging relies on the fact that the ERP components are the same for every stimulus. This does not take into account the random

variation in latency, or jitter, of peaks in the ERP. The effect of jitter is to temporally smear peaks and reduce their amplitude. Woody suggested an approach based on correlating time-shifted individual trials to reduce the effects of jitter [88]. The limitations of the method are that it will not allow the trial-to-trial variation to be investigated and it requires a reference trial for it's correlation process.

Latency differences of later components result in attenuation in the averaged ERP [89]. In particular the variation in latency has most effect at increasing temporal distance from the time point used for synchronisation. This leads to the smearing of later peak positions and attenuation of amplitude. These components are observed as being of lower frequency and longer duration. This characteristic may be purely as a result of using averaged trials. Similarly components not phase locked to stimulus are attenuated. The phase reordering post-stimulus cannot be seen in averages however this important brain dynamic is observable using more recent techniques described in chapter 6.

The ability to effectively recover single trials will allow the investigation of brain dynamics of any given trial within a set of trials. Also the effects of habituation to task and fatigue e.t.c. can be investigated by considering the evolution of ERP over a number of trials [90]. The investigation of trial-to-trial variation for subject group is described in chapter 5.

Chan *et al.*[91] described an improvement on adaptive filtering of a brain stem auditory evoked potential (EP) using an ensemble average as a reference signal. Although he commented on EP trial-to-trial variability, his method did not fully rectify this. The method is an improvement on standard synchronised averaging methods because the number of running averages is reduced.

Filtering approaches that consider the time-varying characteristics of ERPs have yielded improved results over conventional deterministic filters. Adaptive filtering approaches [92] including Kalman filtering [93] have been applied to evoked potentials. Unfortunately this approach suffers from the lack of a valid noise model when applied to ERPs.

The Weiner filter is the optimal deterministic filter in the least mean square error sense when applied to a known deterministic signal with known deterministic noise [94]. The application to ERP filtering has been of the *a posteriori* type [95]. That is an estimate of the statistics of

both the signal (taken from the spectrum of the synchronised average) and noise (estimated as the average spectrum of the recorded waveforms). With the assumptions and estimates considered it provides improved filtering on a subject level however no consideration is given to the time-varying nature of ERPs. In a development of this approach, deWeerd proposed time-varying Weiner filters [96][97]. Simulated ERP waveforms were used to test the performance of the filters. The method was applied to averaged ERPs and is not suited to single trial estimation due to the need for accurate noise models.

The methods discussed so far have not met the requirements set by the characteristics of event-related potentials. In summary the main signal characteristics are time varying nature with only a heuristic model for both the signal itself and the noise. Recent developments in digital signal processing have provided new tools which are more suited to non-stationary signals. In particular the joint time frequency /scale methods which can be grouped under the heading of wavelets.

4.3 Wavelet-Based ERP Filtering

Relevant features in event-related potentials are localised temporally. For example the section of interest may be centred on the time at which a subject presses a button in response to a stimulus. Some noise will occur continuously in time whilst other noise artifacts will be synchronised with some external events but not with the event that produces the ERP. For example the ERP may be obscured by some ongoing mains noise, ongoing EEG and a random transient eye movement. The electrophysiological activity of the brain readily maps to short duration bursts of activity within a given frequency range. For example the short term oscillatory response to a given stimulus. Wavelet methods enable a signal to be decomposed into temporally localised components within a given bandwidth. The multi-scale concept of wavelets maps well with the compound signal produced from many signal generators [98].

Wavelets have been succesfully applied to the analysis of several electrophysiological signals [13][12][71]. This suggests that wavelet based filtering may be suited for the estimation of single sweep EPs. A small number of studies have been carried out investigating the applicability of wavelets to ERP filtering and analysis.

The approach used in transform domain filtering may be employed for use with the wavelet transfom. The process involves transforming the data using the transform of choice. The ideal choice of transform is that which, upon application, separates the desired signal from the undesired noise. Specific transform domain coefficients relating to noise components are selected and their values are set to zero. The non-noise coefficients are left intact. The coefficients are then inverse transformed to produce a filtered (de-noised) signal.

Bartnik *et al.*[99] applied the approach described above to single-trial, auditory evoked potentials (AEPs). The 1 second section of data recorded immediately following the stimulus was assumed to contain the EP. The subsequent 1 second section, following the EP, was assumed to be pure EEG. Regression and discriminant analysis were used to provide the 5 wavelet coefficients that 'best' represented the evoked potential as opposed to the EEG. The remainder were set to zero prior to signal reconstruction by inverse wavelet transform. The reconstruction from 5 coefficients was suggested as being relatively noise free, however, most details were lost.

Thakor *et al.*[100] used multiresolution wavelets in the analysis of averaged EPs. They did not try to recover single trials but the practical methodology employed may be developed further. If Thakor *et al.*'s approach was developed to utilise a constantly updating running average then a method for single trial estimation based on the idea of running averages could be employed provided a small number of trials are used (2-4 and not 16-20). Thakor *et al.*[100] also suggested that wavelets should be used in conjunction with other methods to improve the SNR.

Bertrand *et al.*[101] improved the procedure of [99]. This method used Meyer's wavelets (those based on the DFT of a "wavelets" spectrum) to improve the SNR of averaged middle-latency auditory evoked potentials (MLAEP). Consideration was given to the characteristics of the signal being non-stationary. A time-varying filter adapted to the signal was proposed. However, this was used after synchronised averaging. The wavelet coefficients were chosen manually and the remainder were set to zero prior to reconstruction. A discussion on the search for an optimal filter for evoked potentials was given. This lead to a proposed time-frequency optimal filter in the least mean squared error sense.

Wavelet networks [107] combine wavelets and neural networks and are typically used for

discrimination of ERPs. Heinrich *et al.*[106] applied wavelet networks to the analysis of single trial auditory ERPs. Real EEG was added to simulated ERPs which were used to determine the performance of the approach. The filtered 'ERPs' were good estimates of the original ERPs. The measurement of trial specific time-frequency features permits the analysis of trial-to-trial variation.

In this study a novel method of recovering single trial ERPs from the background EEG was developed and its effectiveness was evaluated [105]. The analysis was based on a type of ERP known as the contingent negative variation (CNV). The method involved the application of the discrete wavelet transform (DWT). The signal was decomposed by a tree-structured filter bank implementation of the DWT. The resulting wavelet coefficients were scaled using an adaptively computed scaling factor. The goal being to maintain trial specific detail whilst attenuating the background EEG. The estimated single trial was recovered using the tree-structured synthesis bank implementation of the inverse DWT.

In order to find the optimum performance for the developed wavelet transform based adaptive filter, a number of different basis functions were explored. The performance of the filter for each case was quantified. The results obtained were compared with those obtained by deterministic, finite impulse response filters.

4.4 Adaptive Wavelet-Based ERP Filtering Technique

Filtering in the wavelet domain is achieved through the scaling (attenuation) of selected wavelet coefficients. By setting the value of the selected coefficients to zero (the approach taken by previous methods) the assumption made is that the specific coefficients represent noise rather than desired signal. If it is the case that the attenuated coefficients were more representative of noise rather than the desired signal then the SNR of the desired signal would be improved.

However whilst this method of hard thresholding the coefficients may improve the SNR, any ERP features that are decomposed into the same time-scale bins as noise will also be attenuated. The recovered single-trial ERP would appear distorted. The main goal of single

trial filtering is to maintain trial dependant response information whilst improving the SNR.

Due to the spectral overlap between the ERP and the unwanted 'noise', the wavelet transform does not completely separate signal from noise. For a given set of coefficients the relative contribution of desired signal and noise components is not deterministic. A method which uses some *a priori* knowledge of the desired signal characteristics would therefore be beneficial. This would allow the coefficients to be scaled with a real value between 0 and 1 to meet the requirements of increasing SNR whilst minimising distortion.

The novel algorithm developed in this study computed the optimum scaling factor for each level of the DWT adaptively [105]. An approach to single trial ERP filtering using the subject average as a template to provide the *a priori* knowledge was developed. The single-trial wavelet coefficients were adaptively scaled using this *a priori* knowledge.

4.4.1 The Adaptive Wavelet-Based Filtering Algorithm

In order to investigate the effectiveness of the developed algorithm a set of 32 simulated single trials ERPs was produced. This enabled the recovered simulated single trial to be compared with the original waveform and thus allowing a quantitative evaluation of the filtering method to be carried out.

To produce the simulated single trials, real EEG was added to a model of a contingent negative variation (CNV) ERP. The model (shown in Fig.4.1) had similar characteristics to those of an averaged CNV. It had a zero mean before stimulus. Immediately following the 'presentation' of the first stimulus, there was an auditory evoked potential. A negative shift follows the EP in anticipation of the impending second stimulus. The second stimulus produced another auditory EP before the ERP returned to the pre-stimulus (baseline) level.

32 simulated single trials were produced by adding 32 different recordings of EEG to the model. The number of trials was chosen to maintain the similarity between the processing of the simulated waveforms and the recorded CNVs of which there were 32 trials from each of 40 subjects. The simulated single trials were bandlimited to 30Hz and the sampling rate was 125Hz, again to reflect the recorded trials. A 512 point section (covering approximately 4

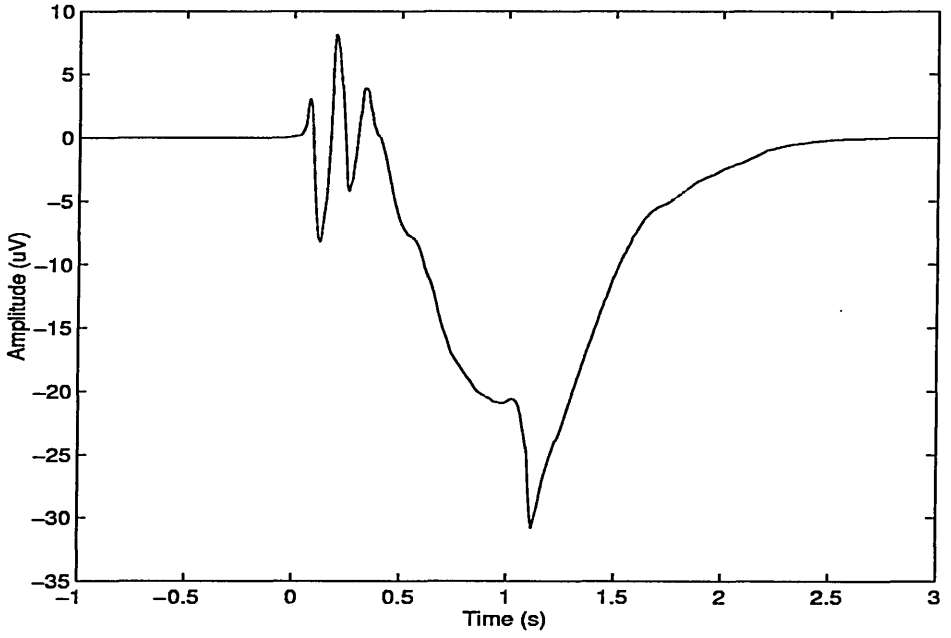

Figure 4.1: A simulated ERP

seconds from 1 second preceding the first stimulus) of each waveform was used in subsequent processing. A simulated single trial is depicted in Fig.4.2.

The filtering technique employed a template to provide the algorithm with *a priori* signal knowledge. In the case of real ERPs, this was the synchronised average of the 32 trials from the same subject,. To replicate the processing of real ERPs, the average of the set of 32 synthetic single trials (shown in Fig.4.3) was used as a template rather than the original simulated ERP which is too dissimilar from the real averages.

An overview of the procedure for the adaptive wavelet based filtering of single trial ERPs developed in this study is provided below. This process was repeated for each single trial.

- Apply the discrete wavelet transform to both the single trial and template waveform.
- For each level of decompositon, use the template coefficients to guide the adaptive algorithm in setting the scaling factor for the single trial coefficients.
- Apply the inverse discrete wavelet transform to the scaled coefficients to construct the,

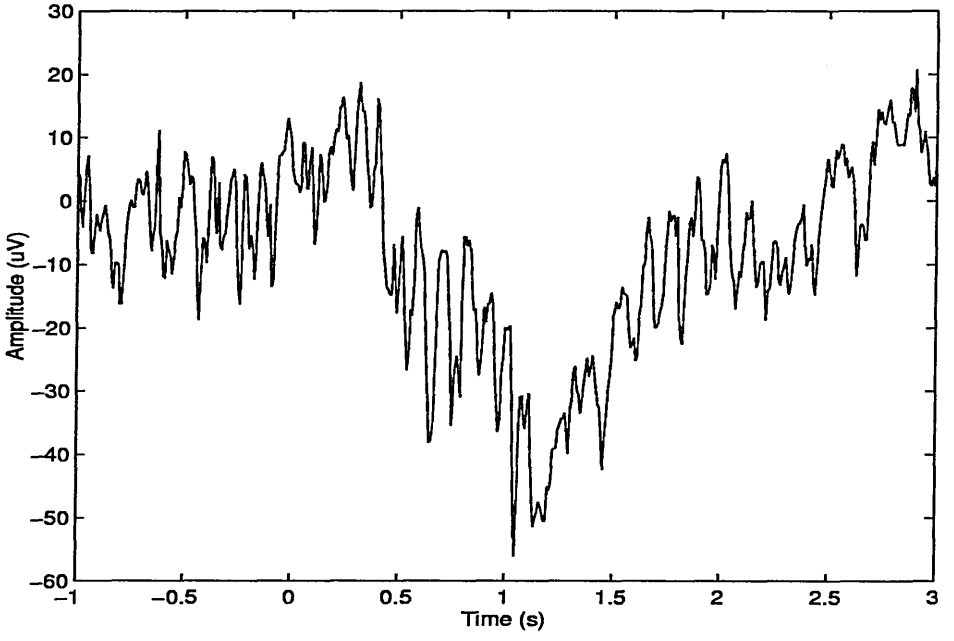

Figure 4.2: A simulated single trial

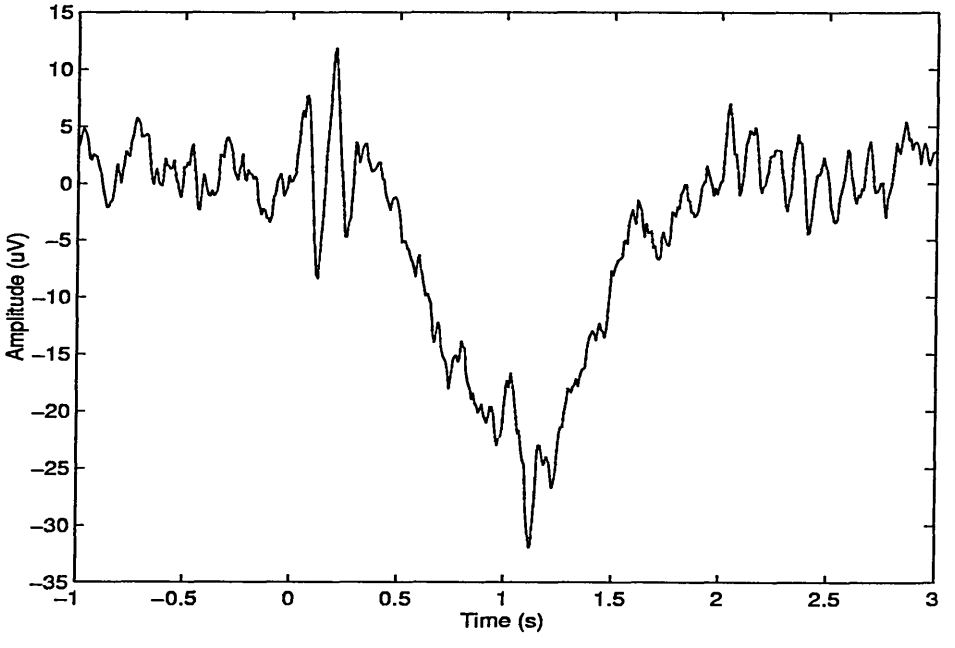

Figure 4.3: The time domain average of 32 simulated single trials

now filtered, single trial waveform.

The details of the approach are now discussed.

Although the wavelet transform is suitable for non-stationary signal analysis, it was found that the negative shift of the CNV dominated the transform coefficients. To improve the time-varying characteristics of the algorithm, the single trial waveform was broken down into a series of sections in the time domain. In effect the filter worked on 8 points of the original signal before moving on to the next 8 points until all of signal has been processed. The choice of 8 points from the 512 points of the whole signal provided a good resolution for the time-varying filter. However, two problems arose from the use of such a small section relating to the practicalities of wavelet filtering: The edge effects introduced by finite length filters had a more significant effect on the recovered data and the number of levels of wavelet decomposition were governed by the signal length. This effected the frequency resolution and hence effectiveness of the wavelet transform. To overcome these effects, a series of longer overlapping windows, centred on the 8 point section of interest, was used to provide a longer section of signal to process. This redundant extra processing had minimal effect on the overall filtering time.

A sliding window technique (Fig.4.4) was used to extract 32 points at a time from both the recorded waveform and the corresponding template.

The 32 point section was filtered using the algorithm discussed below. Following filtering the central 8 points of the 32 point section were used to produce the reconstructed signal. The sliding window was then moved by 8 points before extracting the next 32 point section and repeating the algorithm.

For clarity in the following discussion of the algorithm, the section of the single trial will be called the signal and the section of the template will be called the template.

The discrete wavelet transform (DWT) of both the signal and template were calculated. The resulting wavelet transform consisted of coefficients at a number of levels of decomposition or scales. For a signal of length N points, the maximum number of levels of wavelet transform decompositon, L, is equal to $(log_2 N) - 1$. For each level of decomposition the scaling factor

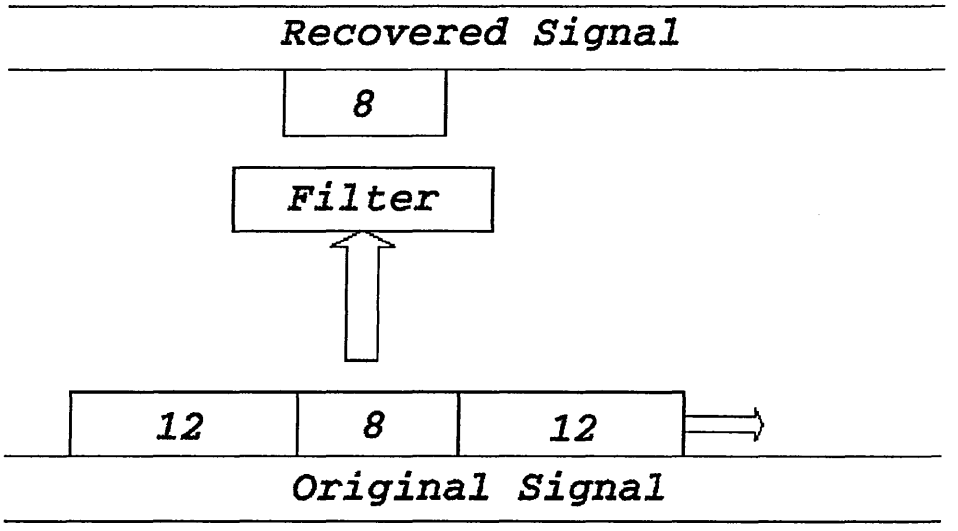

Figure 4.4: The sliding window technique

for the signal coefficients was computed and applied using the procedure shown in Fig.4.5.

- The algorithm parameters were initialised. The scaling factor (SF) and scaling factor increment (INC) were set to 0.5, the midpoint of their range. The Euclidean distance difference (EDD) was initialised to 1.
- The Euclidean distance (ED1) between signal and template coefficents was calculated.
- The following steps were then repeated until any further iterations caused the Euclidean distance between the coefficients of the signal and those of the template to increase. i.e. the optimum scaling factor has been obtained.
- The signal coefficients were scaled by obtained value of SF.
- If the scaling caused the Euclidean distance between the coefficients to be reduced (i.e. ED1 is greater than ED2), the scaling factor value remained unchanged. Otherwise the signal coefficients were restored to their value of the previous iteration and the scale factor was incremented by half its current value.

Once the optimum scaling factors were determined for the section being processed, the

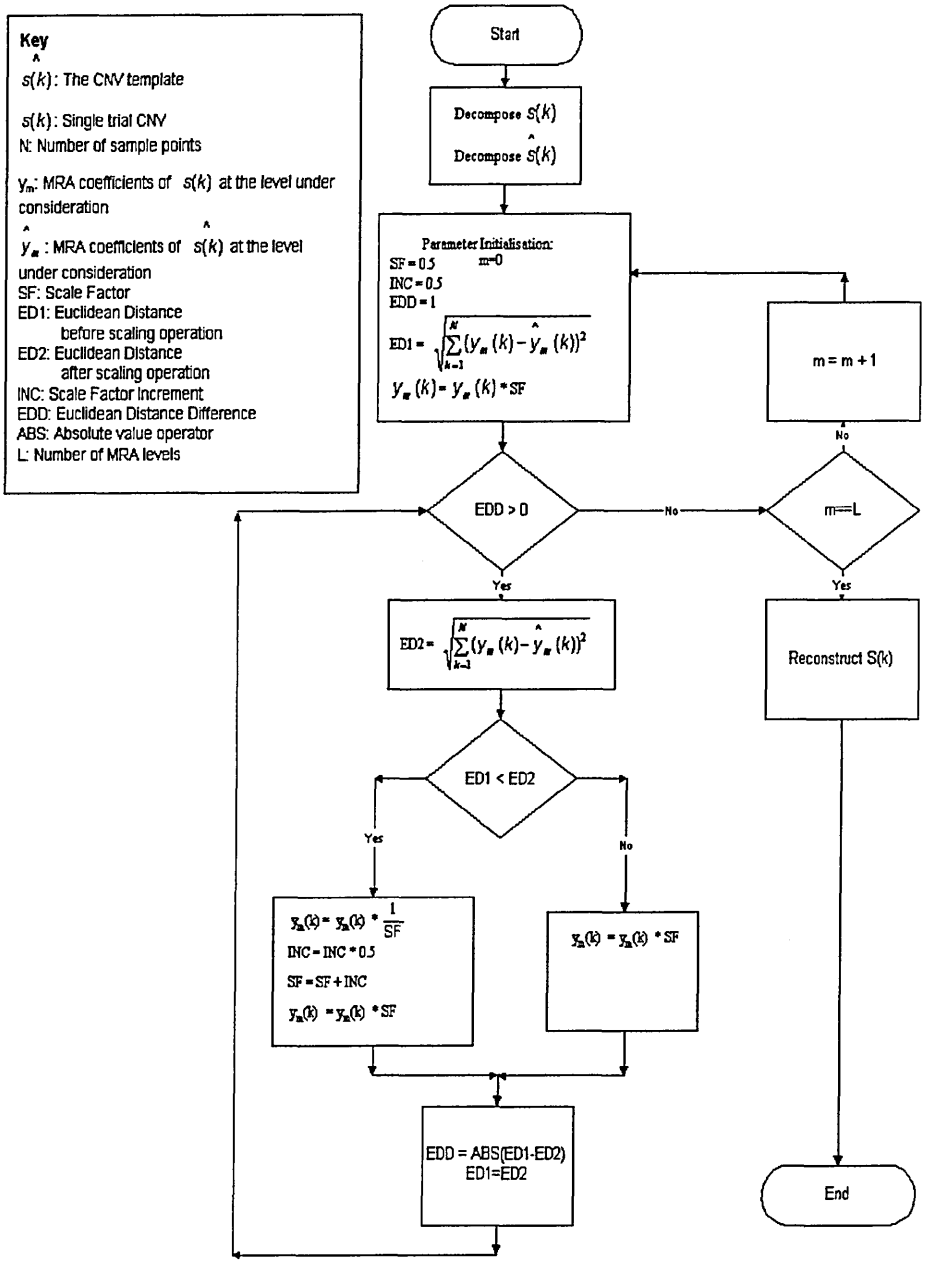

Figure 4.5: The adaptive filtering algorithm

wavelet coefficients were multiplied by the factor. The algorithm was repeated for the next section of the signal.

Following the application of the process to the whole signal, the single trial waveform was reconstructed using the scaled wavelet coefficients. The use of this sectioning technique introduced small discontinuities in the recovered waveform. A subsequent processing step was used to reduce these unwanted, and artificially introduced, features. This was achieved by linear rotation of each 8 point section to coincide with the first point of the following section as depicted in Fig.4.6.

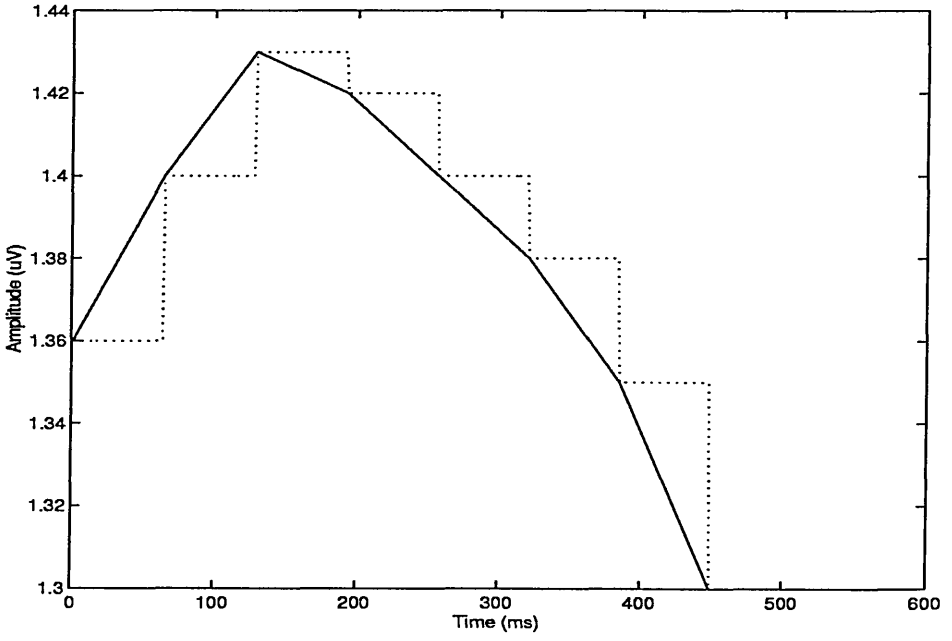

Figure 4.6: The linear rotation technique to remove discontinuities. The dotted line depicts the original signal. The solid line is produced as a result of applying the rotation technique

The resulting estimated single trial had an improved SNR. The filtering process had significantly reduced the background EEG but trial specific detail was maintained.

4.4.2 Analysis of the Effectiveness of the Filtering Technique

The use of simulated rather than recorded CNV waveforms enabled the effectiveness of the method to be quantified. As discussed above, the aim of the filtering algorithm was to improve the signal-to-noise ratio of single trials whilst maintaining trial specific features. The evaluation of the filtering algorithm was based on a comparison of two parameters, the noise factor improvement and signal distortion. Noise factor improvement was the ratio of SNR after filtering (SNR_p) to SNR before filtering (SNR_0). The value of $SNRo$ was computed using (4.1).

$$SNR_0 = \frac{\sum_{k=1}^{N} {S_k}^2}{\sum_{k=1}^{N} {n_k}^2} \tag{4.1}$$

where S, and n were samples of CNV model and the added background EEG respectively. The number of samples N was chosen to be 512 points. The signal-to-noise ratio after the application of the single trial recovery method (SNR_p) was determined using (4.2).

$$SNR_p = \frac{\sum_{k=1}^{N} {\hat{S}_k}^2}{\sum_{k=1}^{N} (\hat{S}_k - S_k)^2} \tag{4.2}$$

where $\hat{S}$ were samples of the recovered simulated single trial. The noise factor improvement was then calculated as the ratio of SNR_p to SNR_0 (4.3).

$$\text{Noise factor improvement} = \frac{SNR_p}{SNR_0} \tag{4.3}$$

The larger the value of the noise factor, the more effective the filtering operation.

The amount of signal distortion after filtering was estimated by comparing the Euclidean distances between the simulated CNV and that of recovered single trial (4.4).

$$\text{Distortion} = \sqrt{\sum_{k=1}^{N} (\hat{S}_k - S_k)^2} \tag{4.4}$$

The smaller the value of the distortion parameter, the closer the recoverd signal is to the desired signal.

For the wavelet analysis and synthesis filters used in this study, the effectiveness of three popular orthogonal filters, namely Daubechies, Coiflet (Coifman), and Symmlet were evaluated. A selection of wavelet basis functions are shown in Fig.4.7. Each filter or basis function can be implemented with a different number of coefficients. For Daubechies all even numbered coefficients between 2-20, for Coiflet 6,12,18,24, and 30 coefficients and for Symmlet all even coefficients between 8-20 were used. The values of the coefficients for these filters are available in reference [67].

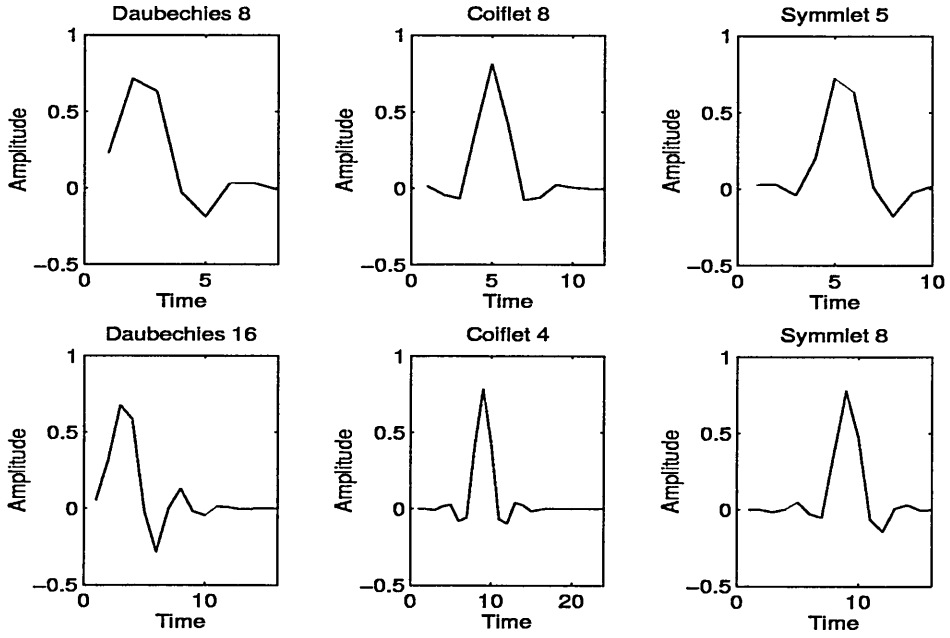

Figure 4.7: A selection of wavelet basis functions

4.5 Comparison of the Developed Method With Other Filtering Approaches

In producing the adaptive wavelet-based filtering technique, a number of decisions were made. These included the choice of transform, the choice of basis function and the method for coefficient scaling. The decisions made were based on the results obtained by comparing a range of alternatives at each stage of development. The effectiveness of the adaptive wavelet-based filtering technique developed in this study was compared with a number of other methods [104]. These methods were deterministic finite impulse response filters and two wavelet packet transform based approaches.

The method for evaluating a given technique was based on that discussed in section 4.4.1. A simulated ERP was produced. This waveform had similar characteristics to those expected from an averaged CNV in a normal subject. Real EEG was added to this ERP to produce a simulated single trial. The use of a simulated trial allowed the effectiveness of the filter to be quantified using measures of SNR improvement (equation 4.3) and distortion (equation 4.4).

To reduce the effect that the characteristics of the simulated single trial may have on a given filtering technique, three different simulated trials were used. Each technique considered was used to filter each of the three trials. An average of the three calculated values was used on an estimate of the performance of each technique.

Lowpass finite impulse response (FIR) filters with 21 coefficients were also used to process single trials. The cutoff frequencies of the filters ranged from 3.1 Hz to 19.2 Hz. The performance of the FIR filtering method was quantified using the measures described.

The wavelet packet transform was used to decompose the single trials. A number of basis functions were compared. Following transformation, the desired basis tree, that spans the overcomplete wavelet packet table, was selected. Two such basis trees were considered, the wavelet basis, which is the same as the discrete wavelet transform, and Wickerhauser's best basis [78], a popular basis designed primarily for signal compression.

For each basis tree a number of coefficients which best represented the waveform were

maintained whilst the remainder were set to zero prior to reconstruction. The number of coefficients to use when hard thresholding was determined experimentally. The number of coefficients needed to reconstruct the CNV model without visible distortion was found to be 30. After decomposition and the selection of the desired basis tree, the coefficients in that tree were sorted in magnitude order. The largest 30 coefficients were kept, the remainder were set to zero. (Bartnik *et al.*'s method [99] used only 5 coefficients resulting in what appeared to be a lowpass filtered estimation of the EP and hence most features were lost.)

Finally the best result from each method was compared with the developed adaptive filter. The traditional approach of synchronised averaging was used to provide a datum for comparison. Note that this is a technique currently employed to improve the signal-to-noise ratio of a number of trials but is not a method for single-trial recovery as such.

4.6 Results and Discussion

The results for the performance of the adaptive wavelet-based filtering algorithm developed in this study are included in this section. This is followed by the results of the comparative study of the developed technique with other filtering approaches.

4.6.1 Results for the Adaptive Algorithm

For each set of variables in the filter design, three single trials were processed and the average result was used for subsequent evaluation. Considering the noise factor improvement and distortion, Daubechies filter with 16 coefficients yielded the best results (Table.4.1). However in all cases, the magnitude of the noise factor improvement was approximately 3 and the amount of distortion was around 1.8×10^{-4}.

The Daubechies 16 wavelet basis function was therefore chosen for subsequent analysis and processing of real CNV waveforms. The results for the application of the algorithm to two simulated single trials is shown in Fig.4.8. The average of 32 simulated single trials is shown in Fig.4.8 **a** and **b** for comparison. The two simulated single trials are shown in **c** and **d**. Note in particular, the noise artifact causing the negative deviation in the baseline EEG

Basis function	**Noise Factor Improvement**	**Distortion x 10^{-4}**
Daubechies 4	2.95	1.803
Daubechies 6	2.99	1.794
Daubechies 8	3.01	1.793
Daubechies 10	2.98	1.801
Daubechies 12	2.97	1.800
Daubechies 14	2.99	1.790
Daubechies 16	**3.01**	**1.789**
Daubechies 18	3.00	1.794
Daubechies 20	2.97	1.800
Coiflet 1	2.95	1.807
Coiflet 2	2.99	1.793
Coiflet 3	2.99	1.792
Coiflet 4	3.00	1.789
Coiflet 5	2.99	1.791
Symmlet 4	2.97	1.799
Symmlet 5	3.00	1.794
Symmlet 6	2.98	1.796
Symmlet 7	2.97	1.800
Symmlet 8	2.99	1.789
Symmlet 9	2.98	1.800
Symmlet 10	2.98	1.792

Table 4.1: Comparison of Basis functions for adaptive wavelet transform based filtering of ERPs. Note that the similarity of the values suggest that choice of basis function is not significant for the filtering application.

before the presentation of the first stimulus at time 0. The results of applying the adaptive filtering algorithm, to the trials shown in **c** and **d** is shown in **e** and **f** respectively. Note that a large amount of background EEG has been removed leaving some ERP detail.

The technique was then applied to the estimation of real single-trial CNV waveforms. Fig.4.9 **a** and **b** show a subject averaged CNV waveform which was used as the template. Fig.4.9 **c** shows a single trial CNV waveform recorded from the same person. Fig.4.9 **d** shows a contaminated (artifact immediately before the first stimulus) single trial CNV waveform recorded from the same person. The result of the adaptive wavelet-based filtering algorithm when applied to these single trial CNV waveforms are shown in Fig.4.9 **e** and **f** respectively. The background EEG is significantly attenuated while the waveform's details are mainly preserved.

Plots of six single trial CNVs, their recovered waveforms and the subject average are shown superimposed in Fig.4.10. From Fig.4.10 it can be seen that for each trial, the recovered waveform (shown in black) is more similar to the averaged ERP (shown in blue) than the original trial (shown in red). Most trial specific details are maintained particularly around the auditory evoked potentials (AEPs) following stimuli presentation at 0 and 1 seconds. It can also be seen that the application of the algorithm maintains the amplitude of those single trials which are larger than the average.

When the above analysis was repeated using the CNV grand average, produced from 20 normal subjects each consisting of 32 trials, as the template, the recovered single trial CNV waveform was not significantly different from that shown in Fig.4.10.

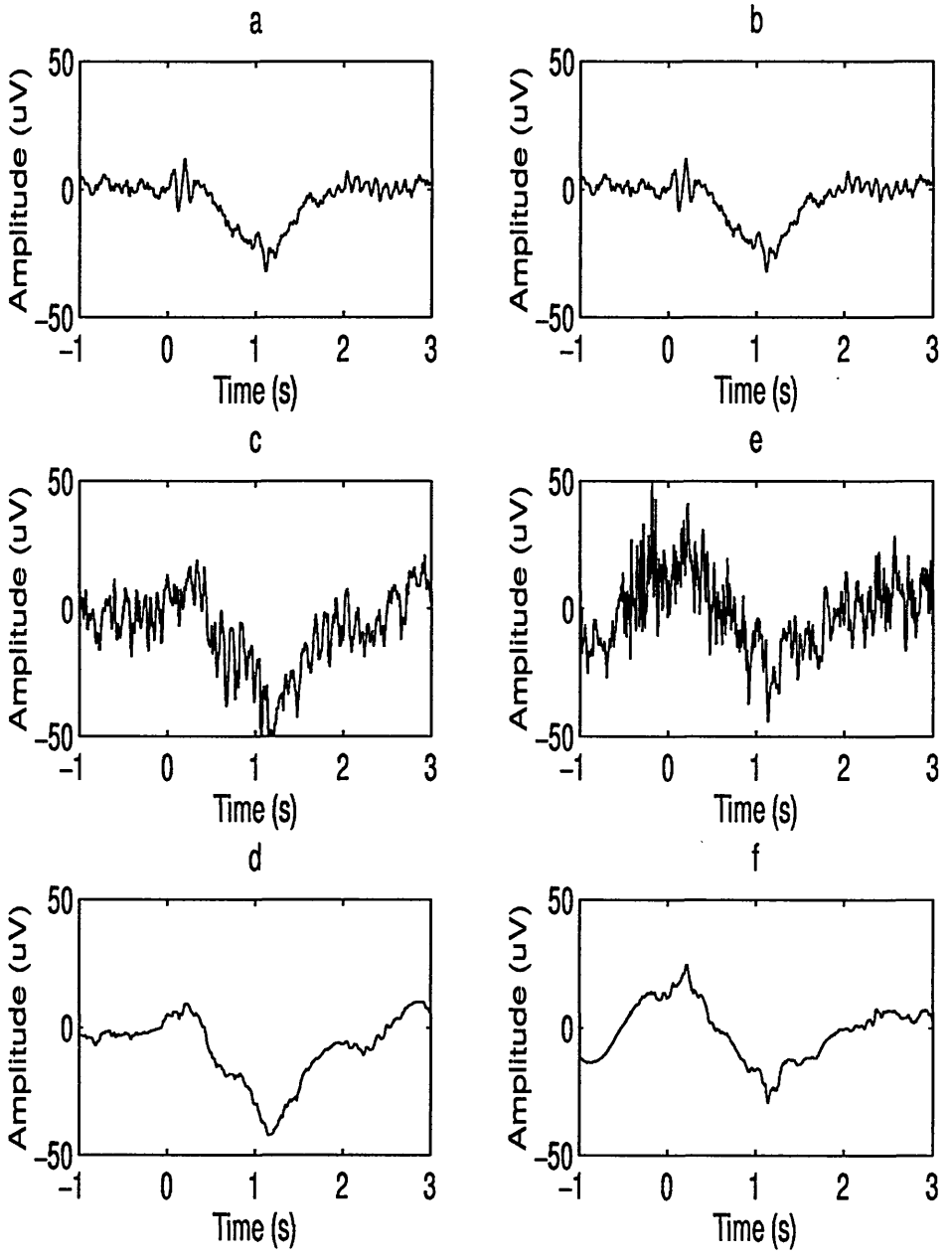

Figure 4.8: **a** and **b** show the average of 32 simulated trials, **c** and **d** are simulated single trials, **e** and **f** are the recovered simulated single trials of c and d respectively

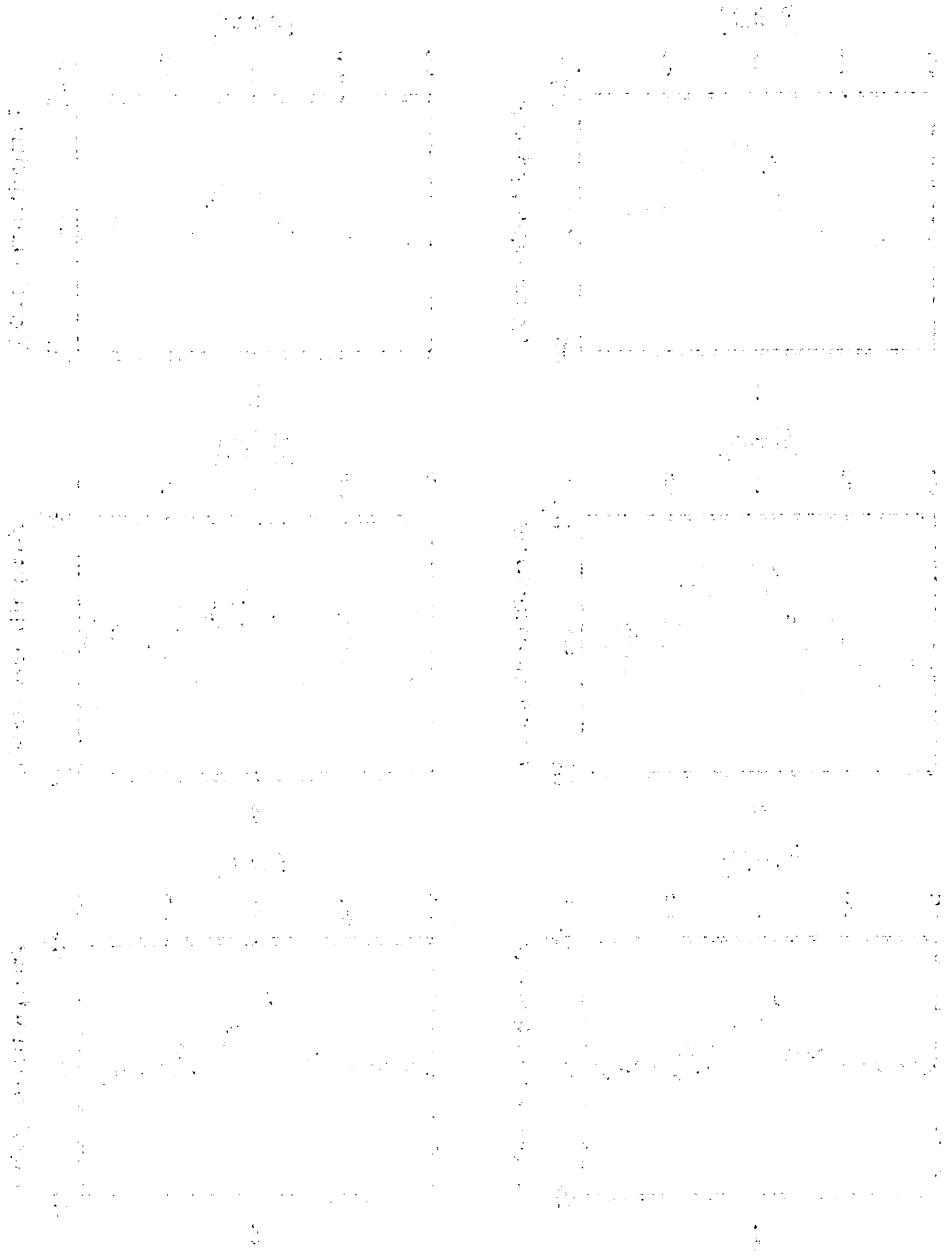

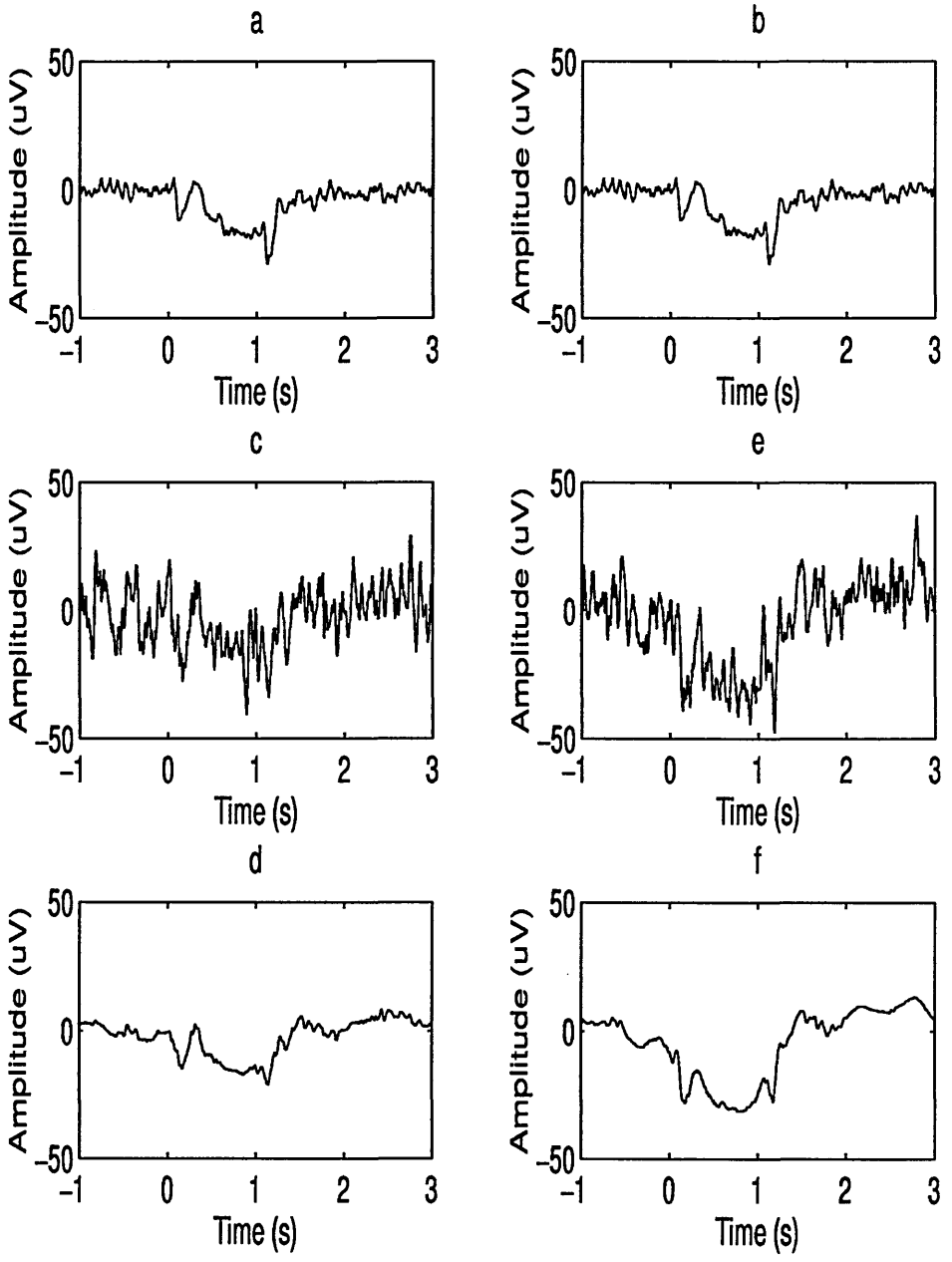

Figure 4.9: **a** and **b** show the average of 32 real trials from a normal subject, **c** and **d** are real single trials, **e** and **f** are the recovered real single trials of c and d respectively

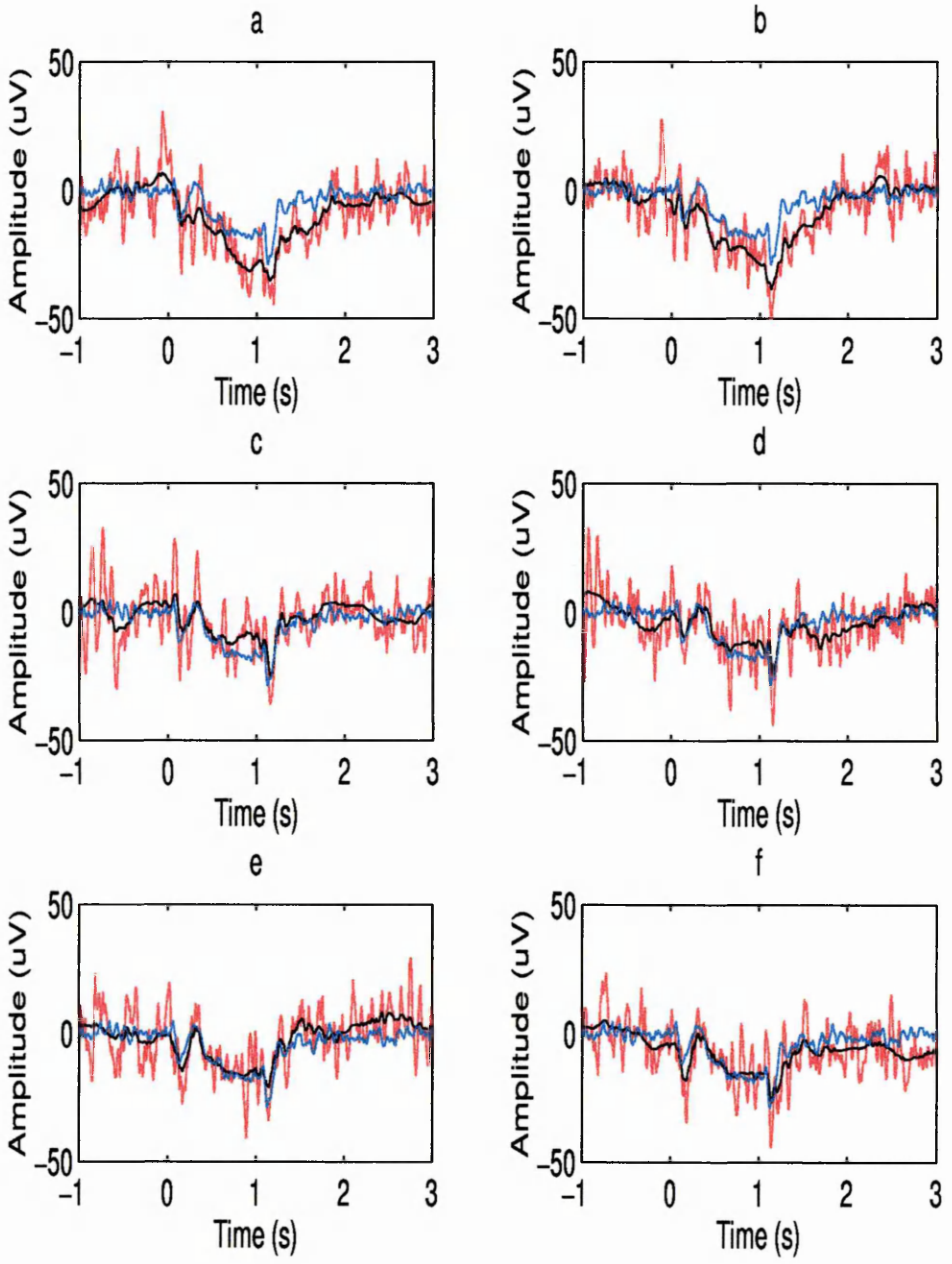

Figure 4.10: A number of recovered single trials recorded from a normal subject. The single trial is shown in red, the average of 32 trials is shown in blue and the recovered single trial is shown in black

4.6.2 Results for the Comparative Study of Wavelet-Based Filtering Approaches

A deterministic filtering approach using a number of 21 tap finite impulse response filters was included for comparison. The results are summarised in Table.4.2.

Cutoff Frequency	Noise Factor Improvement	Distortion $x10^{-4}$
3.1 Hz	**2.71**	**2.007**
6.2 Hz	2.65	2.053
12.4 Hz	2.43	2.230
19.2 Hz	2.30	2.357

Table 4.2: Comparison of FIR filtering of ERPs

From the table it can be seen that the best results were obtained using the lowest frequency range. The energy in a CNV waveform is concentrated in the lowest frequency components. The FIR results reflect this. An estimated simulated single trial produced by FIR lowpass filtering is depicted in Fig.4.11 **d**. The results for FIR lowpass filtering of a real CNV from a normal subject are shown in Fig.4.12 **d**.

It can be observed from both Table.4.2, Fig.4.12 **d** and Fig.4.11 **d** that almost all detail is lost (the filtered waveform is distorted) while a significant amount of background EEG reamins, when FIR filtering is employed.

The following wavelet basis functions were considered for wavelet packet based filtering using Wavelab [108]. Daubechies 2-20, Coiflet 1-5, and Symmlet 4-10. Two popular basis trees, the wavelet basis and Wickerhauser's best basis, were investigated. The results are summarised in the Tables 4.3 and 4.4. The wavelet basis is summarised in Table.4.3. The results employing Wickerhausers best basis are included in Table.4.4.

The average noise factor and distortion did not vary significantly between choice of basis functions. The best result for the thresholding approach for both basis trees considered was used as a representative for the evaluation of that technique. Following reconstruction, the

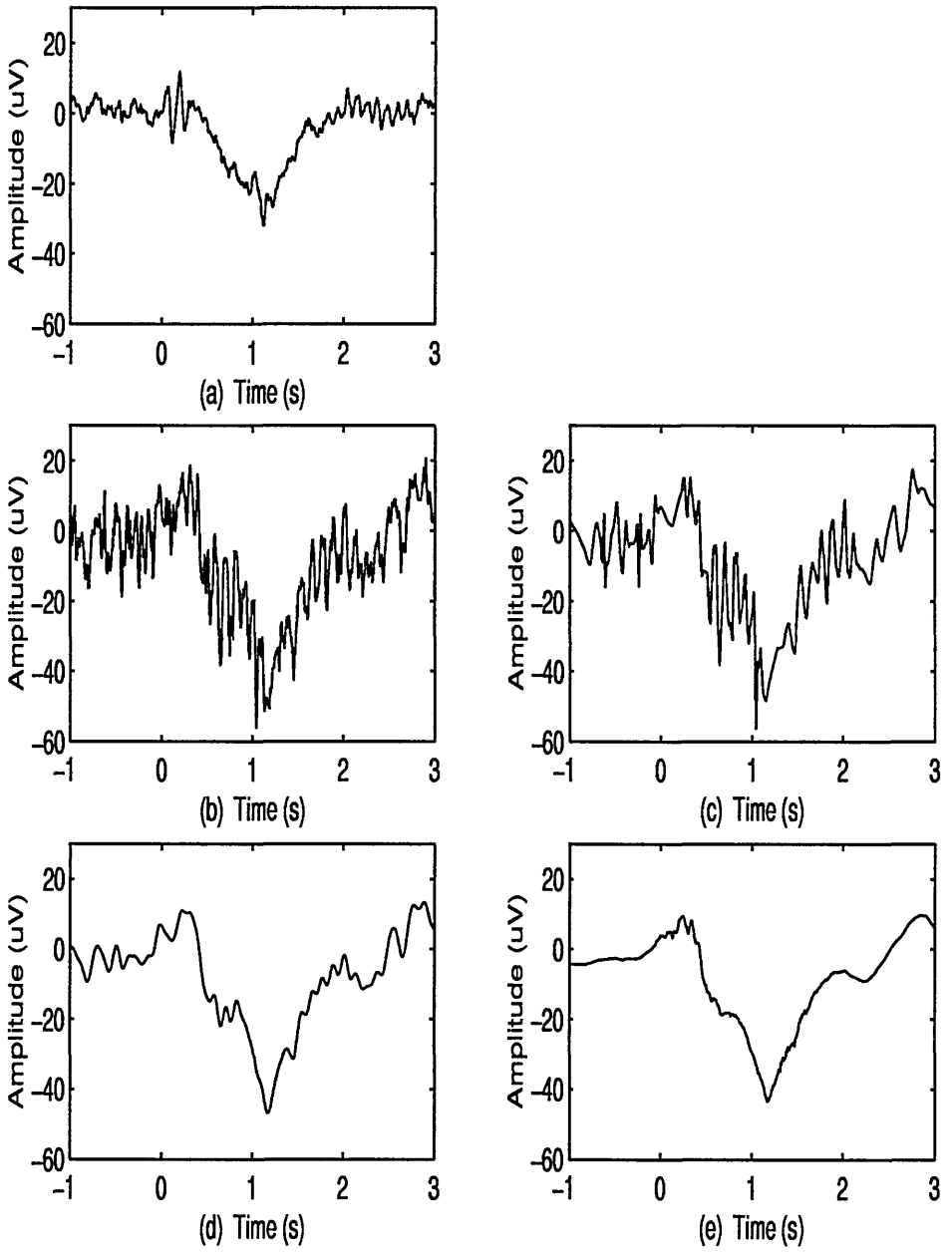

Figure 4.11: A Summary of Single trial recovery methods for a simulated ERP: **a** is the average of 32 simulated trials, **b** is a simulated single trial, **c** is the recovered waveform of **b** using the 30 largest wavelet coefficients of the best basis, **d** is the FIR lowpass filtered vesrion of **b** and **e** is the adaptive wavelet-based filtered version.

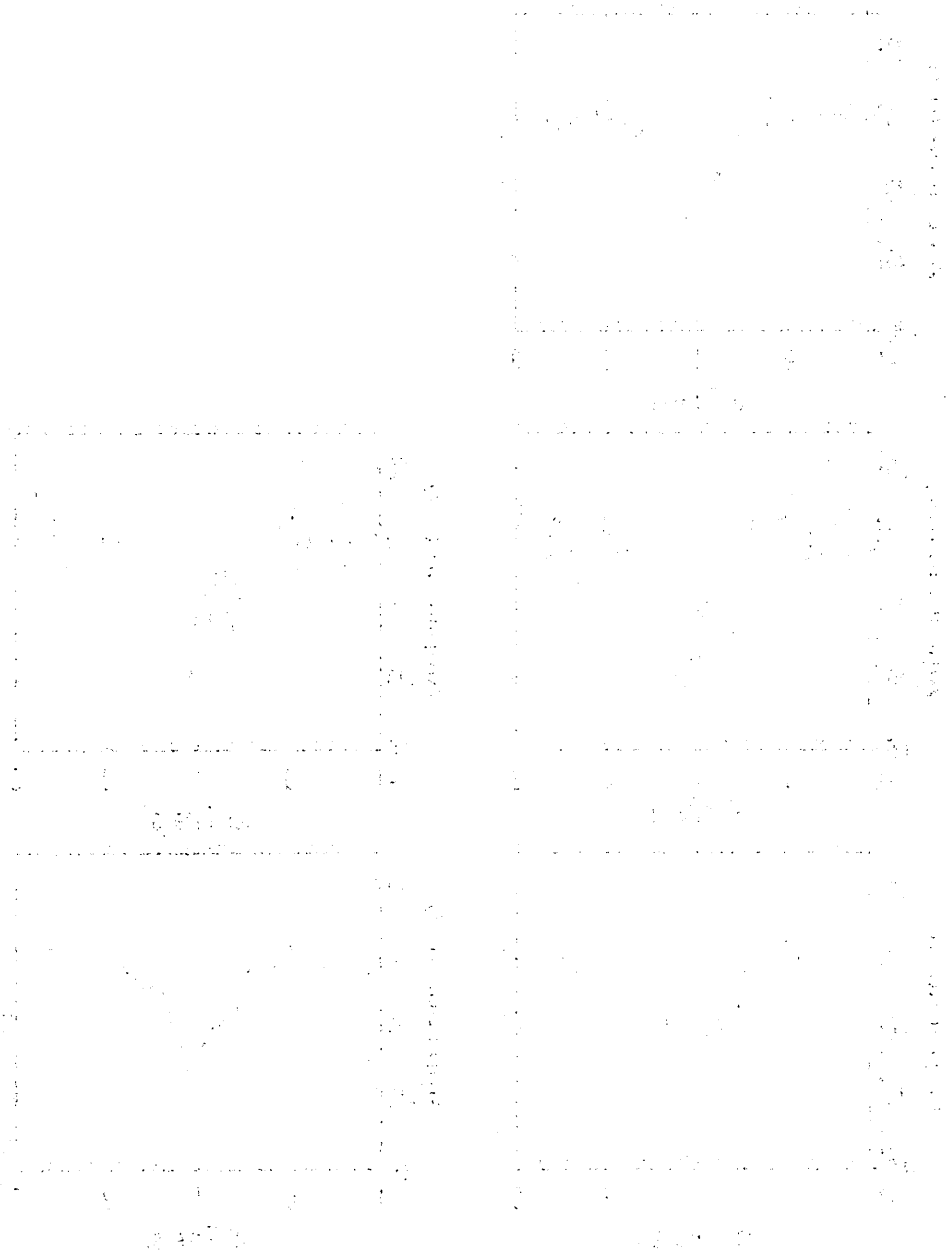

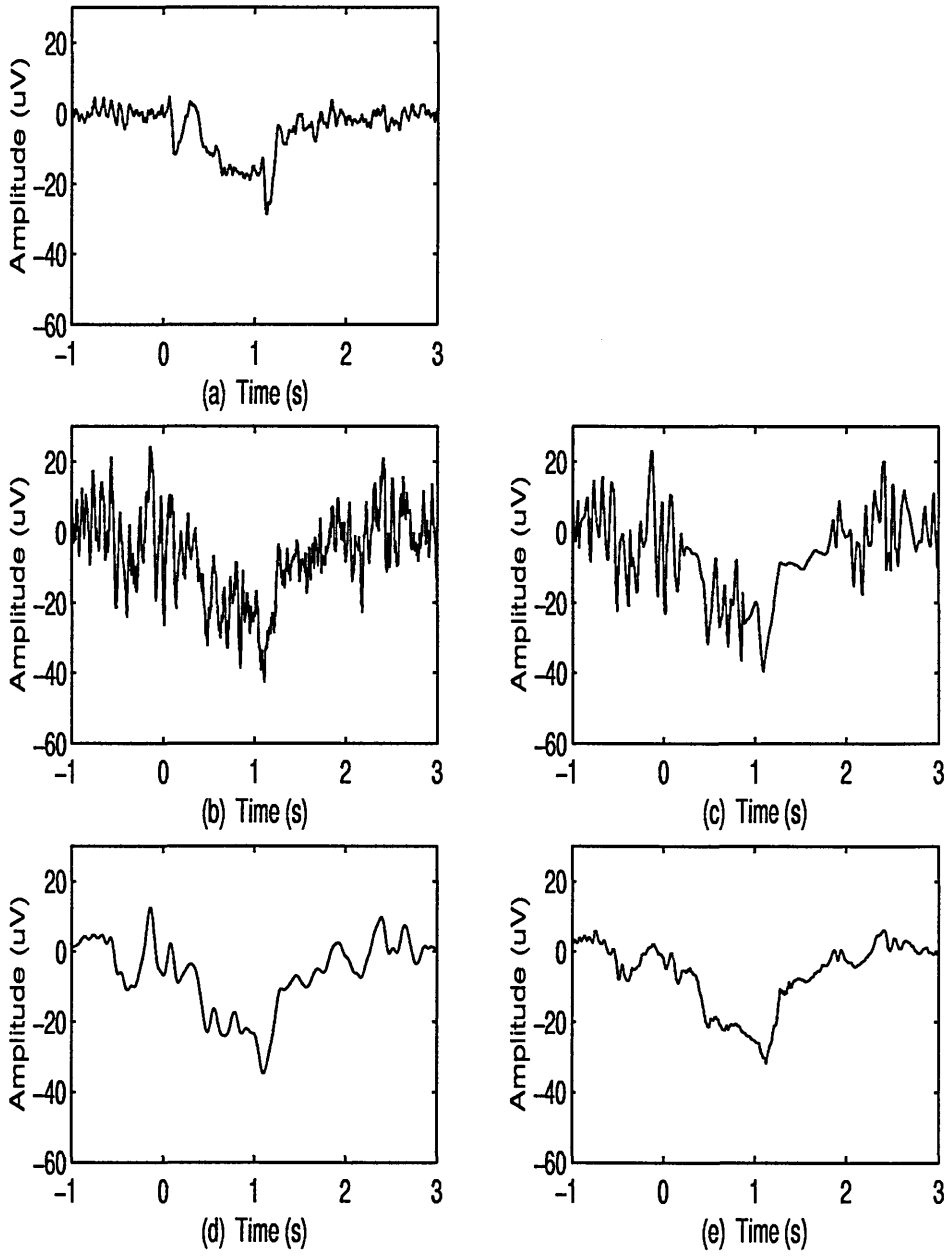

Figure 4.12: A Summary of Single trial recovery methods for a real CNV: **a** is the average of 32 single trials from a normal subject, **b** is a single trial, **c** is the recovered waveform of **b** using the 30 largest wavelet coefficients of the best basis, **d** is the FIR lowpass filtered vesrion of **b** and **e** is the adaptive wavelet-based filtered version.

Basis function	**Noise Factor Improvement**	**Distortion x 10^{-4}**
Daubechies 4	2.29	2.341
Daubechies 6	2.29	2.353
Daubechies 8	2.28	2.370
Daubechies 10	2.30	2.358
Daubechies 12	2.30	2.350
Daubechies 14	2.33	2.347
Daubechies 16	2.31	2.366
Daubechies 18	2.33	2.354
Daubechies 20	2.31	2.35
Coiflet 1	2.32	2.328
Coiflet 2	2.33	2.336
Coiflet 3	2.33	2.329
Coiflet 4	2.30	2.366
Coiflet 5	2.29	2.359
Symmlet 4	**2.36**	**2.315**
Symmlet 5	2.35	2.314
Symmlet 6	2.33	2.341
Symmlet 7	2.31	2.348
Symmlet 8	2.32	2.354
Symmlet 9	2.32	2.338
Symmlet 10	2.35	2.327

Table 4.3: Comparison of basis functions employed for wavelet packet based filtering of ERPs using the wavelet basis. Note that the similarity of the values suggest that choice of basis function is not significant for the filtering application.

Basis function	**Noise Factor Improvement**	**Distortion x 10^{-4}**
Daubechies 4	2.25	2.404
Daubechies 6	2.27	2.389
Daubechies 8	2.26	2.428
Daubechies 10	2.28	2.397
Daubechies 12	2.22	2.440
Daubechies 14	2.31	2.385
Daubechies 16	2.26	2.421
Daubechies 18	2.25	2.408
Daubechies 20	2.28	2.380
Coiflet 1	**2.31**	**2.376**
Coiflet 2	2.27	2.396
Coiflet 3	2.28	2.400
Coiflet 4	2.29	2.394
Coiflet 5	2.28	2.400
Symmlet 4	2.25	2.413
Symmlet 5	2.28	2.390
Symmlet 6	2.27	2.408
Symmlet 7	2.28	2.397
Symmlet 8	2.27	2.411
Symmlet 9	2.29	2.400
Symmlet 10	2.29	2.394

Table 4.4: Comparison of basis functions employed for wavelet packet based filtering of ERPs using Wickerhauser's best basis. Note that the similarity of the values suggest that choice of basis function is not significant for the filtering application.

Filter Method	**Noise Factor Improvement**	**Percentage Improvement**	**Distortion x10^{-4}**	**Percentage Improvement**
Synchronised Average	17.36	100	58.7	100
FIR Lowpass 3.1 Hz Cutoff	2.71	15.6	2.007	342
Coiflet 1 (Best basis)	2.31	13.3	2.376	405
Symmlet 4 (Wavelet basis)	2.36	13.6	2.315	394
Daubechies 16 (Adaptive scaling)	**3.01**	**17.4**	**1.789**	**305**

Table 4.5: Summary of single trial ERP filtering methods

signal is an estimate of the original 'noisy' waveform (Fig.4.11 **c** and Fig.4.12 **c** for simulated and real ERPs respectively). The measures of performance reflect this effect.

The best result for each of the approaches considered was used as a representative of that method for comparison in Table.4.5.

From the Table.4.5 it can be seen that the hard thresholding approach to coefficient attenuation in the wavelet domain leads to a lower performance than that of the FIR filtering approach. Some noise components were represented by large magnitude coefficients in the wavelet domain. The selection of coefficients to keep is based on magnitude and hence does not discriminate between signal detail and noise. In this study, the choice of basis tree appeared not to be very significant. The use of the WT as opposed to the overcomplete (redundant) WPT improved the speed of computation because transform calculated only the time-scale bins that were considered.

4.7 Conclusion

A novel adaptive wavelet-based filtering algorithm was developed and was used for the single trial recovery of a cognitive cortical event-related potential (ERP) known as the contingent negative variation (CNV). A method for evaluating its effectiveness was devised and was used to select the most suitable orthogonal filter (basis function) for the process. It was demonstrated that the method can reduce the background EEG by a factor of 3 while preserving the main features of the CNV waveform.

The adaptive wavelet-based filtering algorithm was compared with a number of similar techniques. The traditional approach of synchronised averaging was used to provide a datum for comparison. A filtering approach based on the wavelet packet transform was also explored. A range of filters and basis trees spanning the wavelet packet table were evaluated.

The results obtained suggested that the choice of basis tree appears not to be very significant. The use of the DWT as opposed to the overcomplete, hence redundant, WPT improved the speed of decomposition. The coefficient scaling method chosen had the most impact on the effectiveness of the filter. The results demonstrated that the developed adaptive DWT based approach was the most effective technique considered.

Chapter 5

Investigation of the Trend of CNV Trial-To-Trial Variation in Schizophrenic Subjects

5.1 Chapter Summary

In this chapter, the study of the trend in trial-to-trial variation of the contingent negative variation (CNV) in schizophrenic subjects is covered. The adaptive wavelet-based filtering algorithm, developed in this study, was used to improve the signal-to-noise ration (SNR) of single trial CNVs from both schizophrenic and matched normal control subjects. An estimate of the power of the negative variation for each trial was obtained. This feature was used to investigate the group trend in CNV trial-to-trial variation. The feature was then used by a Kohonen artificial neural network to classify subject categories based on the trial-to-trial variation infomation.

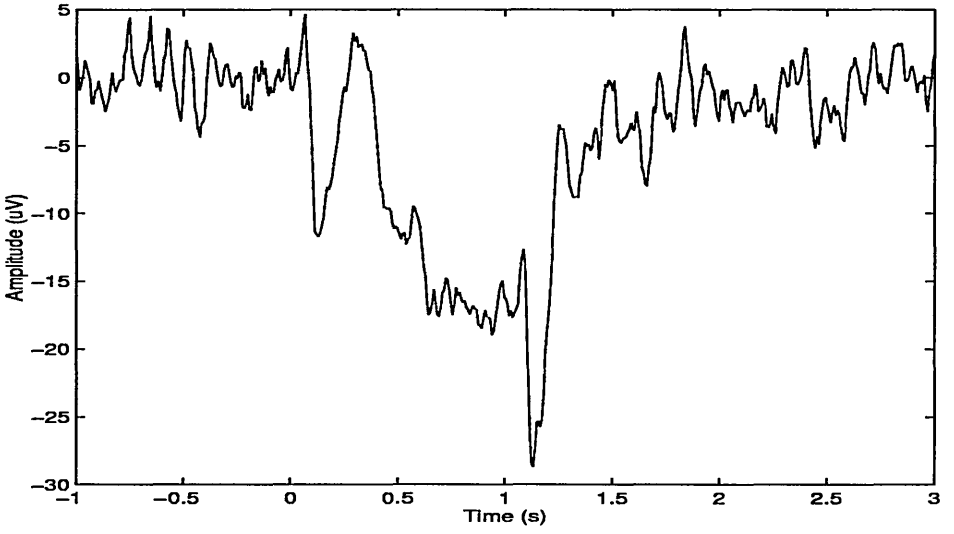

Figure 5.1: A CNV produced as an average of 32 single trials recorded from a normal subject

5.2 Introduction

The contingent negative variation (CNV) is a slow negative potential that develops in the interval between a warning and an imperative stimulus to which a motor response is required in the form of a hand-held button press [28]. As the name suggests, this ERP largely consists of a negative voltage shift in the baseline of the EEG in anticipation of the imperative stimulus (Fig.5.1).

The inter-stimulus interval (ISI) is the section of the CNV between the two stimuli. It is during this time that the CNV is observed.

Various factors effect the magnitude of the CNV [110]. For example omitting the requirement for a motor response to the second stimulus, distraction and age all reduce its magnitude. Attention to task is also related to the CNV magnitude immediately prior to the second stimulus [23]. The attention-arousal model for CNV magnitude changes [110] shows a linear relationship between magnitude and attention (i.e. The magnitude of the CNV increases with an increase in subject attention.) and a non monotonic (inverted U) relationship between magnitude and arousal. (i.e. The magnitude of the CNV initially increases with an increase in subject arousal until a maximal magnitude peak is reached. Any subsequent

increase in arousal results in a decrease in CNV magnitude until at very high levels of subject arousal no CNV is observed.) The CNV increases with conditioning in the early stages and decreasing with inattention and boredom [111]. Hillyard [29] reported that the CNV development period was approximately 10 trials. That is the trial number at which the CNV magnitude ceases to increase any further.

Schizophrenia is a mental illness afflicting about 1% of the population worldwide [113]. The illness presents itself via a diverse range of symptoms including hallucinations and delusions, not all of which need to be present in each subject [114]. Structural abnormalities are known to exist in the brains of schizophrenic subjects [115]. The relationship between abnormalities in ERPs and cognitive impairment in patients has been suggested [116]. The CNV is known to have a generally reduced magnitude in schizophrenic subjects [109][38]. The magnitude of the CNV is thought to reflect the degree of psychotic symptoms in acute schizophrenics. That is the more severe the condition, the smaller the CNV [5]. The reduced CNV amplitude is present in the averaged waveform. There are a number of hypotheses as to the reason for the CNV reduced amplitude in the averaged waveforms. These include:

- an actual reduced amplitude produced by neural subsystems employed during the task [117].
- an increased jitter (relative misalignment of successive trials) in the individual trials resulting in reduced peak amplitude following time domain averaging [112].

The analysis of single trials allows these hypotheses to be considered.

In a previous study [118] in which averaged CNVs were used to investigate the detection of Schzophrenia and othere mental illness, no work on single trial analysis was carried out.

The focus of this work is the understanding of single trial event-related potentials. The aim of this study was to investigate the trend in trial-to-trial variation of CNVs in both normal and schizophrenic subjects with a view to demonstrating that the CNV trial-to-trial variation in normal and schizophrenic subjects is significantly different and that the observed differences may be used to discriminate schizophrenic subjects.

5.3 Experimental Method

32 CNV single trial waveforms, recorded from 20 medicated schizophrenics and their age and sex matched normal control subjects, were analysed. Full subject details including the severity of subjects symptoms and type and dosage of mediaction is provided in [34]. Previous studies [118] have shown that medication does not effect the CNV significantly. The analysis of the effects of any medication on the results have therefore not been investigated in this study.

The group average trial-to-trial variation was first investigated. This allowed the identification of gross trends within the two subject categories. For all normal subjects, the trials were averaged across trial number e.g. the average of trial 1 across normal subjects. Each subsequent set of trials where processed in a similar way until all 32 trials had been averaged. The process was repeated for schizophrenic subjects.

To enable the CNV trial-to-trial variation to be investigated for each individual subject and to facilitate subsequent categorisation, an estimate of each single trial ERP was required. The adaptive wavelet-based filtering algorithm (Chapter 5 [105]) was used to estimate each of the 32 single trials recorded from the 40 subjects under consideration. That is, the individual CNV trials were recovered from the background EEG. Full details of the subjects, the recording system and procedure are provided in [118].

The CNV amplitude, the main feature in the CNV, was the focus for classification. This measure has been successfully used in other studies [34] for the classification of schizophrenic subjects.

To represent the inter-stimulus interval (ISI) by a suitable parameter, the power of a section of the CNV from the ISI was calculated. The ISI covers the 1 second period from the presentation of the first stimulus until the occurrence of the second stimulus. The first 300 ms section of the ISI contains the auditory evoked potential (AEP) produced in response to the first stimulus and contains no relevant cognitive components. The 64 sample values (corresponding to 0.5 s section of the ERP prior to the presentation of the imperative stimulus) were selected for analysis. This is the section in which the CNV amplitude is generally maximal and since it is immediately prior to the imperative stimulus it contains

cognitive information relating to attention. The section's power (P) was computed using equation 5.1.

$$P = \sum_{k=187}^{250} {S_k}^2 \tag{5.1}$$

where S_k represented the samples of the section of each CNV signal (note, the section of interest included sample numbers 187 to 250 inclusive). As 32 trials were recorded from each subject, this operation produced 32 values representing a measure of the CNV trial-to-trial variations for each subject.

Even after the application of the wavelet-based adaptive filtering the estimated single trials CNVs contained some residual background EEG. This resulted in unnaceptable fluctuations in the trial-to-trial variation of each subject. The trial-to-trial variation was therefore characterised by its trend. This was achieved by fitting a polynomial to the 32 CNV power values. Several different polynomials were considered but a 5th-order polynomial was finally chosen heuristically.

A type of artificial neural network known as the Kohonen self organising feature map [83] was used to detect possible clusters formed as a result of similar CNV trial-to-trial patterns.

The Kohonen map used had a square topology as shown in Fig.5.2. The parameters for network learning (as suggested by Haykin [82]) were as follows,

The network weights were initialised to random values between 0.45 and 0.55. During the first 10000 iterations, the learning rate was reduced linearly from 0.4 to 0.1 and the neighbourhood size was reduced from 5 to 1. Then the learning rate was reduced linearly from 0.1 to 0.01 over another 20000 iterations and the neighbourhood size was set to zero. In updating the weights for the neurons in the neighbourhood region, their topological distance to the winning neuron was taken into account [82]. The weights of the neurons closer to the winning node were updated more strongly as compared with those further away. This was achieved by using a Gaussian function described as,

$$f(d,n) = e^{-(\frac{d^2}{2n^2})} \tag{5.2}$$

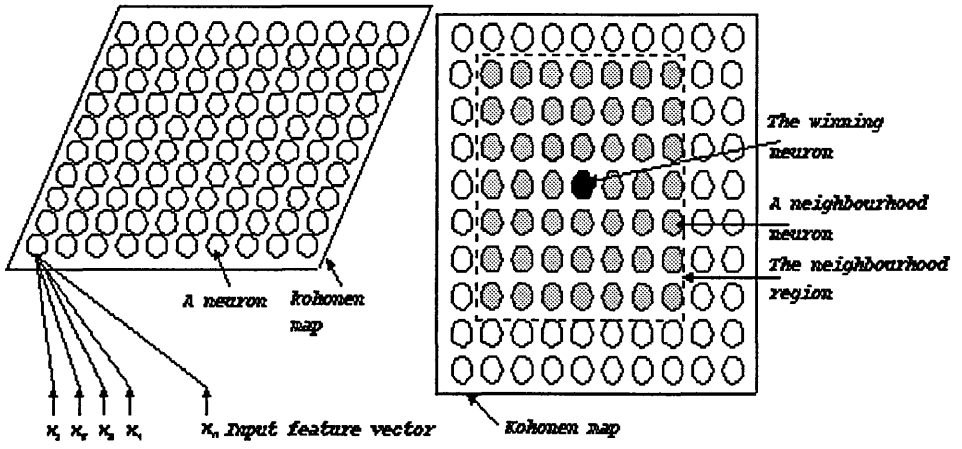

Figure 5.2: The topology of the Kohonen self organising feature map

where, d represents the topological distance of a given node from the winning node and n is the size of the neighbourhood region.

To ensure any clustering is purely a representation of the trial-to-trial variations, the 32 data points of each polynomial were normalised between 0 and 1. The polynomials could not be used directly as input to the Kohonen network as this would have resulted in clusters which represented both the magnitudes of the CNV waveforms as well as their trial-to-trial variations. Therefore the data used as input to the Kohonen network were 40 polynomials, each consisting of 32 values, and normalised between 0 and 1.

5.4 Results and Discussion

The group average trial-to-trial variation is illustrated in Fig.5.3. This shows the category specific, gross trend in CNV development.

From Fig.5.3 it can be seen that there are differences between the average trial-to-trial

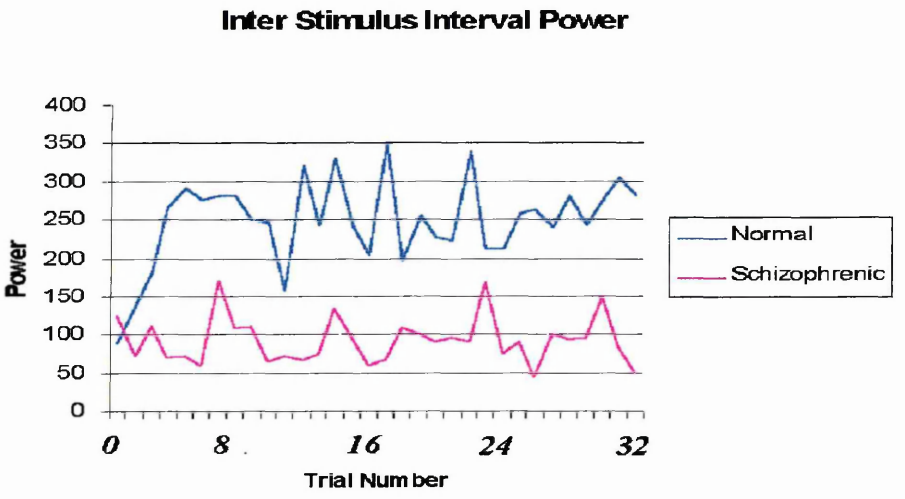

Figure 5.3: The average trial-to-trial variation of ISI power of 32 single trials averaged for normal and medicated schizophrenic subjects

variation in normal and schizophrenic subjects. In normal subjects, their was an increase in amplitude of the CNV over the first 6 trials before reaching a steady state. This gradual increase in amplitude may relate to novelty and habituation to task. It supports the CNV development period of 10 trials reported by Hillyard [29]. These systematic changes may be attributed to the alteration of the rate of post-synaptic summation in response generation pathways [7].

The trend in schizophrenic subjects is for a steady state in CNV amplitude. This may be a result of the effect of averaging a collection of randomly varying trials. The gross trends observed suggested that the groups may be separable based on the evolution of the CNV power over the increase in trial number. The analysis of individual trials was necessary for this purpose.

The general consistency of the patterns' trends during first 6 trials in normal subjects might be a reflection of a more orderly learning process and increasing attention in performing the required experimental tasks in that subject category. These findings indicate that the first 6 trials may be more informative in analysing the schizophrenics states than the remaining CNV trials.

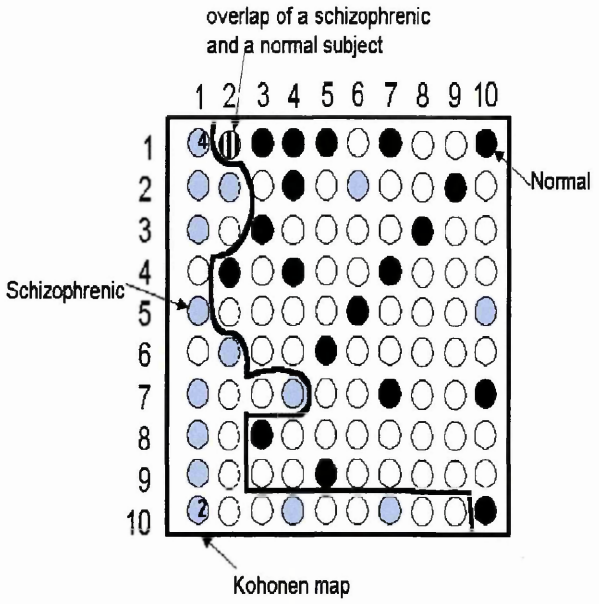

Figure 5.4: The Kohonen self organising feature map showing categorisation of normal and medicated schizophrenic subjects. The numbers 2 and 4 on circles in the left hand column show 2 and 4 overlapping normal subjects respectively.

The Kohonen map following training is shown in Fig.5.4. The numbers on the top and left hand sides of the map represent the neurons coordinates. The normal and schizophrenic subjects are represented by circles with different shadings.

As can be observed in Fig.5.4 the network identified two main clusters representing the two categories. The ability of the Kohonen network to form these clusters suggested that the CNV evolved significantly differently from one trial to the next in the two subject categories.

5.5 Conclusion

A study of contingent negative variation (CNV) trial-to-trial variation in 20 medicated schizophrenics and their normal control subjects was carried out. The results reported in this study are unique in that for the first time it was demonstrated that there is a significant difference between the CNV trial-to-trial variation in normal and schizophrenic subjects.

The findings of this study also indicated that the first 6 trials provide valuable information concerning the development of the CNV. It is known that the CNV amplitude is related to attention and task habituation. The early development of the CNV in normal subjects reflects these cognitive processes. In schizophrenic subjects however, the higher variation in the trend of CNV development may suggest a much less orderly approach to task habituation and may reflect difficulty in maintaining attention.

Using the Kohonen network, it was possible to differentiate the majority of schizophrenics from normal subjects on the basis of their CNV trial-to-trial variations. Early detection of schizophrenia is difficult. This study has provided another avenue to improve the understanding of the disorder and a novel approach for it's identification.

Chapter 6

Development and Application of a Phase Analysis Technique

6.1 Chapter Summary

In this chapter,[1] the phase dynamics of the brain relating to P300 ERP genesis in a visual spatial attention task are investigated. A new technique to visualise these dynamics was developed and applied. The technique focuses on the alpha band activity, in particular the event-related phase dynamics. Independent component analysis (ICA) was used to filter the recorded ERP's into spatially fixed, temporally independent components. The phase dynamics of a number of components were then investigated.

6.2 Introduction

The EEG activity within the 8-13 Hz frequency range is known as the alpha rhythm. It has been suggested that alpha rhythms may reflect a controlling mechanism of brain functions

[1]The work in this chapter was carried out whilst visiting the computational neurobiology laboratory of the Salk Institute at San Diego, California, USA.

[119]. They have recently been associated with cognitive processing in auditory P300s [127]. Despite a large number of functional correlates of the alpha rhythm the genesis of this EEG activity is not exactly known. It has been suggested that the rhythm may be produced by a number of distributed generators [64].

The most common and important model of EEG is that the activity at any instant is the algebraic sum of statistically independent signal and noise components [7]. This model has however been challenged on the grounds that the pre-stimulus EEG affects the subsequent EP [87].

The model may be classified further by the considering the spectral components of each signal generator. The spectrum of the EEG may be analysed using Fourier techniques. This allows the EEG to be separated into a number of components each having a specific frequency range [119]. For example the alpha band covers frequencies in the range 8-13 Hz whilst beta encompasses those frequencies between 17 and 30 Hz [56]. The spectral components produced by a generator (both signal and noise) may be controlled by both amplitude and phase modulation.

Pfurtscheller [55] introduced the terms event-related desynchronisation (ERD) and event-related synchronisation (ERS) to describe the amplitude attenuation of rhythmic components. The attenuation or blocking of rhythmic EEG components such as the alpha band is termed ERD. The result of event-related regionally induced oscillations which are not phase locked is termed ERS. The technique calculates the energy of a specific frequency band at each point in time from a number of scalp locations. Scalp maps show the relationship between coherent and incoherent regions in response to the task. The consideration of both the ERD and ERS produced in response to a task provides a measure of the dynamics of the brain.

A similar technique that considers the envelope of alpha activity is reported by Kaufman [50]. The technique uses the variation from the mean of bandpass filtered ERPs from several scalp locations. The results show location dependent alpha amplitude modulation.

The case for event-related phase reordering of harmonics which result in the observed ERP has been suggested by Basar [120] and Brandt [51] amongst others. This phase resetting or

locking of oscillations has been linked to temporary recruitment of disparate groups of neurons to perform a cognitive task [121][122]. The short-term synchronisation of topographical distinct regions of the brain has been proposed as a mechanism for learning [123].

The terms evoked and induced rhythms are commonly used to describe tightly or loosely phase coupled event-related oscillations respectively. [124]. Non phase-locked components are oscillations that are not synchronised with the moment of stimulus, although they may relate to information processing [17]. The averaging procedure employed in traditional ERP analysis focuses on phase-locked components. Non phase-locked components are attenuated by the process of averaging.

Jervis *et al.* [125] carried out an investigation to establish whether auditory evoked potentials are predominantly due to phase reordering of the background signal (EEG) or to an added signal. They showed that whilst both explanations produce a phase ordering their results were inconclusive in determining which model is the most valid.

Kolev and Yordanova [126] used a min/max approach to identify phase relationships. The phase of the bandpass filtered single-trial AEPs was quantised based on the time of occurrence of the wave extrema. That is, when do the minimum and maximum values occur. This resulted in a binary coded string which was then used in an averaging process of all trials to obtain a histogram of wave extrema occurrence. The technique was applied to the analysis of AEPs, in particular age-related differences in alpha phase-locking which were used to differentiate two age groups based on their phase response.

Brandt [51] also studied alpha phase dynamics in EPs. The phase resetting of both auditory and visual EPs were investigated. The methodology employed was similar to that of Kolev and Yordanova [126]. Each single trial was bandpass filtered between 8-13 Hz to extract the alpha band. The pre-stimulus peak to peak latency was measured to determine if the trial had relatively stable alpha characteristics and hence could be included in subsequent analysis. The phase angle at the time of stimulus was calculated using the latency difference between the stimulus and the pre-stimulus peak or trough of the waveform. Brandt showed the effect of pre-stimulus alpha amplitude and phase on the N1 in both auditory and visual EP components. The results concerning the dynamics of alpha components in the EEG showed partial phase resetting in EP morphology.

Due to the large amounts of data involved in ERP analysis, waveforms are typically summarised by averaging. The averaged data loses single trial information that is not phase locked to the stimulus. Phase in this context means the time of occurance of a feature (a peak for example) in a given single trial relative to the time of stimulus. The process of synchronised averaging maintains features that have the same polarity and time of occurance in the majority of individual trials. The same averaging process attenuates features that do not occur at the same point in time as that of the average. Hence, if a feature has a high variance in time of occurance amongst individual trials (the feature is not strongly phased locked to stimulus) then it will be severely attenuated (possibly lost) by the averaging process.

The desire for analysis of single trials has produced a number of techniques, some of which are discussed in this thesis.

A number of consecutive single trial ERPs can be combined to produce a two dimensional image in which the horizontal and vertical axis represent time and trial number respectively [128]. The amplitude of peaks in individual trials is portrayed by colour. The contribution of each single trial to the ensemble average is highlighted by this approach. To enhance trends in the image, is common to apply a moving average or low pass filter [129]. The image approach to visualisation and analysis of single trial ERPs may be extended by sorting the order of trials based on some experimental factor such as reaction time [59]. This ERP image facilitates the investigation of features such as those locked to response. Jung *et al.*[59] applied the ERP image technique to the activation of independent components produced by independent component analysis (ICA).

ICA is a spatial filtering technique that deconvolves linear mixtures of independent sources [18]. Makeig *et al.*[80] first reported the application of ICA to EEG analysis. It is known that topographically distinct regions of the brain are responsible for different processing tasks. For example the visual cortex, a large region located to the rear (posterior) of the brain, is responsible for vision. In the analysis of single trial event-related potentials the technique decomposes an ERP recorded from e scalp electrodes into c ($c \leq e$) spatially fixed electrophysiologic signal sources (components) whose activations are temporally independent.

Makeig *et al.*[130][89] applied ICA to the analysis of components of the P300 in a visual spatial attention task. Their work is explained first and then the work carried out in this

study follows from section 6.3.2 (Study Specific Experimental Method) onwards. For a group of ten normal subjects, ICA was used to spatially filter each subject's averaged ERPs into functionally independent components. Those components whose activations contributed most to the generation of the late positive complex or P300 where considered. The results of Makeig *et al.* are included and discussed here because they form the basis of the work carried out in this study. The same data were used in this study hence further details are provided in the experimental method section.

A plot of the six most significant components for the 10 subjects and their scalp projections is shown in Fig.6.1. The most significant ICA components were deemed to be those with the largest amplitude variance during the time period of interest. Those components of particular importance are those whose activations have a peak that corresponds both in time and polarity to peaks in the averaged ERP.

The plot shows the activation of a number of ICA components (in colour) along with the envelope of of the data (in black) over a period of 400ms. The envelope of the data represents the most negative and positive values for all channels at each instance in time [130].

The scalp maps show contours of equal potential that would result when the activation of the corresponding component are back projected (through the ICA mixing matrix) onto the sites of the recording electrodes. This allows the location of possible signal generators to be estimated.

It can be seen from Fig.6.1 that ICA identifies several components that contribute to the genesis of the P300 or late positive complex. In particular note the symmetrically lateral scalp maps of the n1l and n1r components. The activations of these components were found to be left and right visual field selective [130]. Along with the N1b component the two components contribute significantly to the genesis of the N1 peak that would be observable in the ensemble average.

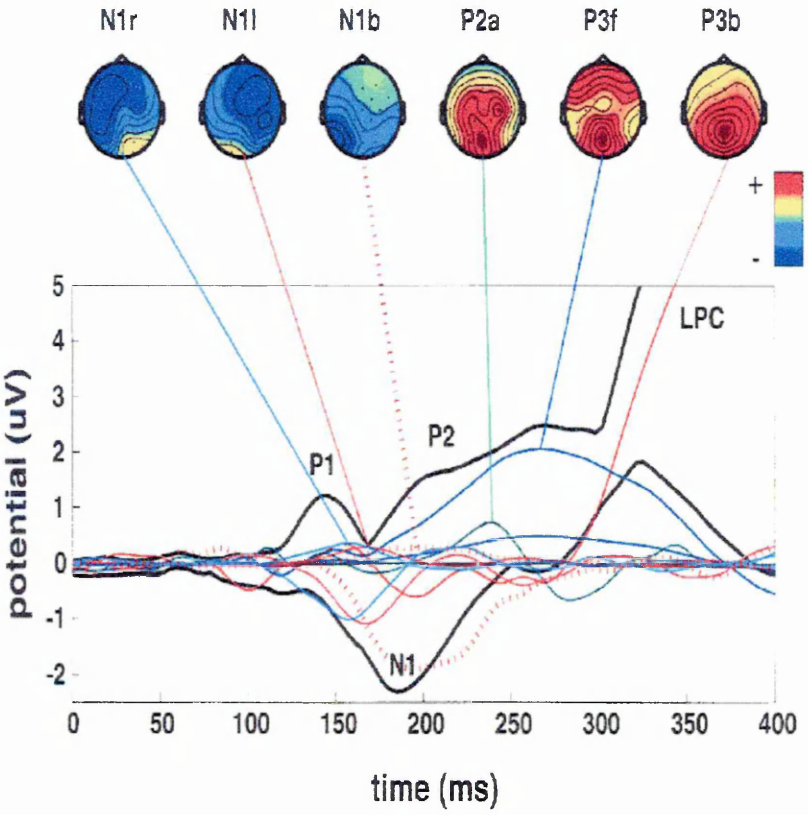

Figure 6.1: The six most significant ICA components in the genesis of the early components of the P300. Produced using the data from Makeig *et.al.*[130]

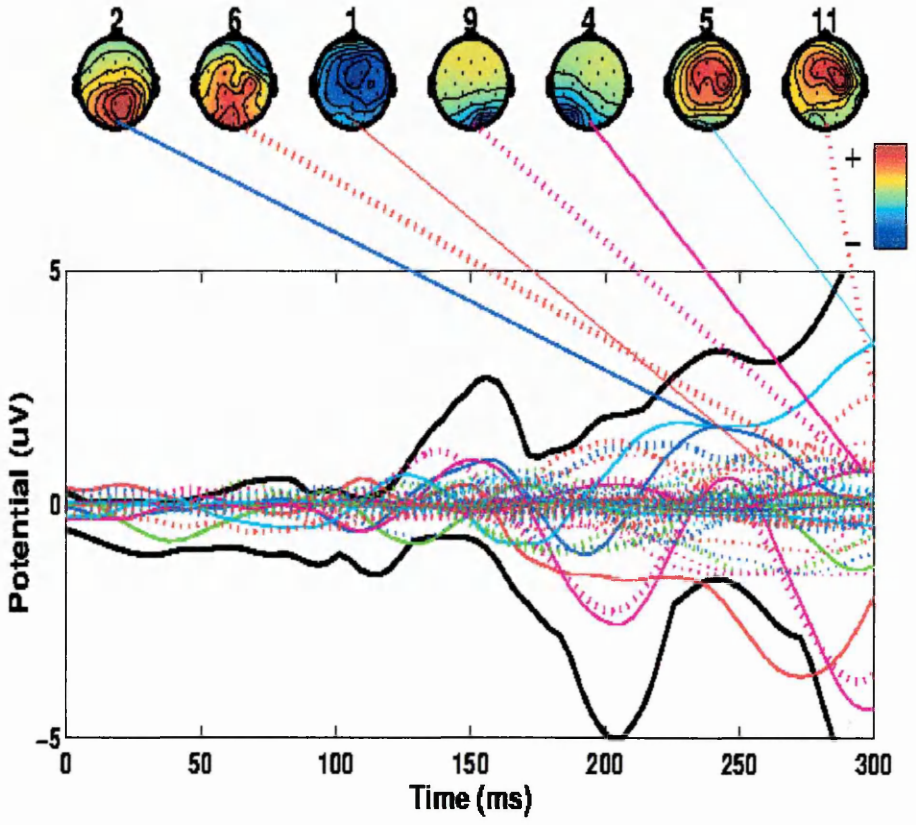

Figure 6.2: ICA Components of a single subject contributing N1 and P1

Independent component analysis was then applied to all trials of a single subject. A plot of the activations of the seven most significant components in terms of the generation of the N1 and P1 peaks for all tasks, and their scalp projections is shown in Fig.6.2.

Two components (number 4 and 9) observed in the single subject for all 512 trials exhibit similar scalp projections to those observed in the group average. The component responses to attended targets in the left and right visual fields were considered separately. The left visual field was considered to be targets appearing in the two leftmost boxes out of the possible five. Similarly the right visual field was considered to be the two right most targets. For attended targets (those to which the subject is to respond) appearing the the left hand

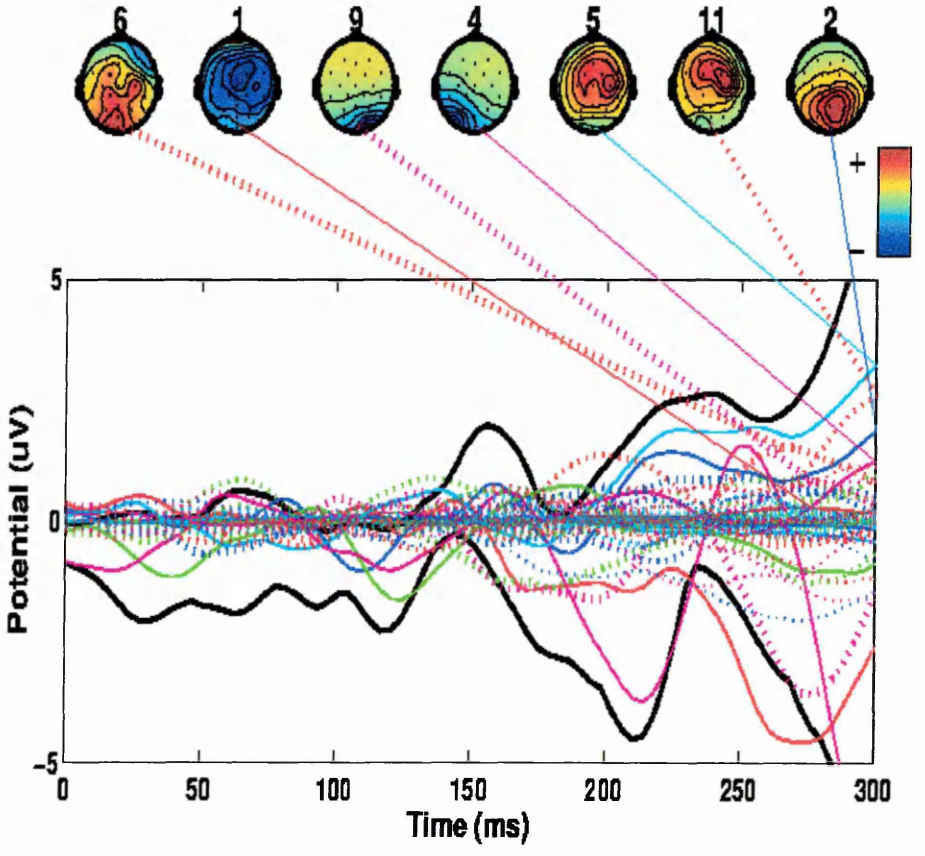

Figure 6.3: ICA components for targets in the left visual field

visual field it can be seen from Fig.6.3 that component 4 contributes most to the generation of the N1 peak whilst component 9's contribution is attenuated from that of all trials.

Conversely, for attended targets appearing the the right hand visual field it can be seen from Fig.6.4 that component 9 contributes most to the generation of the N1 peak whilst component 4's contribution is attenuated from that of all trials.

In this study a further investigation into the response and visual field selectivity of these components was carried out. A novel technique for analysing event-related phase dynamics was developed and applied to the activation of these components. Phase dynamics in this

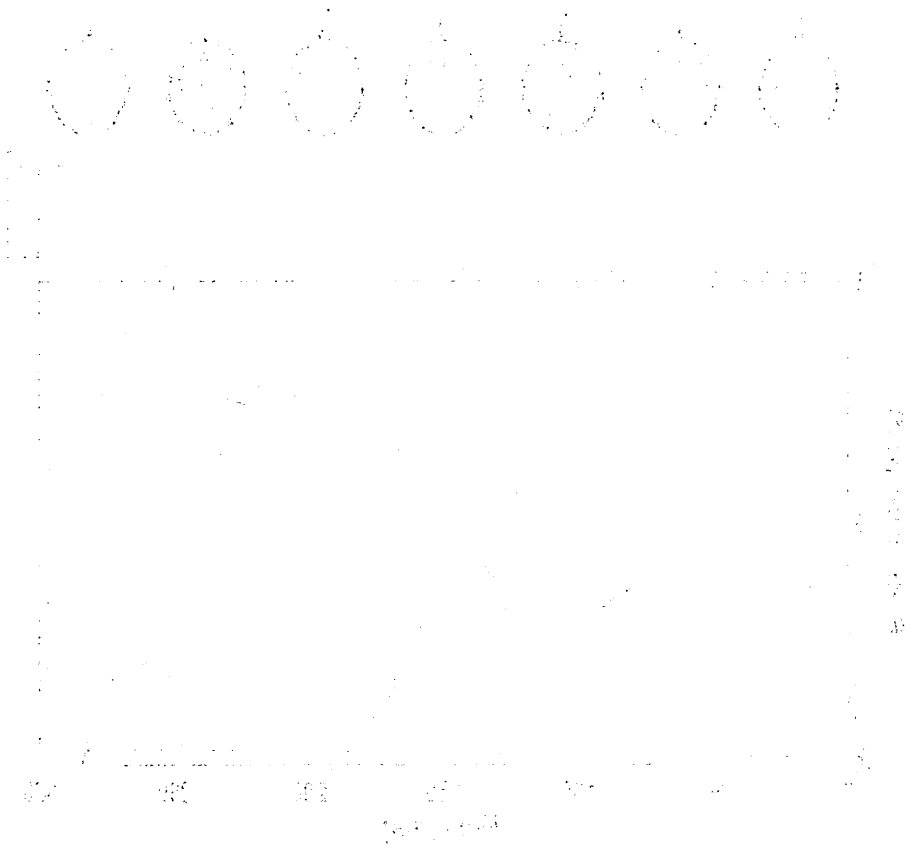

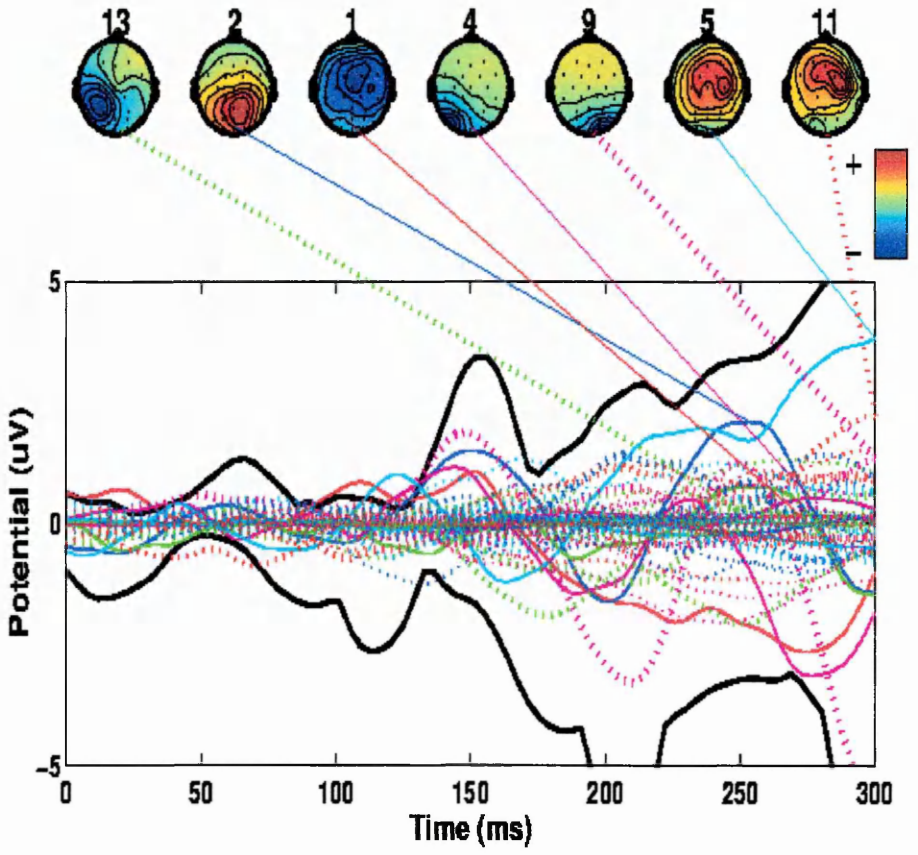

Figure 6.4: ICA components for targets in the right visual field

context relates to how a narrowband waveform changes its phase (in the single frequency sense) in response to the presentation of the stimulus.

The dominant frequency of the ICA component activations was around 10 Hz. This corresponded to the alpha frequency band well known in EEG research. Further it can be seen that the early positive and negative peaks in the P300 were spaced approximately 50 ms apart which correspond to a 10 Hz characteristic. The genesis of the early components in relation to phase and amplitude models was investigated. The mechanisms controlling the activation of these two components were studied using the phase analysis technique and Makeig's event-related spectral perturbation (ERSP) [54]. The amplitude and inter-trial

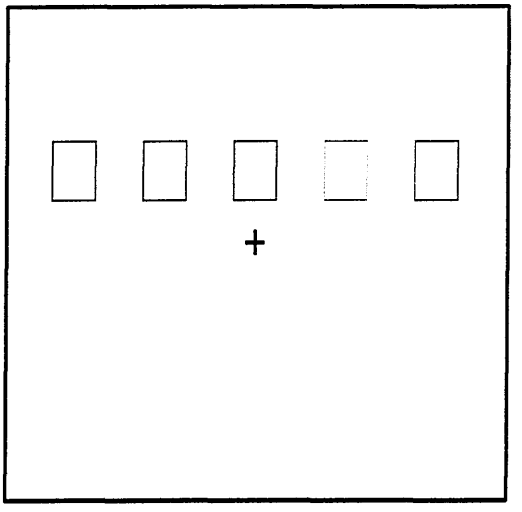

Figure 6.5: The visual spatial attention task

coherence of the alpha band components were also calculated.

For the purposes of comparison, the analysis techniques were applied to single trials as recorded at two scalp electrodes that were located above the most likely source of the ICA components considered.

6.3 Experimental Method

6.3.1 Subjects and Task

P300 ERPs were recorded during a visual spatial attention task [89]. Ten right handed volunteers with normal or corrected to normal vision participated in the task. The subjects were asked to fixate on a cross in the centre of a black screen. Five empty 1.6 cm square boxes where displayed horizontally 0.8 cm above a central fixation cross as shown in Fig.6.5. The horizontal visual angles from the central cross were 5.5, 2.7, 0, -2.7, -5.5 degrees.

Each of the boxes was designated in turn as the target box (coloured green) for one hundred trials. The subjects were asked to spatially attend the target box whilst maintaining visual

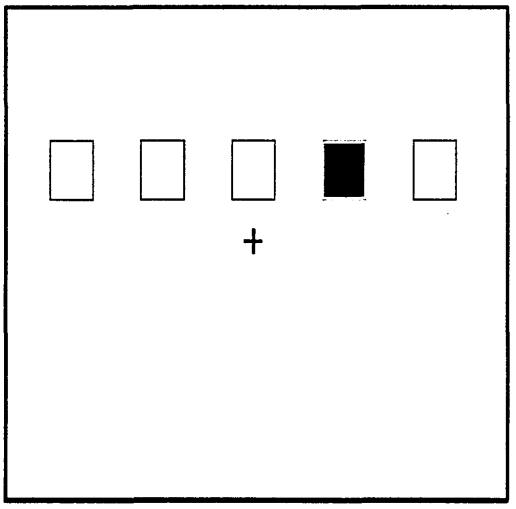

Figure 6.6: The visual spatial attention task showing a target

fixation on the cross in the centre of the screen. The subjects were instructed to respond to stimuli (filled white squares) appearing in the target box (Fig.6.6) by pressing a button.

For each target, 500 stimuli were displayed for 117 ms in of each the boxes in a pseudo random sequence. A non-target was classified as the filled white square appearing in any box other than the target, as illustrated in Fig.6.7 for example.

The occurrence of a stimulus in each box was equiprobable. The inter-stimulus interval was 250-1000 ms in 4 equiprobable 250 ms steps.

EEG for each trial was recorded from 29 electrodes at locations based on a modified international 10-20 system [89]. The recording system anti-aliasing filter had a cut off frequency of 50 Hz. The sampling rate was 512 Hz. Following recording, the effects of line noise were reduced by the application of a 40 Hz lowpass digital filter. Individual trials with ocular artifacts greater than 70 μV where discarded.

One subject from the 10 was selected at random. ICA was used to decompose the subject's single trial data for each of the 500 stimuli.

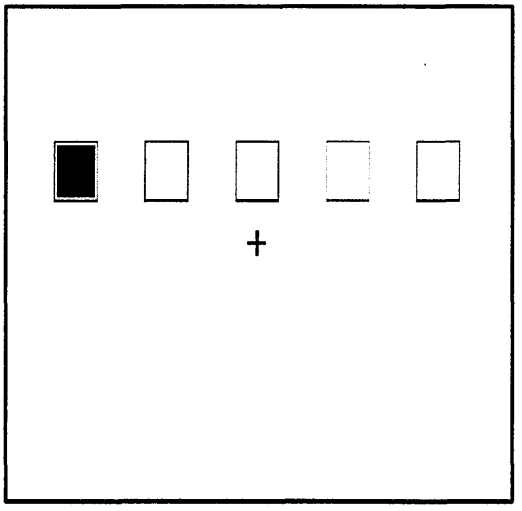

Figure 6.7: The visual spatial attention task showing a non target

6.3.2 Study Specific Experimental Method

Phase Sorted ERP Image

For each single trial activation of each ICA component under consideration, the power spectral density (PSD) was calculated [45]. The PSD enabled the peak alpha frequency to be identified. That is, the frequency within the range 7 - 13 Hz that has the most power. A 3 Hz bandpass filter centred on the peak alpha frequency was produced for each trial. Ideally the bandpass filter would be able to extract only the peak alpha frequency to enable a true measure of phase to be obtained. In practice this was not possible. The bandwidth was chosen as a compromise between being wide enough so as to reduce the effects of non-ideal digital filters and narrow enough to improve the accuracy of phase estimation. The resulting filter was used to extract the alpha band of the signal.

The Hilbert transform (See Chapter 3) was applied to the alpha band to obtain an estimate of instantaneous phase angle throughout the time course. The resulting 90 degree phase shift, inherent to the Hilbert transform, can effectively be ignored since all trials are phase shifted equally. The phase at stimulus was estimated by considering the phase angle over five samples centred on the stimulus. The number of samples chosen was a compromise

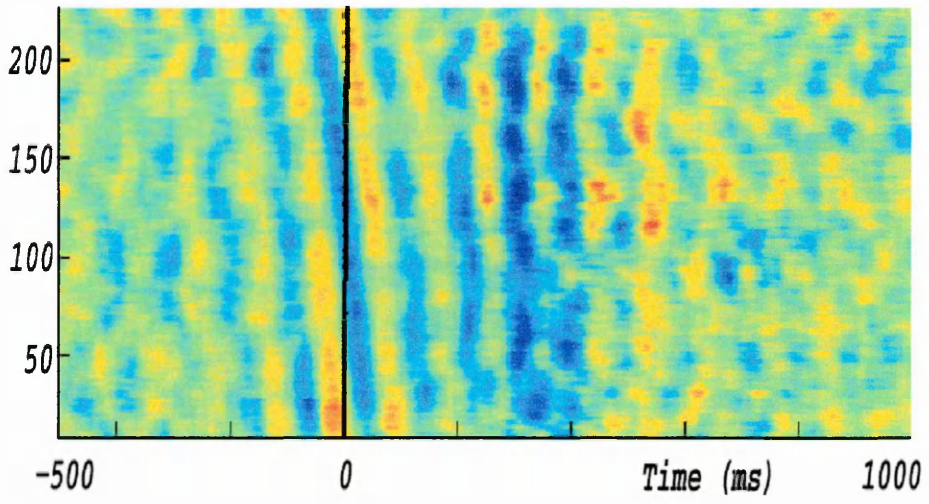

Figure 6.8: An alpha phase-sorted ERP image with time in ms on the horizontal axis and trial number vertically.

between reducing the effects of 'noisy' trials and the complexity of curve fitting a sine wave to a known transient waveform. This non-stationarity is as a result of the need to use a real bandpass filter to extract the alpha band. The phase angles of the five samples were 'unwrapped' [131] to remove any wrapping effects as the angle changes from 2π to 0. The mean phase angle was then calculated modulo 2π.

The single estimate of phase angle, in the range 0 - 2π, was used to determine the position of the single sweep relative to the other sweeps in the 'image'.

An image was constructed indexed horizontally by time and vertically by trial. The single trials where ordered on the calculated phase angle at stimulus. A 15 point moving average filter was applied to the image to reduce the effects of noise. The only post-recording filtering employed was the ICA spatial filtering hence the activations were not noise free. When the alpha phase-sorted image was produced for data recorded from a single scalp electrode, no post-recording filtering was carried out.

Analysis of Phase Sorted ERP Image

The phase-ordered image facilitates the visual analysis of the effects of the alpha phase at stimulus on the ensuing ERP. This is achieved by highlighting the relationship of features of any single trial with those of all other trials focussing in particular on the temporal position of peaks with respect to the time of stimulus. The image shown in Fig.6.8 has a cyclic relationship with the starting point chosen arbitrarily. After one complete cycle the image wraps around so that the bottom and top trials of the image are contiguous. The image is a result of placing several single sweeps next to each other, which are then viewed from above. The similarity between trials is enhanced following the application of a 15 point moving average filter [73]. The resulting peaks in colour (yellow for positive polarity, blue for negative) correspond to peaks (positive polarity) and troughs (negative polarity) in each single trial. When there is no similarity between single trials, the image has a random colour distribution, the baseline region for example. When neighbouring trials exhibit similar features, the colour remains almost constant for the region of similarity.

The assumption made was that at the point of stimulus the brain is in a random state (an assumption that is made in most ERP analysis). In a large sample of trials there will be a uniform distribution of alpha phase angle at this point. The diagonal lines of fixed colour reflect this. Starting at the time of stimulus, from the bottom of the image, the phase angle rotates through 2π radians linearly until the top of the image. The yellow line is the peak of each trial following sorting on this feature. After one complete cycle the image wraps around so that the bottom and top of the image are next to each other. The peak line has advanced (or retarded) 100 ms in one cycle. This reflects the dominant 10 Hz characteristic that was investigated.

The most striking feature is centred on the stimulus. The image can be thought of as looking down on a liquid. The yellow represents the tops of the waves whilst the blue is the trough. At stimulus, the waves travel at an angle to the vertical. If we take a section through the wave at the time of stimulus we would see one cycle of a cosine wave. Starting from the bottom of the image there is the crest of the wave (yellow) as we move through the trials vertically the amplitude drops (becomes blue) and then rises once more to the crest (yellow) of the preceding wave. We have moved through one complete cycle of the range of phase

angles. The image is wrapped around so that the top of the image and bottom of the image are contiguous. The diagonal waves can now be thought of as a screw thread. The pitch of the screw thread is 100 ms. That is in one complete cycle of the image the wave has moved forward 100 ms. The 100 ms period is a result of the dominant 10 Hz characteristic frequency.

The presence of this feature at stimulus is as a result of the ordering of trials whilst constructing the image. The existence of the feature before and after stimulus is as a result of the inertia of alpha band signals. The alpha band waveform can be thought of as a randomly phase modulated 10 Hz sine wave. As we move away from the point of ordering, the compounding effect of the modulation becomes more significant, hence noticeable. The image approaches an almost random distribution of phase angle at 500 ms pre-stimulus when compared with the uniform distribution at stimulus.

The peak line is not vertical which would show a constant phase angle in all trials at that particular point in time. If this were the case then this would reflect phase synchronisation or alignment.

Other Analysis Techniques Employed

The ensemble average for the component activations was included for comparison and completeness. The average represents the component's contribution to the ERP.

The inter-trial coherence (ITC) [45] (see Chapter 3) was calculated for the peak alpha frequency of the components PSD for each single trial. This provided a measure of phase synchronisation. The ITC becomes significant above the red line.

The root mean squared (RMS) of the alpha amplitude throughout the duration of the ERP was calculated. This allowed the additive model for ERP genesis to be considered along with the phase synchronistaion model.

The PSD shows the peak alpha amplitude for the set of trials considered. This value is used in the production of most plots as discussed above and is provided for interest.

The scalp map shows the projection of the signal source under investigation onto the surface

of the scalp. In the simple case this is a single electrode. In the case of an ICA component, the projection is more complex suggesting a source within the cortex.

The event-related spectral perurbation (ERSP) [54] (See Chapter 3) for the component under consideration was also calculated. The ERSP provided a measure of the combined time-frequency changes throughout the group of trials. The application of this technique established the broad band dynamics of the waveforms under analysis as opposed to the narrow band characteristics highlighted through the phase-sorted ERP image.

6.4 Results and Discussion

The results for the analysis of the two ICA components (numbered 4 and 9) from a single subject are presented. The components were selected because they contributed to the genesis of the N1 peak (Fig.6.2) and exhibited scalp projections that suggested signal sources within the visual cortex. The results for the analysis of component 4 is provided first. The corresponding results for component 9 follow. For comparison the results for the analysis of the unfiltered data direct from the scalp electrode is then provided.

6.4.1 Component 4

The ICA components of the subject's response to the two leftmost targets is shown in Fig.6.3. From Fig.6.3 it can be seen that component 4 is the major contributor to the genesis of the N1 peak. That is the activation of component 4 has the largest negative peak approximately coinciding with the N1 peak of the averaged ERP.

The analysis of the activation of component 4 in response to targets presented in the left visual field (the two left most boxes) whilst the subject is mentally attending the left visual field is shown in Fig.6.9.

The power spectral density showed that the peak alpha frequency of this component was 9.5 Hz. The component scalp map suggested a source within the left hemisphere of the visual cortex.

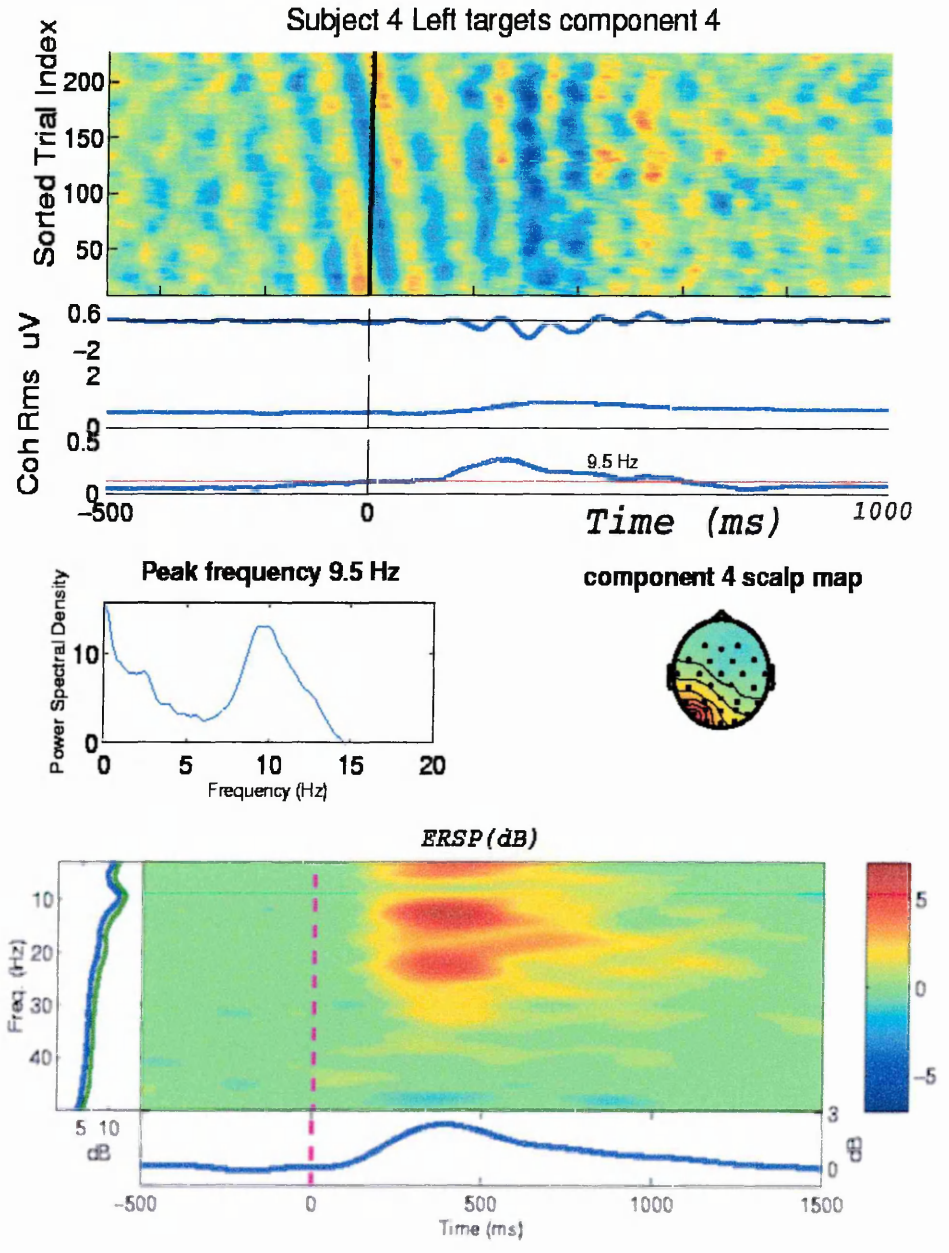

Figure 6.9: Component 4 response to attended targets in the left visual field

From the phase sorted ERP image it can be seen that the phase ordering produces the uniform distribution of alpha phase angle at the time of stimulus. The effects of the slight random frequency modulation of the alpha band between trials is illustrated by the almost random distribution of phase angle at 500 ms pre-stimulus.

The most interesting feature was observed in the 600 ms following the presentation of the stimulus. After 200 ms the waves rotated from their diagonal alignment to become vertically aligned. That is the distribution of phase angles has moved from being uniform at stimulus to being normally distributed about a narrow range of angle. At 400 ms the peaks had become vertically oriented reflecting a phase synchronisation. That is the individual single trials have approximately the same alpha phase angle at that point in the genesis of the ERP. This phase synchronisation was maintained for a few cycles until after 600 ms when the distribution tended toward being random once more.

We can see by looking at the time domain average of the trials that the baseline (pre-stimulus area) is flat. This characteristic is maintained until approximately 200 ms when a 10 Hz burst can be seen. This corresponded to the phase alignment of the individual trials.

Once the phase alignment of individual trials had disappeared (after approximately 600 ms post-stimulus) the alpha burst observed in the time domain response became attenuated before the the ERP returned to the pre-stimulus baseline.

The RMS of the amplitude of the averaged alpha waveform during the time period of the ERP showed an increase in alpha power.

The inter-trial coherence (ITC) for the frequency of interest (9.5Hz in this case) provided a measure of phase synchronisation. The plot shows that the ITC becomes significant (i.e. above the red line) for the time period of the ERP (200-600 ms post-stimulus). The ITC peaks at approximately 400 ms post-stimulus reflecting the phase alignment of the individual trials.

The ERSP showed a broadband amplitude increase, relative to baseline, in the time period of 200-600 ms post-stimulus. In particular note the three most significant time-frequency features during the 200-600 ms time period in the approximate frequency ranges 0-2 Hz, 12-16 Hz and 20-25 Hz. Note also that there was no significant amplitude increase in the

alpha band.

In terms of the alpha band, the contribution of this component to the genesis of the ERP is a product of both alpha phase synchronisation and an relatively small increase in alpha (energy). There was a significant broadband amplitude increase.

The ICA comoponents of the subject's response to the two rightmost targets is shown in Fig.6.4. From Fig.6.4 it can be seen that component 4 does not contribute significantly to the genesis of the N1 peak.

The analysis of the activation of component 4 in response to targets presented in the right visual field (the two right most boxes) whilst the subject is mentally attending the right visual field is shown in Fig.6.10.

From the phase sorted ERP image it can be seen that within the 200 ms post-stimulus, the waves rotated from their diagonal alignment to become vertically aligned. This synchronisation was maintained until approximately 600 ms post-stimulus.

The time domain average of the trials shows the baseline (pre-stimulus area) is flat and extends until approximately 150 ms post-stimulus when a 10 Hz burst could be seen. This corresponded to the early phase alignment of the individual trials. Following the dissipation of the alpha burst (after approximately 600 ms post-stimulus) the ERP returned to baseline within 200 ms.

The RMS of the amplitude of the averaged alpha waveform over the time period showed no increase in alpha power during the presence of the ERP.

The inter-trial coherence (ITC) showed that the ITC becomes significant after only 150 ms. The ITC peaked at approximately 300 ms. The alpha coherence was significant until 500 ms.

The ERSP showed an alpha amplitude decrease in the period 150-500 ms post-stimulus with an increase in amplitude of a narrow frequency band centred on approximately 15 Hz. There was a broadband amplitude increase in the 600-900 ms period which include the alpha band.

The contribution of this component to the genesis of the ERP is purely a product of alpha

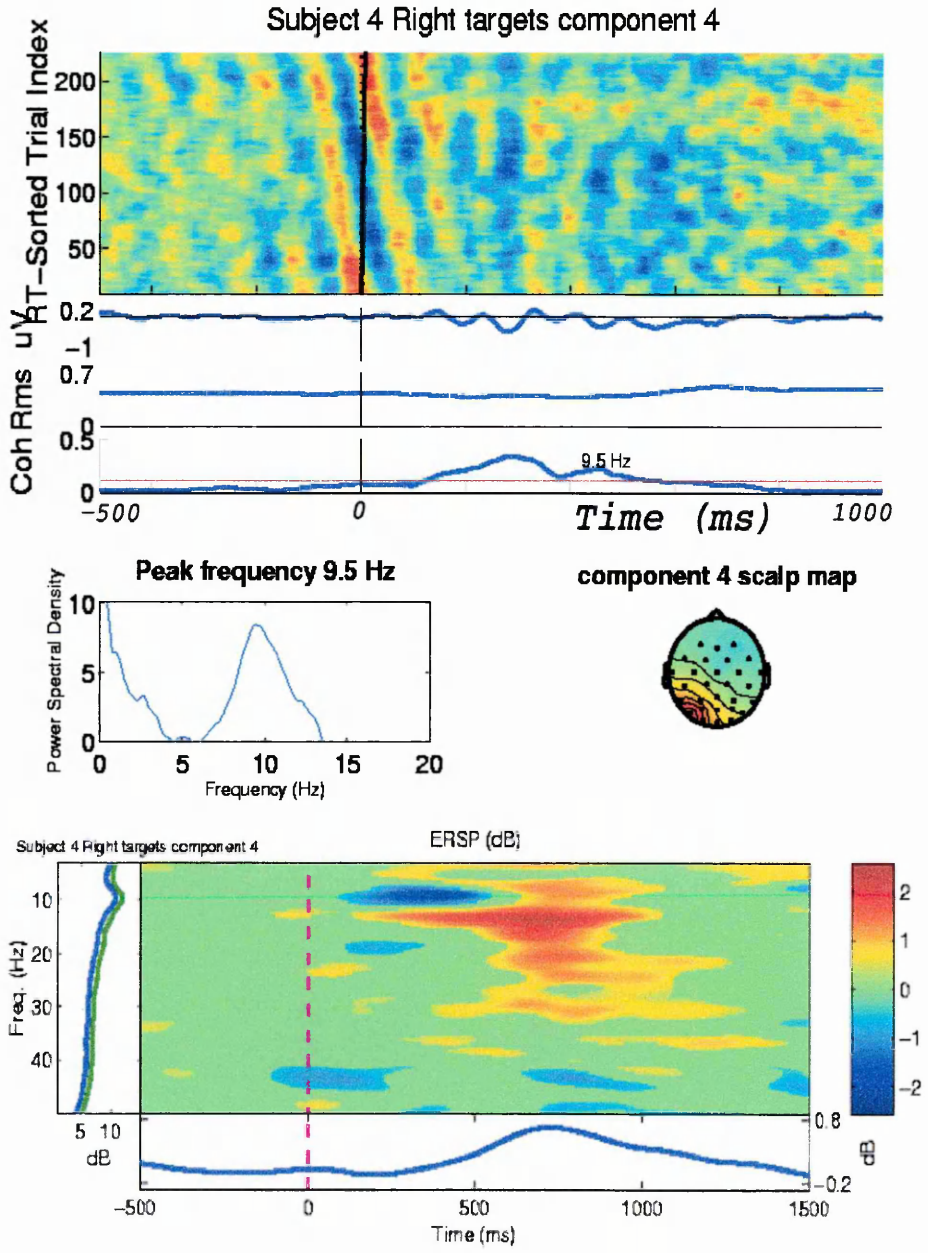

Figure 6.10: Component 4 response to attended targets in the right visual field

phase synchronisation. There was a significant post ERP broadband amplitude increase.

The two remaining task conditions that were investigated are when targets appear in the non-attended visual field. That is when the subject is told to attend left but targets appear in the right visual field or targets that appear in the left visual when the subject is attending right.

The analysis of the activation of component 4 in response to targets presented in the left visual field (the two left most boxes) whilst the subject is mentally attending the right visual field is shown in Fig.6.11.

From the phase sorted ERP image it can be seen that a weak phase synchronisation occurred at approximately 200 ms post-stimulus. Almost immediately the distribution of phase angle tended toward being random once more.

The time domain average of the trials showed little deviation from the pre-stimulus baseline level. A small peak was produced at 200 ms.

The RMS of the amplitude of the averaged alpha waveform over the time period of the ERP showed an increase in alpha power at approximately 200 ms post-stimulus.

The inter-trial coherence (ITC) showed no significant phase synchronisation.

The ERSP showed an early amplitude increase, relative to baseline, in the time period starting almost immediately at stimulus presentation and lasting for approximately 300 ms for frequencies in the 8 -16 Hz range.

The contribution of this component to the genesis of the ERP was a purely product of small alpha amplitude increase. No phase synchronisation occurred.

The analysis of the activation of component 4 in response to targets presented in the right visual field (the two right most boxes) whilst the subject is mentally attending the left visual field is shown in Fig.6.12.

From the phase sorted ERP image it can be seen that a phase synchronisation occurred at approximately 150ms post-stimulus. The synchronisation was maintained until 400 ms post-stimulus, when the distribution of phase angle tended toward being random.

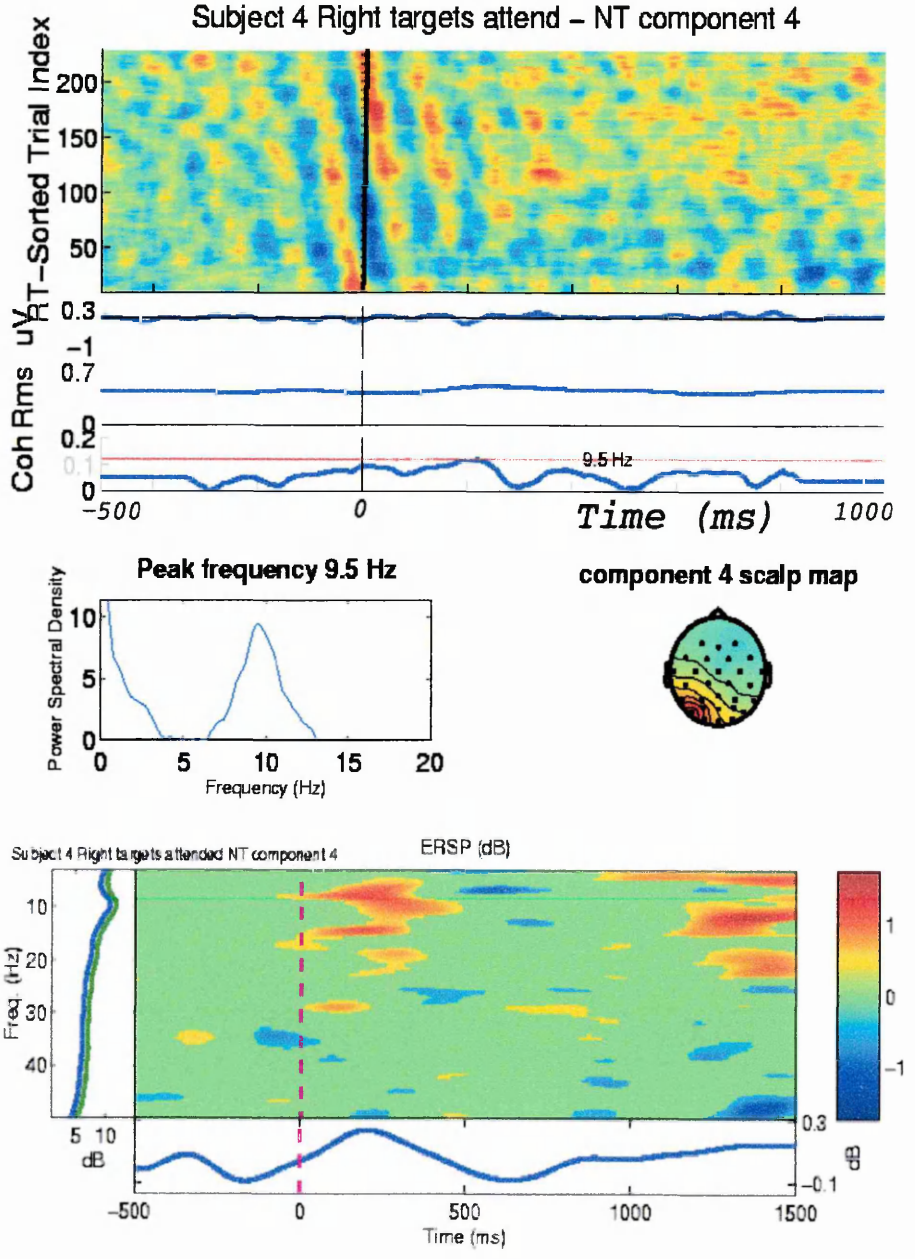

Figure 6.11: Component 4 response to targets in the left visual field whilst attending right

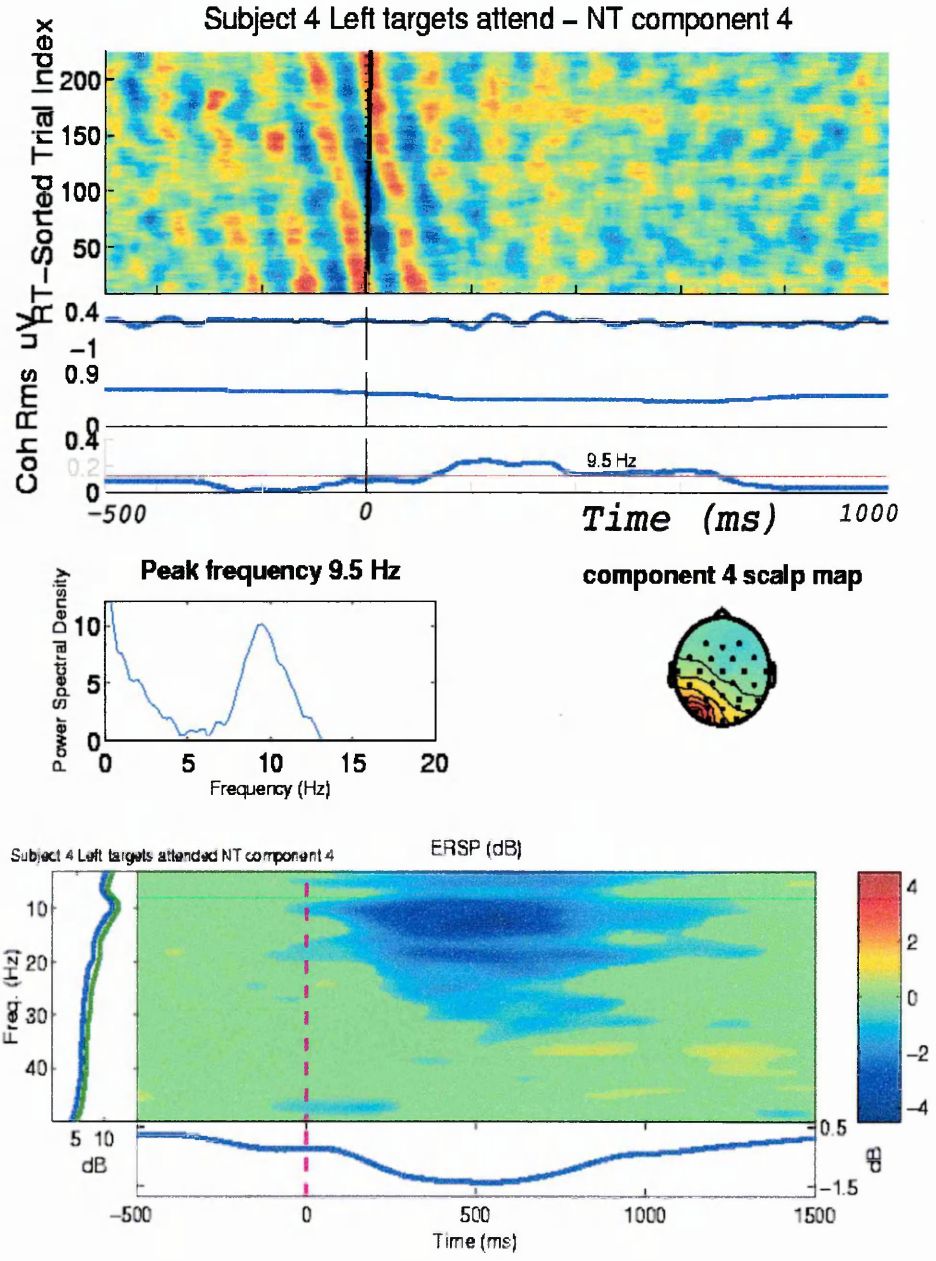

Figure 6.12: Component 4 response to targets in the right visual field whilst attending left

We can see by looking at the time domain average of the trials that a burst of approximately 10 Hz frequency, was produced in the period 150-400 ms post-stimulus. Following this alpha burst, the ERP returned to the pre-stimulus baseline.

The RMS of the amplitude of the averaged alpha waveform over the time period of the ERP showed an decrease in alpha power.

The inter-trial coherence (ITC) showed a significant phase synchronisation in the period 150-400 ms post-stimulus.

The ERSP showed a broadband amplitude decrease, relative to baseline, in the time period starting almost immediately at stimulus presentation and lasting for approximately 800 ms. In particular note the distribution of the significant time-frequency features.

The contribution of this component to the genesis of the ERP was a product of alpha phase synchronisation. Indeed there was a significant broadband amplitude decrease including the alpha band.

The results for component 4 for the four task combinations considered suggest differing control mechanisms in each case. The analysis of the laterally symmetrical component 9 was investigated for comparison.

6.4.2 Component 9

The ICA comoponents of the subject's response to the two leftmost targets is shown in Fig.6.4. From Fig.6.4 it can be seen that component 9 does not contribute significantly to the genesis of the N1 peak.

The analysis of the activation of component 9 in response to targets presented in the left visual field (the two left most boxes) whilst the subject is mentally attending the left visual field is shown in Fig.6.13.

The power spectral density showed that the peak alpha frequency of this component was 9.75 Hz. The component scalp map suggested a source within the right hemisphere of the visual cortex.

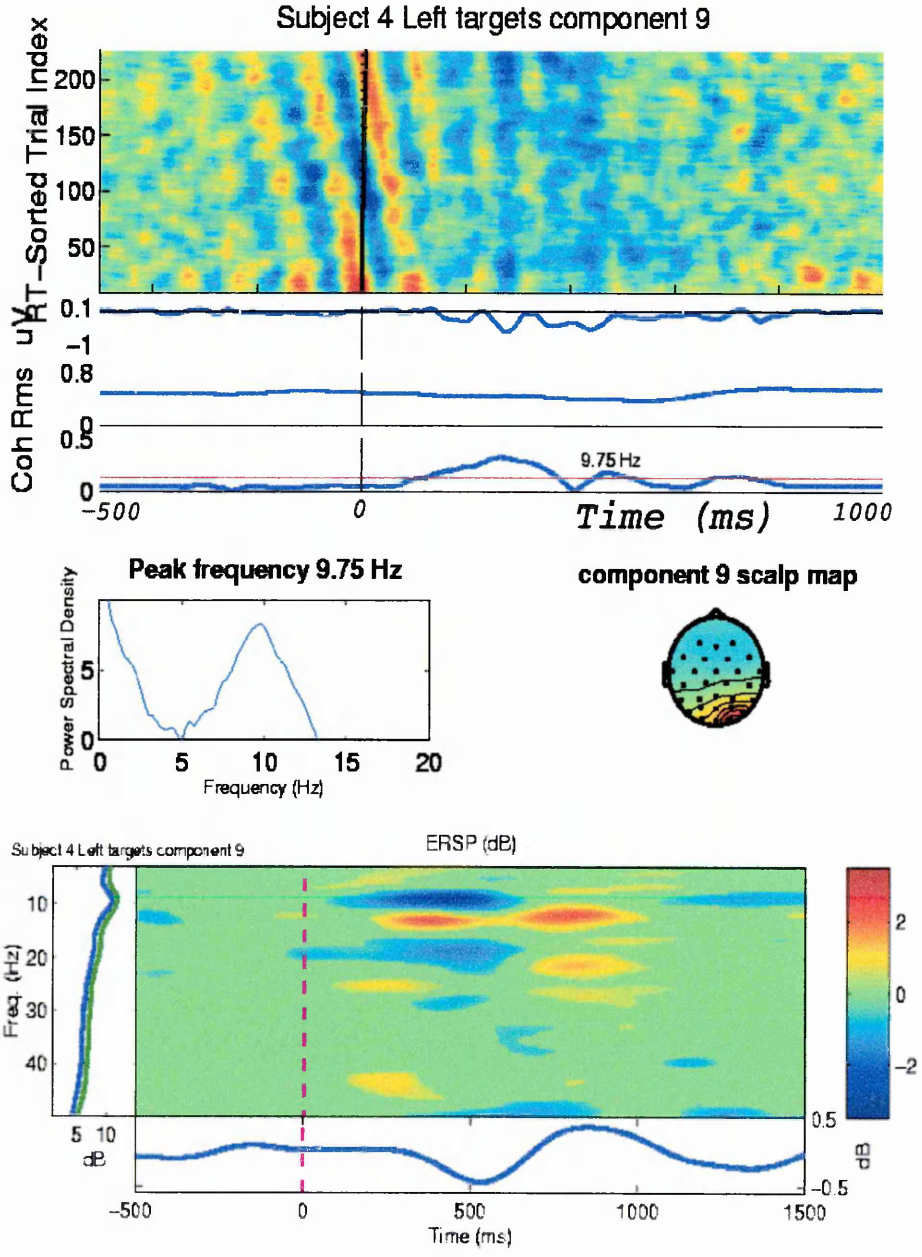

Figure 6.13: Component 9 response to attended targets in the left visual field

From the phase sorted ERP image it can be seen that by 200 ms post-stimulus, the waveforms rotated from their diagonal alignment to become vertically aligned. This phase synchronisation was maintained for a few cycles until after 500 ms when the distribution tended toward being random once more.

We can see by looking at the time domain average of the trials that the baseline (pre-stimulus area) is flat. This characteristic was maintained until approximately 150 ms when a response could be seen. The voltage deviation returned to baseline after 500 ms. Activity was still present until 800 ms post-stimulus.

The RMS of the amplitude of the averaged alpha waveform during the time period of the ERP showed a noticeable decrease in alpha power.

The inter-trial coherence (ITC) became significant after only 150 ms. The main coherent activity lasted until 400 ms although some bursts of coherent activity were observed at approximately 500 ms and 700 ms following stimulus presentation.

The ERSP showed an alpha amplitude decrease in the period 150-600 ms post-stimulus with an increase in amplitude of a narrow frequency band centred on approximately 15 Hz. There were amplitude increases in the 600-900 ms period for two narrow bands centred on 13 and 22 Hz approximately.

In terms of the alpha rhythm, the contribution of this component to the genesis of the ERP was purely a product of phase synchronisation. A marked decrease in alpha energy was observed.

The ICA comoponents of the subject's response to the two rightmost targets is shown in Fig.6.3. From Fig.6.3 it can be seen that component 9 is the major contributor to the genesis of the N1 peak.

The analysis of the activation of component 9 in response to targets presented in the right visual field (the two right most boxes) whilst the subject is mentally attending the right visual field is shown in Fig.6.14.

From the phase sorted ERP image it can be seen that by 200 ms post-stimulus, the waves rotated from their diagonal alignment to become vertically aligned. This synchronisation

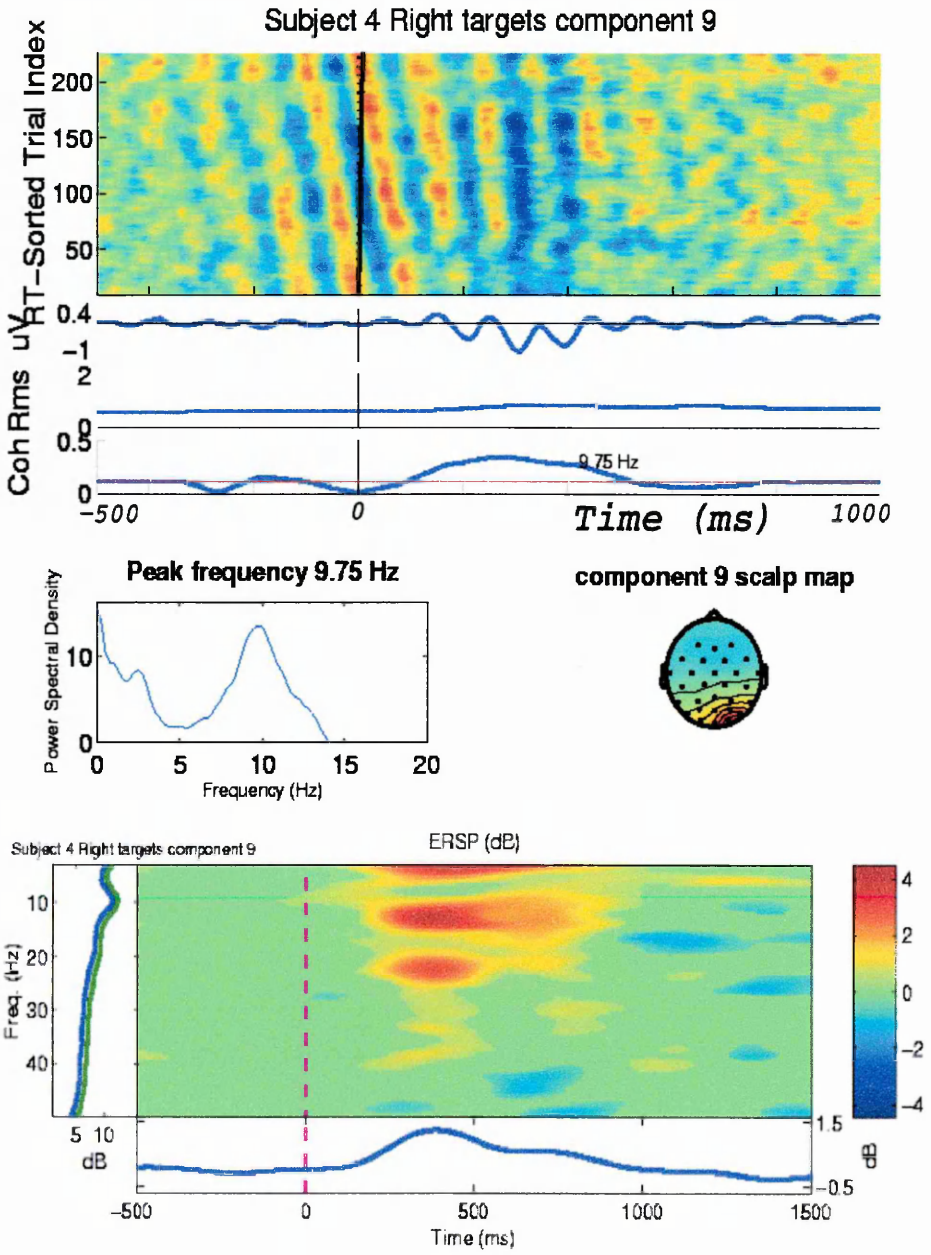

Figure 6.14: Component 9 response to attended targets in the right visual field

was maintained until approximately 600 ms post-stimulus.

The time domain average of the trials shows a relatively flat pre-stimulus baseline. The characteristics of which were maintained until 100 ms after stimulus presentation when a 10 Hz burst began. This alpha burst lasted until approximately 600 ms post-stimulus. After which, the ERP returned to the pre-stimulus baseline.

The RMS of the amplitude of the averaged alpha waveform over the time period increased during the presence of the ERP.

The inter-trial coherence (ITC) became significant after only 100 ms. The ITC peaked at approximately 250 ms and remained significant until 500 ms.

The ERSP showed a broadband amplitude increase, relative to baseline, in the time period of 200-600 ms post-stimulus. In particular note the three most significant time-frequency features during the 200-500 ms time period in the approximate frequency ranges 0-2 Hz, 12-16 Hz and 20-25 Hz. The amplitude of the two lower frequency components was significantly increased until approximately 800 ms following stimulus presentation. Note also that there was no significant amplitude increase in the lower frequency range of the alpha band.

In terms of the alpha band, the contribution of this component to the genesis of the ERP is a product of both alpha phase synchronisation and an relatively small increase in alpha (energy). There was a significant broadband amplitude increase.

The two remaining task conditions that were investigated are when targets appear in the non attended visual field. That is when the subject is told to attend left but targets appear in the right visual field or targets that appear in the left visual when the subject is attending right.

The analysis of the activation of component 9 in response to targets presented in the left visual field (the two left most boxes) whilst the subject is mentally attending the right visual field is shown in Fig.6.15.

From the phase sorted ERP image it can be seen that a phase synchronisation occurred at approximately 200 ms post-stimulus. At approximately 400 ms post-stimulus, the distribution of phase angle tended toward being random once more.

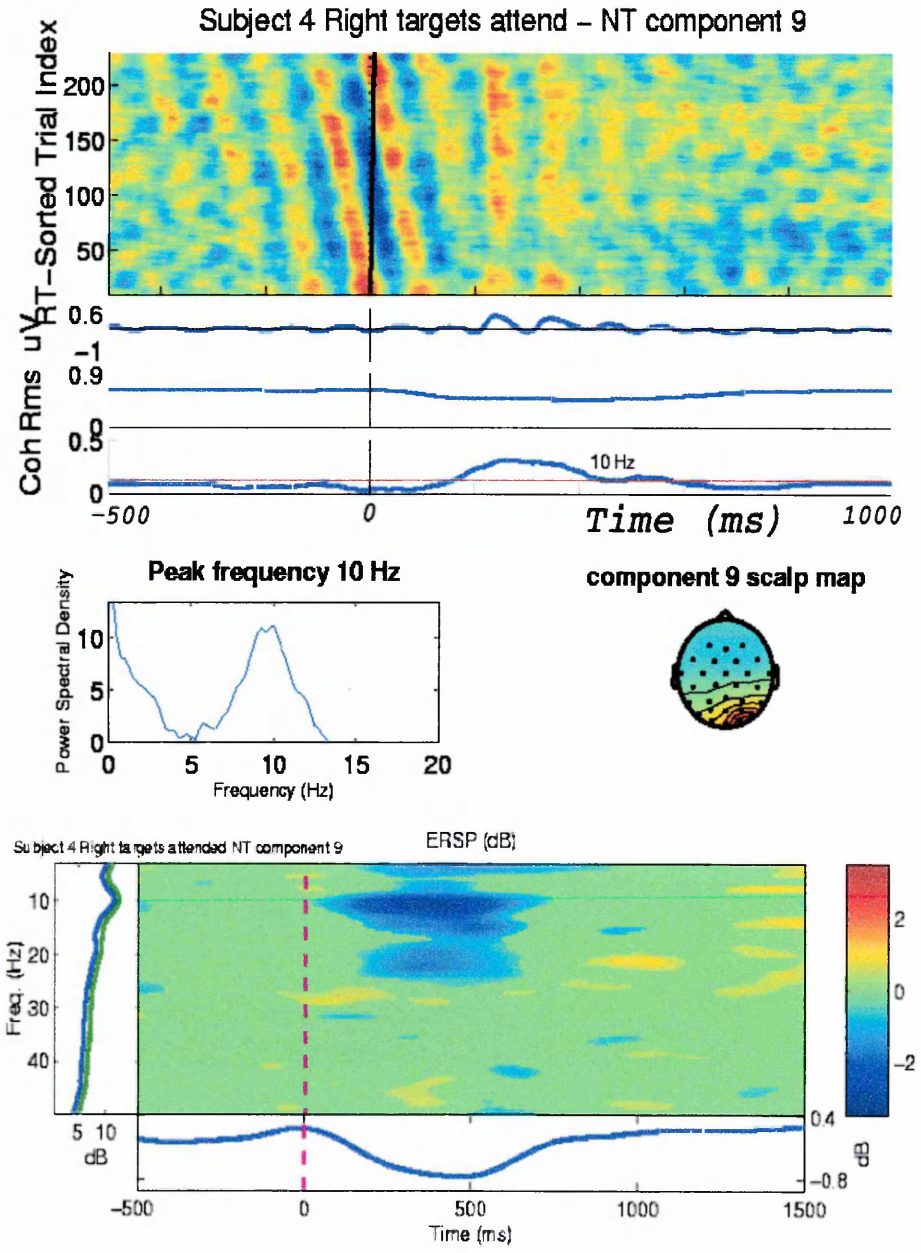

Figure 6.15: Component 9 response to targets in the left visual field whilst attending right

A burst of approximately 10 Hz frequency, was produced in the period 200-600 ms post-stimulus. Following this alpha burst, the ERP returned to the pre-stimulus baseline.

The RMS of the amplitude of the averaged alpha waveform over the time period of the ERP showed a relatively large decrease in alpha power.

The inter-trial coherence (ITC) showed a significant phase synchronisation in the period 200-400 ms post-stimulus.

The ERSP showed a broadband amplitude decrease, relative to baseline, in the time period starting almost immediately at stimulus presentation and lasting for approximately 600 ms. In particular note the distribution of the significant time-frequency features.

In terms of the alpha rhythm the contribution of this component to the genesis of the ERP was a product of phase synchronisation. There was a significant broadband amplitude decrease including the alpha band.

The analysis of the activation of component 9 in response to targets presented in the right visual field (the two right most boxes) whilst the subject is mentally attending the left visual field is shown in Fig.6.16.

From the phase sorted ERP image it can be seen that a weak phase synchronisation occurred at approximately 300ms post-stimulus. Almost immediately the distribution of phase angle tended toward being random once more.

The time domain average of the trials showed little deviation from the pre-stimulus baseline level. A small burst of alpha activity was observed between 200 and 600 ms.

The RMS of the amplitude of the averaged alpha waveform over the time period of the ERP showed a slight increase in alpha power at approximately 200 ms post-stimulus. A post ERP decrease in alpha power was also observed.

The inter-trial coherence (ITC) showed a phase synchronisation between 200 and 400 ms with a relatively low significance.

The ERSP showed amplitude increases, relative to baseline, in the time period between 250 and 500 ms following stimulus presentation for narrow frequency bands approximately

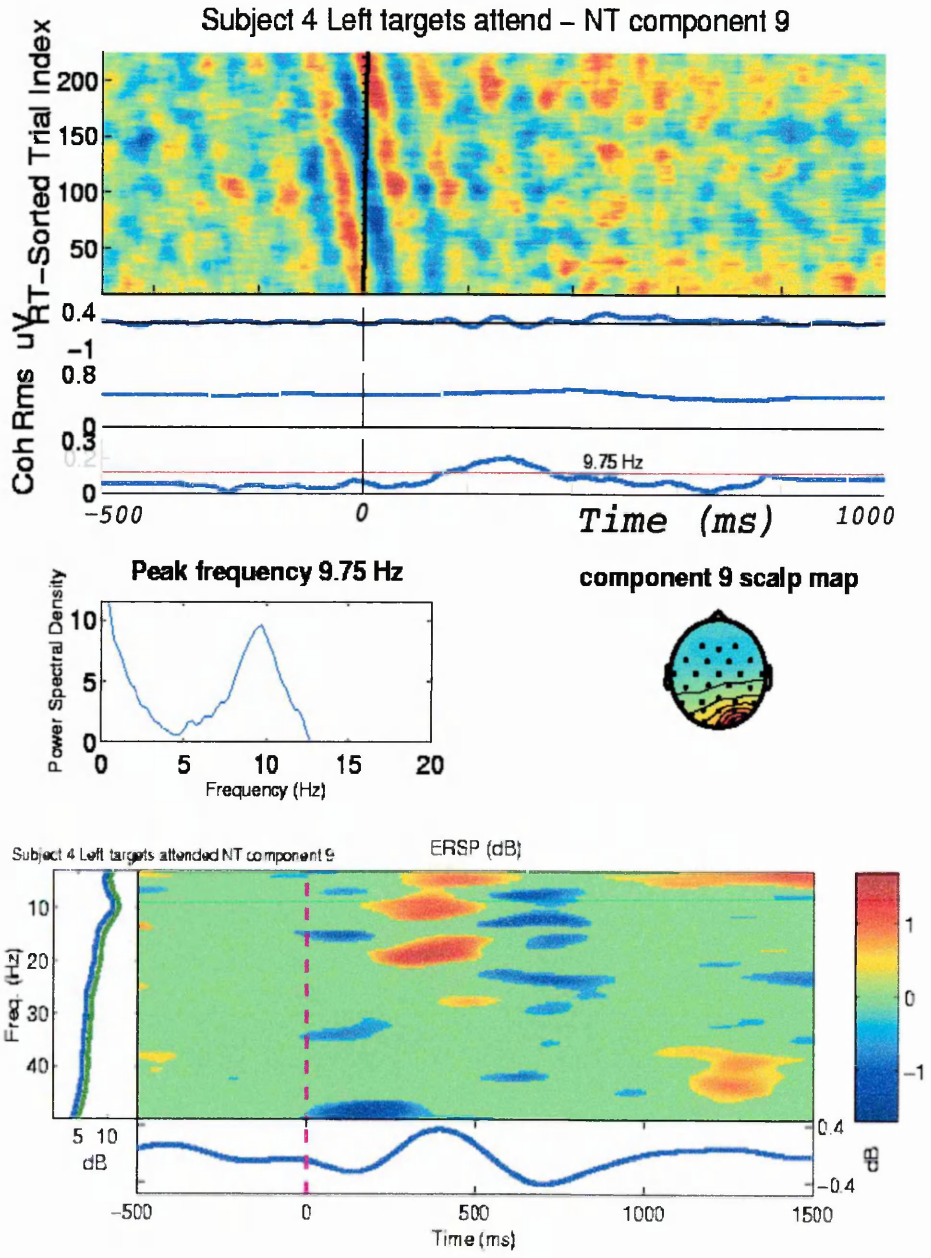

Figure 6.16: Component 9 response to targets in the right visual field whilst attending left

centred on 2, 10 and 18 Hz.

In terms of the alpha rhythm, the contribution of this component to the genesis of the ERP was a product of a small alpha amplitude increase and phase synchronisation with a comparatively low significance.

6.4.3 Unfiltered Scalp Recordings

For comparison, the single scalp electrode that was nearest to the identified independent component in the left hemisphere of the visual cortex was investigated. The scalp electrode that reflected the laterally symmetric component in the right hemisphere was also analysed.

Fig.6.17 depicts the results when attended targets appear in the left hand visual field. That is the subject is attending left and the target appears to the left.

Fig.6.18 depicts the results when attended targets appear in the right hand visual field. That is the subject is attending right and the target appears to the right.

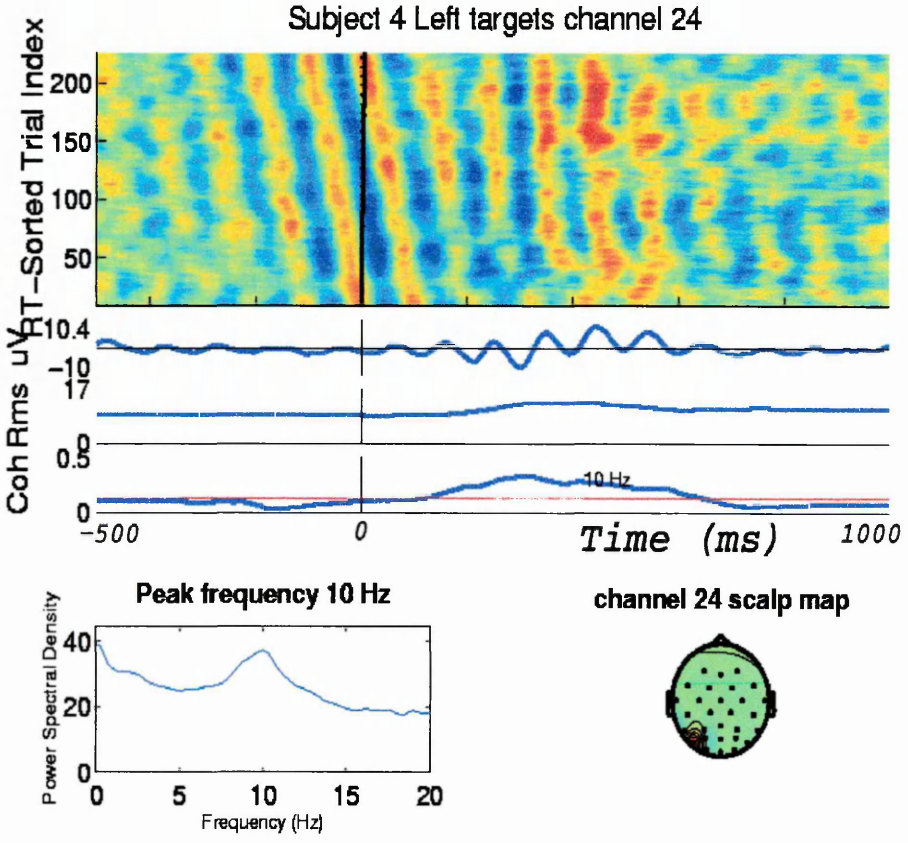

Figure 6.17: Channel 24 response to targets in the left visual field when attending left

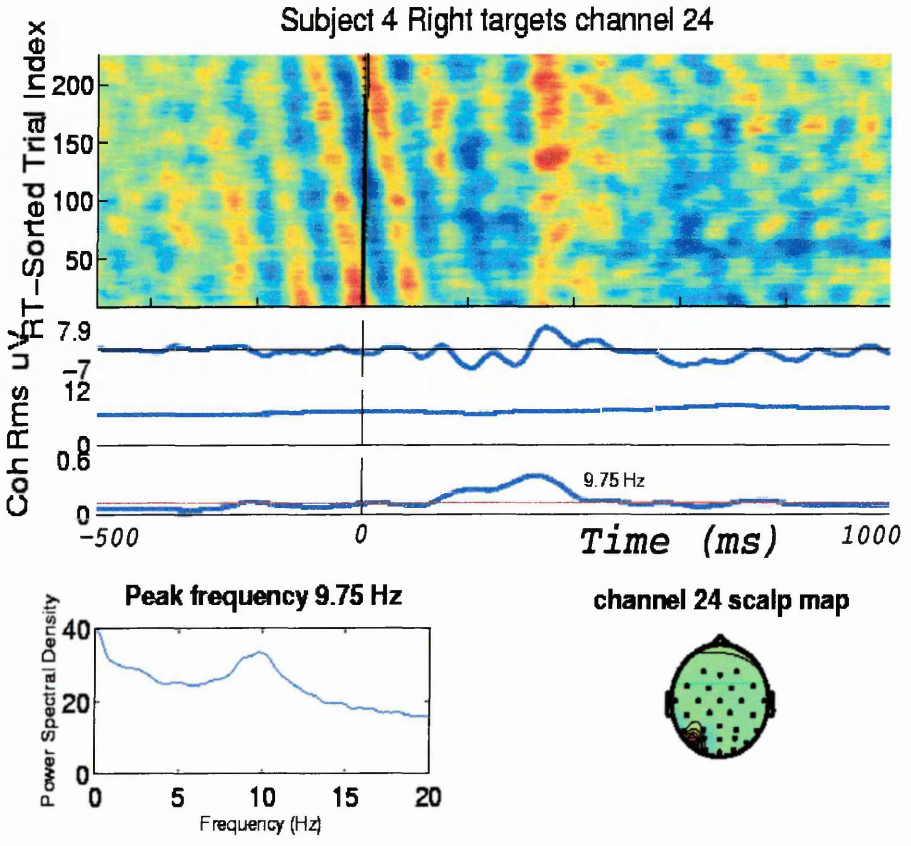

Figure 6.18: Channel 24 response to targets in the right visual field when attending right

6.5 Conclusion

A new technique, the phase sorted erpimage, was developed to investigate the phase dynamics of ERPs. This was successfully applied, along with other techniques, to the investigation of independent component analysis (ICA) component activations in a visual spatial attention task. Two components with scalp projections that suggested sources with the visual cortex were analysed.

There were differences in the component activations in response to targets being in the left or right visual field. The scalp projections of components 4 and 9 suggested that they represent homologous and physiologically plausible signal generators within the visual cortex. The mechanisms controlling the activation of these two components was investigated. The time domain response of components 4 and 9 were analysed in terms of the contribution of alpha power changes and phase synchronisation to the genesis of the ERP. The results are summarised in Fig.6.19 and further reinforce the symmetry and independence of the components.

The similarity between the analysis of the raw data from the scalp electrode and that activation of the independent component further illustrates the power of ICA as a spatial filtering technique for EEG analysis. The analysis of the unprocessed single trials demonstrated the effectiveness of the phase sorted ERP image in the investigation of event-related phase dynamics. The technique yields good results when applied to noisy data.

The results suggest that two laterally symmetrical regions of the visual cortex are visual field selective.

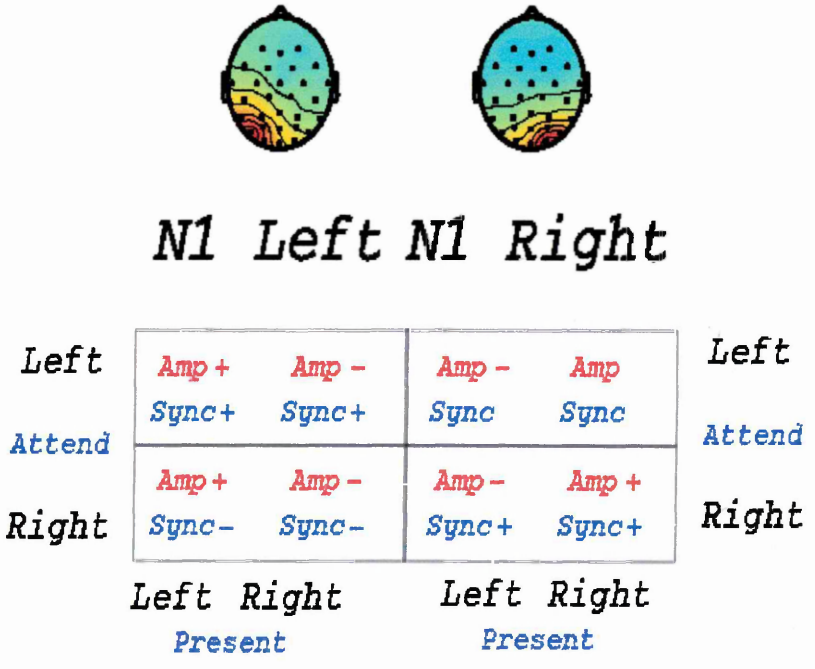

Figure 6.19: A summary diagram showing phase and amplitude symmetry between the two homologous independent components

Chapter 7

Conclusions and Further Work

7.1 Chapter Summary

This chapter provides a conclusion to the study. Some suggestions for further work are provided.

7.2 Chapter Conclusions

The trial-to-trial variation had immediate effect on the recovery of event-related potentials (ERPs) from the larger amplitude background electroencephalogram (EEG). A novel technique for estimating single trial ERPs was developed and evaluated. The method was based on the wavelet transform which provided a representation of the ERP in the combined time and scale domain. The choice of the wavelet transform based approach reflected the time-varying characteristics of ERPs. The developed adaptive wavelet-based filtering algorithm was used for the single trial recovery of a cognitive cortical event-related potential (ERP) known as the contingent negative variation (CNV).

A method for quantitatively evaluating its effectiveness was devised and was used to select the most suitable orthogonal filter (basis function) for the process. The adaptive wavelet-

based filtering algorithm was compared with a number of other possible techniques. The traditional approach of synchronised averaging was used to provide a datum for comparison. A filtering approach based on the wavelet packet transform was also explored in which a range of filters and basis trees spanning the wavelet packet table were evaluated.

The results obtained suggested that the choice of a particular basis tree appears not to be very significant. The method chosen for coefficient scaling had the most impact on the effectiveness of the filter. The results demonstrated that the developed adaptive wavelet-based filtering approach was the most effective technique considered. The method could reduce the background EEG by a factor of 3 while preserving the main features of the CNV waveform.

The ability to effectively estimate single trial ERPs allowed the analysis of the trial-to-trial variation of an ERP in schizophrenic and matched normal subjects. A study of contingent negative variation (CNV) trial-to-trial variation in 20 medicated schizophrenics and their normal control subjects was carried out. The study showed distinct differences in the time evolution of the CNV waveforms with trial numbers between each of the two subject categories. The findings of this study indicated that the first 6 trials provide valuable information concerning the development of the CNV.

The possibility of using the trend of the trial-to-trial variation for the purpose of subject classification was investigated. Using the Kohonen self-organising artificial neural network, it was possible to differentiate the majority of schizophrenic from normal subjects on the basis of their CNV amplitude trial-to-trial variation. Since trial-to-trial variation carries cognitive information, this study successfully revealed that schizophrenic subjects undergo a different cognitive process during the CNV recording experiments as compared with normal subjects.

A new method for the analysis of the event-related phase dynamics was developed. The technique was applied to P300 ERPs produced in a visual spatial awareness task. The genesis of the P300 and its relationship to the alpha rhythm was investigated for two spatially fixed, temporally independent signal sources identified following independent component analysis. The scalp projections of the two components suggested that the sources were within the visual cortex. The mechanisms controlling the activation of these two components, in terms of the contribution of alpha power changes and phase synchronisation was investigated.

There were differences in the component activations in response to targets being in the left or right visual field. The results suggested that the two physiologically plausible components were homologous and that two laterally symmetrical regions of the visual cortex are visual field selective.

The power of the phase analysis method was illustrated following successful application to data taken directly from scalp electrodes. The similarity between the analysis of the raw data from the scalp electrode and that activation of the independent component further demonstrates the power of ICA as a spatial filtering technique for EEG analysis. Similarly, the analysis of the unprocessed single trials showed the effectiveness of the phase sorted ERP image in the investigation of event-related phase dynamics. The technique could successfully be applied to noisy data.

7.3 Thesis Conclusion

This study lead to the development of novel joint time-frequency techniques that facilitated increased understanding of event-related potentials. Wavelet transforms are ideally suited to the characteristics of single channel ERPs. For higher frequencies, their high temporal resolution at the expense of frequency resolution and the opposite of lower frequencies reflects the current classification of ERP components in terms of bursts of activity within frequency bands.

For ERP noise reduction, the ability to separate components with overlapping spectra but occuring at temporally different locations is essential. Wavelet transforms lend themselves to these non-stationary waveforms. The effectiveness and importance of wavelet based filtering to single trial ERP recovery was demonstrated by facilitating the investigation of trial-to-trial variation of ERPs and the subsequent analysis resulting in identification of schizophrenic subjects.

The ability to estimate the phase of a single frequency component from a single trial ERP at a given instance in time has allowed the event-related phase dynamics to be investigated. This has lead to a greater understanding of the complex mechanisms involved in the genesis

of ERPs.

Wavelets and other joint time-frequency analysis techniques are ideally suited to the filtering and analysis of single trial ERPs.

7.4 Suggestions for Further Work

The suggestions for further work are separated into two sections. The first focuses on wavelet based filtering of single channel ERPs. The second concerns the application of ICA and wavelets for the analysis of multichannel data.

7.4.1 Wavelets

The effectiveness of the wavelet based filtering algorithm could be improved in three areas.

Firstly, the development of a wavelet basis function more suited to single trial ERP recovery. However, the investigation undertaken in this study suggested that the basis function had minimal effect on the SNR improvement. This is to be expected since the constraints on wavelet design lead to functions with similar frequency responses. The application of optimal wavelets may be more suited to signal or feature detection.

Secondly, the use of the overcomplete wavelet packet transform could be developed further with the aim of selecting the best basis tree in terms of filtering performance. An information theoretic approach to basis tree selection, similar to Wickerhauser's algorithm, with the aim being SNR improvement as opposed to signal compression.

Finally, The development of an 'intelligent' coefficient scaling system. The results from this study suggested that the method for selecting and attenuating the signal coefficients in the wavelet domain was the most significant factor in SNR improvement. A method employing fuzzy logic and/or an artificial neural network may be able to learn which time frequency components are more related to noise than desired signal and hence attenuate the coefficients accordingly. This may lead to the development of a coefficient scaling method that does not rely on a time and phase locked average.

An improved single trial recovery method would facilitate a more detailed investigation of ERP trial-to-trial variation by allowing more subtle features to be considered. This may lead to the possibility of correlating trial-to-trial variation with the severity and types of symptoms in schizophrenia and other psychiatric disorders.

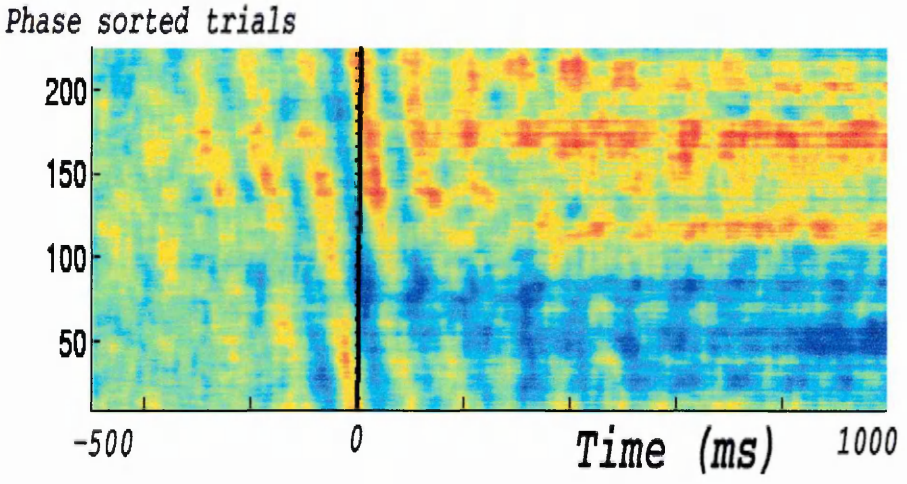

Figure 7.1: The phase-sorted ERP image of an ICA component exhibiting a late d.c. offset dependent on alpha phase at stimulus

7.4.2 ICA and Wavelets

The combination of independent component analysis and joint time-frequency methods is ideally suited to the analysis of multi-channel ERPs. ICA provides a spatial filter which separates the recorded data into temporally independent components. The activation of these components can subsequently be analysed using joint time-frequency techniques.

The results in this study have shown that the activation of two physiologically plausible components, identified by the ICA algorithm is modulated by some underlying mechanism. The source and characteristics of this mechanism could be explored. Perhaps by the application of ICA to the activation of a component.

An observation made during this study was that a centrally located component in the visual cortex (almost beneath the OZ electrode) exhibited a post-stimulus d.c. offset dependent on alpha phase at stimulus as shown in Fig.7.1.

The effect can be more easily seen when the single trials are separated into two groups dependent on phase at stimulus. The plot of the average of each group is shown in Fig.7.2.

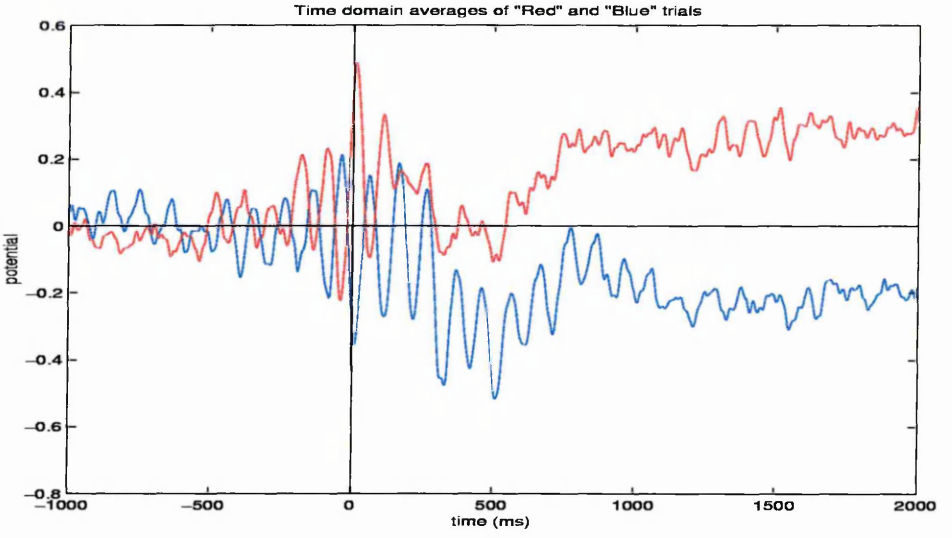

Figure 7.2: The time domain averages of trials with a late d.c. offset dependent on alpha phase at stimulus

Several other components exhibited this characteristic. This may be a fruitful area of investigation. From and engineers perspective, this may relate to storing the state of the brain at the time of stimulus, prior to dealing with it.

Finally ICA and the techniques developed in this study may be employed for single trial recovery. Jung *et al.* [59] have reported some results in this area. A development is to use the phases sorted erpimage, as produced in this study, to observe and quantify the event-related alpha phase shift for each trial. Using this information the single trials can be stretched to align peaks of interest.

Appendix A

Refereed Journal Publication

Adaptive multiresolution analysis based evoked potential filtering

M.R.Saatchi
C.Gibson
J.W.K.Rowe
E.M.Allen

Indexing terms: Multiresolution analysis, Wavelet transform, Signal detection, Evoked potentials

Abstract: Evoked potentials (EPs) are electrical activities of the brain synchronised with external stimuli. They have proved valuable for the understanding of the functioning of the brain and in investigating several brain related disorders. EPs are usually obscured by the background electroencephalogram (EEG) and thus require appropriate filtering. As the frequency spectra of the EEG and EPs overlap, the application of deterministic filters on their own is usually inadequate. Synchronised averaging improves the signal-to-noise ratio; however it inhibits measurement of the important variations which develop from one EP recording or trial to the next. The presence of these variations also makes an averaged EP a distorted version of an EP which evolves with time. A novel adaptive filtering algorithm based on the wavelet transform method of multiresolution analysis (MRA) was developed and was successfully used for single trial recovery of a type of EP known as the contingent negative variation (CNV). Both simulated and real CNV waveforms were processed. A technique to evaluate the effectiveness of the developed method was devised and was used to select the best orthogonal filter among Daubechies, Coifman and Symmlet for the adaptive MRA based filtering operation. The technique enabled the magnitude of the background EEG to be reduced by a factor of 5 while preserving the main features of the CNV waveform.

1 Introduction

The electrical activity of the brain, electroencephalogram (EEG) was first described by Caton [1]. The EEG represents the spontaneous electrical activity of the brain. In addition to the EEG, it is also possible to record electrical activities of the brain which are synchronised to the occurrence of external stimuli such as visual and auditory stimuli. These waveforms are known as evoked potentials (EPs). Cognitive EPs are known as event-related potentials (ERPs) and they require the subject to co-operate during the recording by recognition or response.

EPs are a valuable tool for understanding of the functioning of the brain and thus they have proved effective for investigating a number of brain related disorders including schizophrenia [2, 3], Huntington's disease [4] and Parkinson's disease [5]. They complement the information obtained using the methods such as computerised tomography (CT) and magnetic resonance imaging (MRI).

The techniques for the recording of EPs are now well established. The principal difficulty in analysing EPs is that they have a very poor signal-to-noise ratio. The magnitude of an EP is up to 30μV. This is embedded in the background EEG which has a magnitude up to 100μV. As the spectra of EPs and the background EEG overlap, the use of deterministic filters on their own usually does not result in an adequate reduction of the background EEG.

The magnitude of the background EEG is significantly reduced by the process of synchronised averaging. In this process a number of EPs recorded under similar experimental conditions are averaged. The assumptions are that the background EEG is an additive random signal which is uncorrelated with the desired EPs and the individual EPs are consistent in amplitude and latency from one recording or trial to the next. However the cognitive processes such as learning, memory and attention play an important role in the generation of many EPs causing an averaged EP to be an approximation of the true EP. In a number of studies ways of improving the effectiveness of averaging have been explored. These include: latency correction [6] and selective averaging by cross-covariance [7]. Another shortcoming of the averaging method is that it inhibits measurement of the trial-to-trial variations as EPs evolve in amplitude and latency from one trial to the next. For example, in normal subjects the amplitude of a type of cognitive EP known as the contingent negative variation (CNV) initially increases and then decreases with time [8]. The cause(s) of these may be related to factors such as fatigue, learning and variation in the level of attention. The impairment of cognitive processes in subjects with

IEE Proceedings online no. 19971319

Paper first received 14th November 1996 and in revised form 11th April 1997

M.R. Saatchi, C. Gibson and J.W.K. Rowe are with the School of Engineering, Sheffield Hallam University, Pond Street, Sheffield S1 1WB, UK

E.M. Allen is with the Department of Clinical Neurophysiology, Plymouth General Hospital, Derriford Road, Plymouth PL6 8DH, UK

disease and Parkinson's disease may make their EP trial-to-trial variations different from those in normal subjects. The measurement and quantification of this information can thus provide valuable clinical information about the disorder.

In several studies, attempts were made to recover single trial EPs from the background EEG. These included autoregressive modelling [9], Kalman filtering [10] and adaptive filtering [11]. The difficulty with such methods is that they rely on assumptions which are difficult to fulfil. For example, to use conventional adaptive filtering an EEG record is required. This must be closely correlated with the contaminating EEG and it must also be uncorrelated with the desired EP.

Recent advances in the field of wavelet transforms [12] and their successful applications in the analysis of various signals, including biomedical signals [13], pointed to the possibility of using them to develop methods for the recovery of EPs. In a study, it was demonstrated that, by performing the wavelet transform of an EP and setting its specific wavelet transform coefficients to zero before performing the inverse wavelet transform, the contribution of the background EEG can be significantly reduced [14]. In another study, a time varying filter was developed using the wavelet transform and was successfully applied to two types of EPs [15]. The problem with the current wavelet transform based methods of EP recovery is that the signal-to-noise ratio improvement is achieved by causing significant loss in EPs details.

In this study, an adaptive filtering algorithm based on the wavelet transform method of multiresolution analysis (MRA) was developed. This algorithm was successfully used for the recovery of a type of cognitive EP known as the contingent negative variation (CNV). Several orthogonal filters were considered for the MRA process and the effectiveness of each for the recovery of the CNV waveform was evaluated.

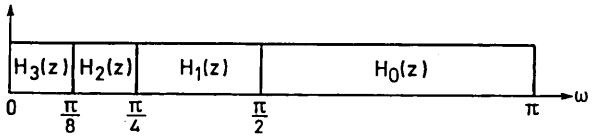

Fig.1 *Frequency responses of analysis filters*

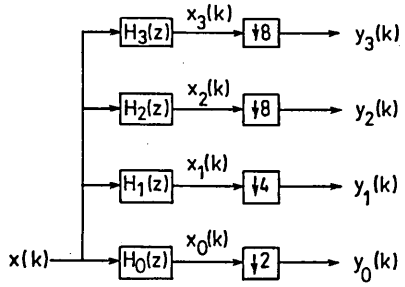

Fig.2 *Tree-structured analysis filter bank*

2 Multiresolution analysis

MRA is an application of the wavelet transform. Detailed description of the method is provided in many articles, for example [16–18]. The MRA technique decomposes a signal using a set of filters with frequency responses shown in Fig. 1. The network to achieve this is based on Fig. 2. It should be noted that $\downarrow n$ represents decimation (down sampling) by a factor n. The amount of decimation in each branch of the Fig. 2 is proportional to the bandwidth of the filter preceding the decimator in that branch.

Suppose $H(z)$ and $G(z)$ are the frequency responses of a highpass filter and a lowpass filter, each with the cut-off frequency of $\pi/2$. The desired frequency responses of Fig. 1 can be realised by a set of filters expressed as [18],

$$\begin{aligned} H_0(z) &= H(z) \\ H_1(z) &= G(z)H(z^2) \\ H_2(z) &= G(z)G(z^2)H(z^4) \\ H_3(z) &= G(z)G(z^2)G(z^4) \end{aligned} \quad (1)$$

In practice, the equivalent of Fig. 2 shown in Fig. 3 is used as it is easier to implement. The signal can be reconstructed from its MRA coefficients (i.e. $y_0(k)$, $y_1(k)$, ...) using the structure shown in Fig. 4. This network is based on a synthesis lowpass filter $G_s(z)$ and a synthesis highpass filter $H_s(z)$. The filters $G(z)$, $H(z)$, $G_s(z)$ and $H_s(z)$ are very closely related and therefore, given $G(z)$, the other three filters can easily be derived from it [18]. The analysis and synthesis filters must satisfy a number of conditions to ensure perfect reconstruction (i.e. $\hat{x}(k) = x(k)$ [18].

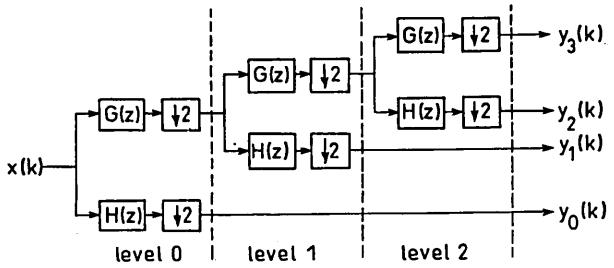

Fig.3 *Equivalent of analysis filter bank*

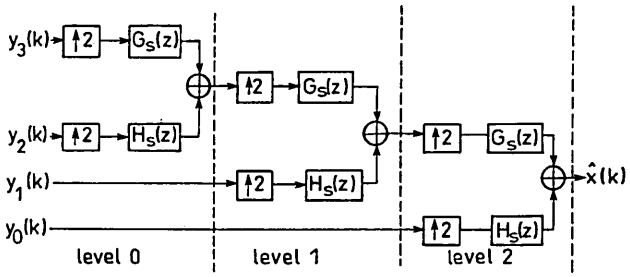

Fig.4 *Tree-structured synthesis filter bank*

3 Contingent negative variation and its preprocessing

The CNV is a cortical EP which consists of slow surface negativity in the EEG that depends on the association or contingency of two successive stimuli [19]. The first stimulus (S1) serves as a warning stimulus for the second imperative stimulus (S2) to which a response of some sort (usually motor) is made. An averaged CNV waveform from a normal subject is shown in Fig. 5. The CNV is thought to be generated principally by the frontal cortex as well as the midbrain including frontal association, motor and somatosensory zones [20]. The CNV is a cognitive EP because its generation depends on a sequence of brain activities such as attention, recognition, memory and motivation [19]. The CNV has been extensively studied in schizophrenia because symptoms such as inattention

and lack of motivation are characteristic symptoms of the condition [2, 3].

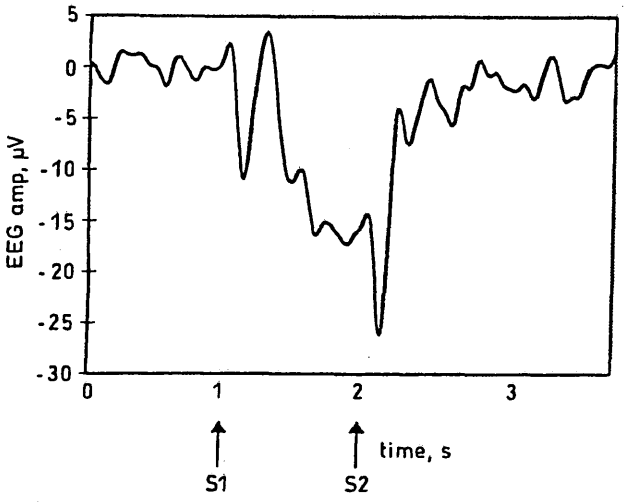

Fig.5 *Averaged CNV waveform in normal subject*

The CNV recording system and the required preprocessing procedure are described in [21]. The system consisted of an EEG machine, a personal computer, a unit which amplified, filtered, and digitised the signals. The passband of the filter was 0.1 to 30Hz. Programmable gain amplifiers were used to improve the accuracy of signal digitisation. The signals were digitised with a 12-bit analogue to digital converter using a sampling rate of 125Hz.

Thirty two CNV waveforms (trials) were recorded per subject from the convexity of the scalp (vertex) using silver–silver chloride electrodes and with the linked earlobes as reference. The duration of each trial was 12 seconds. The warning (S1) and imperative (S2) stimuli, were presented at 1 and 2 seconds, respectively. S1 was a click and S2 was a continuous tone. The subjects were asked to terminate the tone by pressing a hand-held push-button. All data recordings were carried out in an EEG recording room by an experienced EEG technician.

4 Description of adaptive multiresolution analysis based filtering algorithm

A basic procedure for the MRA method of recovering an EP from the background EEG is as follows. (i) Decompose the waveform using MRA network of Fig. 3. (ii) Select the MRA coefficients at one or more levels and set these to zero. This selection needs to be carried out heuristically. (iii) Reconstruct the signal using the network of Fig. 4. As the MRA coefficients at some levels are more representative of the background EEG, this operation will improve the signal-to-noise ratio. This process can be improved by scaling the MRA coefficients with a value between 0 and 1. As the required scaling factor needs to determined heuristically, this technique is inefficient.

The algorithm developed in this study was based on the principle described above; however, the optimum scaling factor for each level of the MRA was computed adaptively. The algorithm required a CNV template. Two forms of templates were possible. The first was subject specific template obtained by averaging 32 CNV trials from the subject whom individual trials were required. The other was the CNV grand average produced by obtaining the averaged CNV waveforms (over 32 trials) from a number of subjects (in this study 20 subjects) and averaging the resulting waveforms. The latter template is only for the recovery of the CNV waveforms from the subjects of the category where the CNV grand average was obtained.

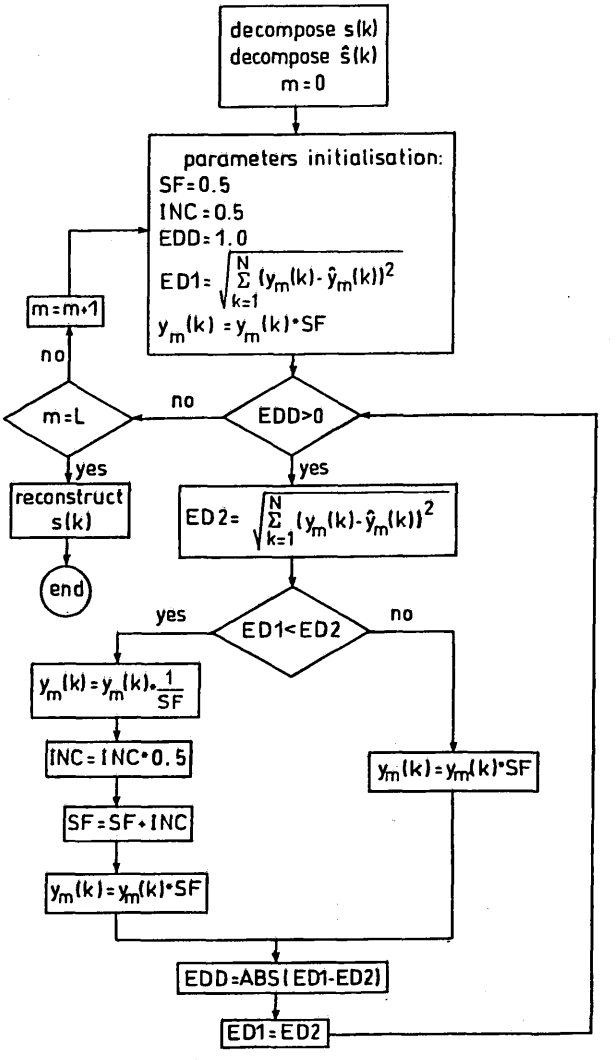

Fig.6 *Flowchart for adaptive MRA filtering algorithm*
$\hat{s}(k)$: CNV template
$s(k)$: single trial CNV
N: number of sample points
y_m: MRA coefficients of $s(k)$ at level under consideration
$\hat{y}_m$: MRA coefficients of $\hat{s}(k)$ at level under consideration
SF: scale factor
ED1: Euclidean distance before scaling operation
ED2: Euclidean distance after scaling operation
INC: scale factor increment
EDD: Euclidean distance difference
ABS: absolute value operator
L: number of MRA levels

The operation of the adaptive MRA based filtering algorithm is outlined in the flowchart of Fig. 6. Initially, both the single trial CNV waveform ($s(k)$) and the CNV template ($\hat{s}(k)$) were decomposed using the network shown in Fig. 3. Then, the MRA coefficients at each level ($y_0(k)$, $y_1(k)$, ...) were scaled using the following procedure. The initial Euclidean distance (ED1) between the MRA coefficients of the two signals at the level under consideration were computed. The scaling factor (SF) and scaling factor increment (INC) were initialised to 0.5. The Euclidean distance difference (EDD) parameter needs to be initialised with a positive value for the algorithm to start correctly. The significance of SF, INC and EDD becomes clear once the rest of the algorithm is described. The MRA coefficients of the single trial CNV at the level under consideration were scaled by current value of SF (initially,

0.5). If this scaling caused the Euclidean distance between the MRA coefficients of the single trial CNV and those of the corresponding CNV template to be reduced (i.e. ED1 > ED2), the scaling factor value remained unchanged. Otherwise, (i) the MRA coefficients of the single trial CNV at the level under consideration were restored to their original values, (ii) the scale factor was incremented by half its current value, and (iii) the MRA coefficients at the level under consideration were scaled with the new scaling factor. Following this, the absolute value of the difference between the current and previous Euclidean distances was computed. The current Euclidean distance was reinitialised with the previous Euclidean distance value. The process continued until any further scaling caused the Euclidean distance between the MRA coefficients of the single trial CNV and those of the CNV template to increase. The MRA coefficients at the remaining levels were scaled similarly. For a signal of N points, the number of MRA levels, L, is equal to $\log_2^N - 1$. This operation resulted in an optimum scaling factor for the MRA coefficients at each level. Following this process, the single trial CNV was reconstructed using the scaled MRA coefficients.

5 Analysis procedure

The adaptive MRA filtering algorithm was implemented as described in the previous Section. Tests were carried out to ensure the software worked correctly. Perfect reconstruction was achieved when the output of the network shown in Fig. 3 was used directly as input to Fig. 4. It was observed that subsectioning of the CNV waveform and its template would improve the filtering operation. With this scheme, each section was processed by the algorithm independently. However, this caused discontinuities in the reconstructed signal. To minimise this effect, a section of the signal consisting of 32 samples was processed, and the eight samples at the centre of the section were kept. Then the next section of the waveform was selected such that the eight samples at the centre of the section were the continuation of the eight samples kept from the previous operation. This process was repeated until the complete waveform was processed.

To be able to evaluate the effectiveness of the method, it was necessary to use simulated rather than recorded CNV waveforms. A simulated CNV waveform consisted of a piecewise CNV model to which real EEG was added. The piecewise CNV model, together with a simulated CNV waveform, are shown superimposed in Fig. 7. The simulated CNV is a very simplified representation of the CNV waveform, and therefore many components such as those developed as a result of the onset of stimuli are not represented.

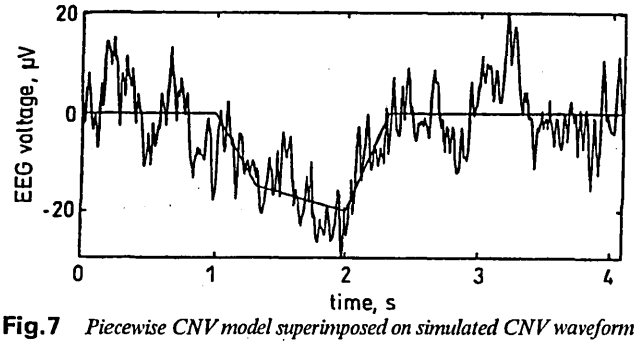

Fig.7 *Piecewise CNV model superimposed on simulated CNV waveform*

The estimate of the evaluation of the CNV recovery method was based on computation of noise factor and signal distortion. Noise factor is the ratio of signal to noise power ratio after filtering operation (SNR_p) to signal to noise power ratio before the filtering process (SNR_0).

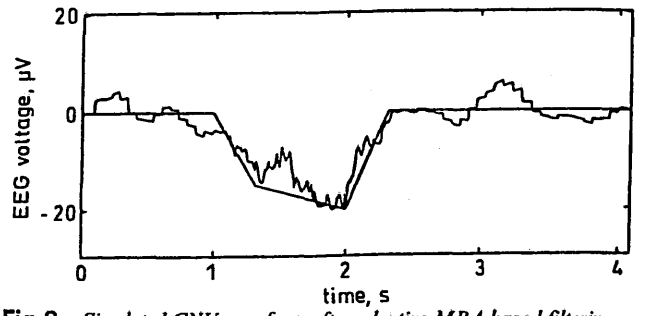

Fig.8 *Simulated CNV waveform after adaptive MRA based filtering*

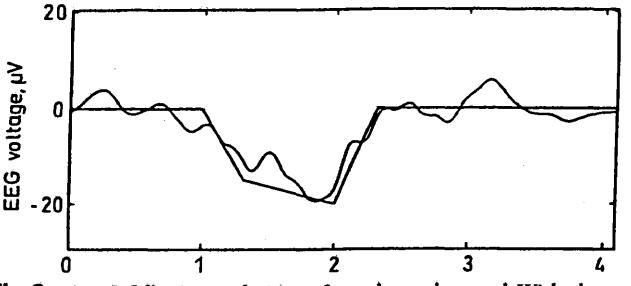

Fig.9 *Fig. 8 following application of wavelet packets and Wickerhauser best basis algorithm*

The value of SNR_0 was computed by

$$SNR_0 = \frac{\text{piecewise CNV model power}}{\text{additive EEG power}} = \frac{\sum_{k=1}^{N} \hat{s}_k^2}{\sum_{k=1}^{N} n_k^2} \quad (2)$$

where $\hat{s}_k$ and n_k are samples of the piecewise CNV model and the background EEG, respectively. The number of samples (N) was 512 points. The signal-to-noise ratio after the application of the CNV recovery method (SNR_p) was estimated using

$$SNR_p = \frac{\text{recovered simulated CNV power}}{\text{residual EEG power}} = \frac{\sum_{k=1}^{N} s_k^2}{\sum_{k=1}^{N} (s_k - \hat{s}_k)^2} \quad (3)$$

where s_k are samples of the recovered simulated CNV. It should be noted that $(s_k - \hat{s}_k)$ are samples of the estimate of the residual background EEG. The larger the value of the noise factor, the more effective would be the process of EP recovery. The amount of signal distortion after filtering was estimated by comparing the Euclidean distances between the piecewise CNV model and that of recovered CNV waveforms. The smaller is the magnitude of this parameter, the smaller would be the amount of distortion.

For the analysis and synthesis networks of Figs. 3 and 4, it was decided to use three popular orthogonal filters, namely Daubechies, Coiflet (Coifman), and Symmlet, and to evaluate their effectiveness (in recovering the simulated CNV) with different number of coefficients. For Daubechies all even numbered coefficients between 2 and 20, for Coiflet 6, 12, 18, 24, and 30 coefficients and for Symmlet all even coefficients

between 8 and 20 were tried. The coefficients for these filters are available in [22].

6 Results and discussion

Considering the magnitudes of noise factor and distortion, Daubechies filter with 16 coefficients, Coiflet filter with 6 coefficients and Symmlet with 20 coefficients provided best results. In each of these three cases, the magnitude of the noise factor was about 5.2 and the amount of distortion was about 6.3×10^{-5}.

The output of the adaptive MRA based filtering algorithm for the simulated CNV waveform of Fig. 7 is shown in Fig. 8. The Daubechies filter with 16 coefficients was used for this process. Traces of discontinuities are still visible in the recovered waveform. To completely remove these and to further attenuate any residual background EEG, the recovered waveform was processed using the wavelet packets and the best basis algorithm of Wickerhauser. The resulting waveform is shown in Fig. 9. The techniques and methods of implementation of wavelet packets and the best basis algorithm of Wickerhauser are described in detail in [23]. For this operation, Daubechies filter with 16 coefficients was used and the signal was reconstructed with the 25 largest Wickerhauser best basis coefficients. It should be noted that signal decomposition using wavelet packets is similar to that of MRA except that, when using wavelet packets, the outputs of both lowpass and highpass filters are decomposed at each level.

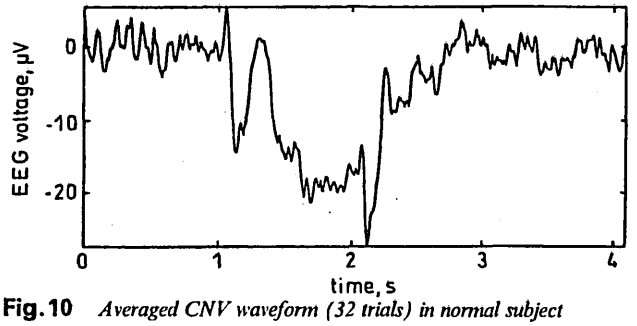

Fig. 10 *Averaged CNV waveform (32 trials) in normal subject*

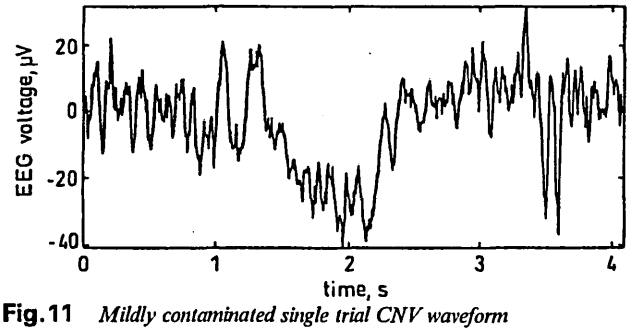

Fig. 11 *Mildly contaminated single trial CNV waveform*

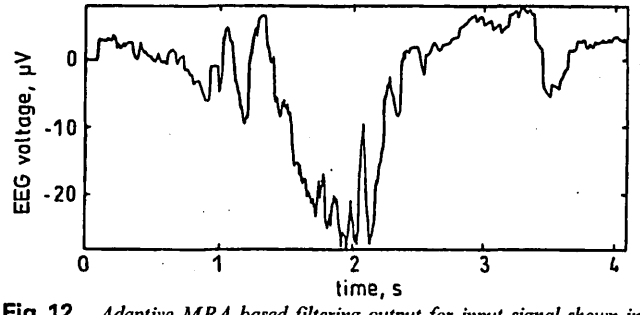

Fig. 12 *Adaptive MRA based filtering output for input signal shown in Fig. 11 and the template shown in Fig. 10*

Fig. 10 shows an averaged CNV waveform. Fig. 11 shows a mildly contaminated single trial CNV waveform recorded from the same person. The output of the MRA based filtering algorithm for this single trial CNV waveform is shown in Fig. 12. The template used was the averaged CNV (Fig. 10). As can be observed, the background EEG is significantly attenuated while the waveform's details are mainly preserved. Fig. 13 shows the waveform obtained by processing Fig. 12 with the techniques of wavelet packets and Wickerhauser best basis algorithm. The procedure followed to obtain Figs. 12 and 13 was similar to that followed to obtain Figs. 8 and 9. When the above analysis was repeated using the CNV grand average as the template, the recovered single trial CNV waveform was not noticeably different from that shown in Fig. 13. This shows that, if it is not possible to obtain an averaged CNV waveform from the person to use as the template, the CNV grand average (provided it is obtained from the same subject category) may be used as the template.

Fig. 12 shows a severely contaminated single trial CNV waveform recorded from the subject whose averaged CNV is shown in Fig. 10. The recovered CNV following the filtering operation is shown in Fig. 15. Again, the CNV waveform is clearly visible in the recovered signal.

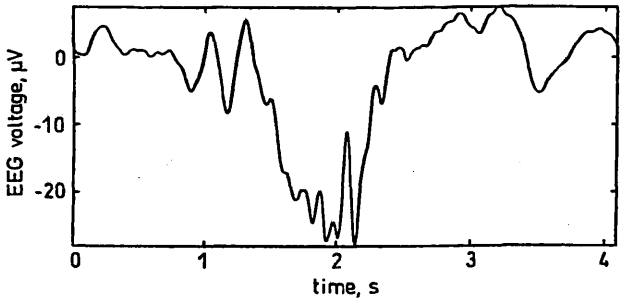

Fig. 13 *Fig. 12 following application of wavelet packets and Wickerhauser best basis algorithm*

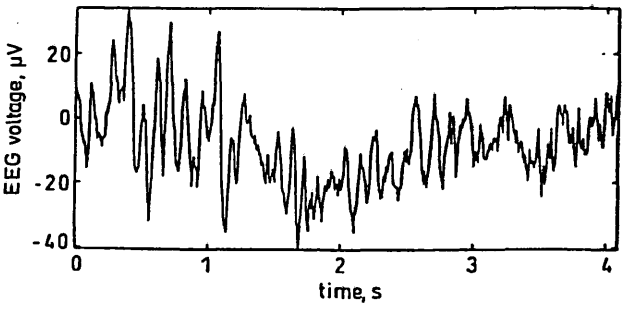

Fig. 14 *Severely contaminated single trial CNV waveform*

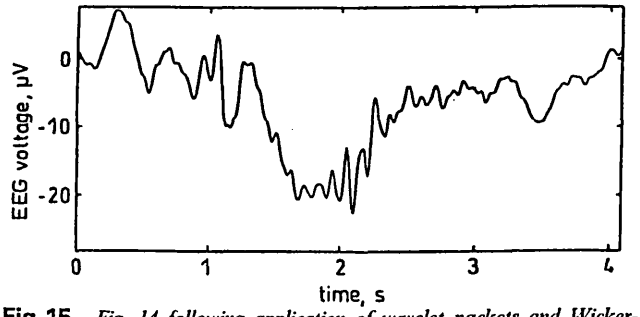

Fig. 15 *Fig. 14 following application of wavelet packets and Wickerhauser best basis algorithm*

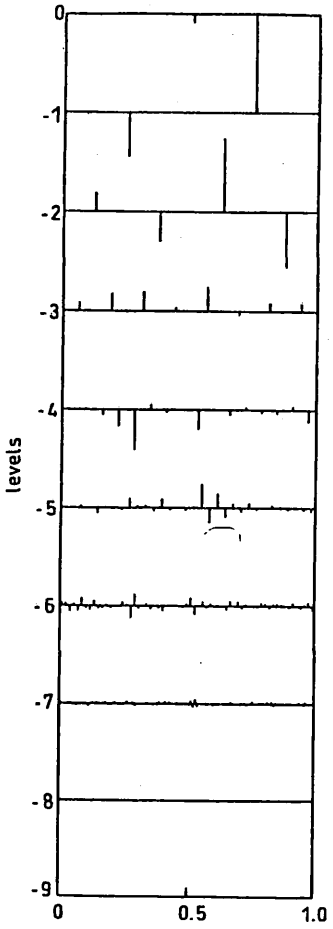

Fig. 16 *Spike plot of MRA coefficients for Fig. 10*

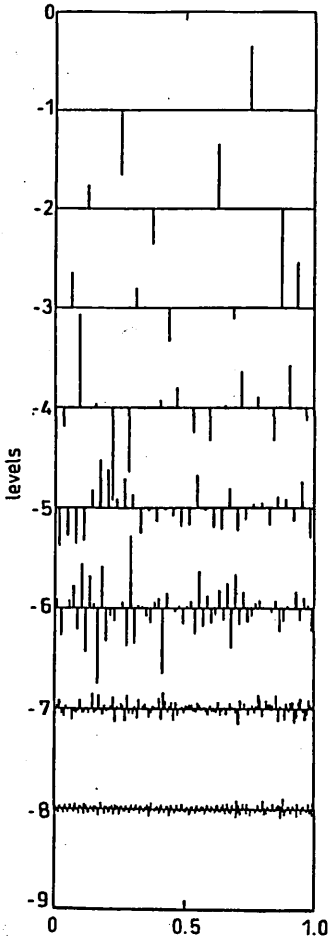

Fig. 17 *Spike plot of MRA coefficients for Fig. 14*

A spike plot of the MRA coefficients of the averaged CNV waveform of Fig. 10 is shown in Fig. 16. As the length of the CNV waveform was 512 points, the signal is decomposed to eight levels. The convention of representing the coarsest level as level –1 is used here. The spike plots of MRA coefficients for Figs. 14 and 15 are shown in Figs. 17 and 18, respectively. Comparison of Figs. 16, 17 and 18 indicates that the levels –5 to –8 are significantly attenuated by the filtering process. This is to be expected as the CNV energy is mainly concentrated at very low frequencies.

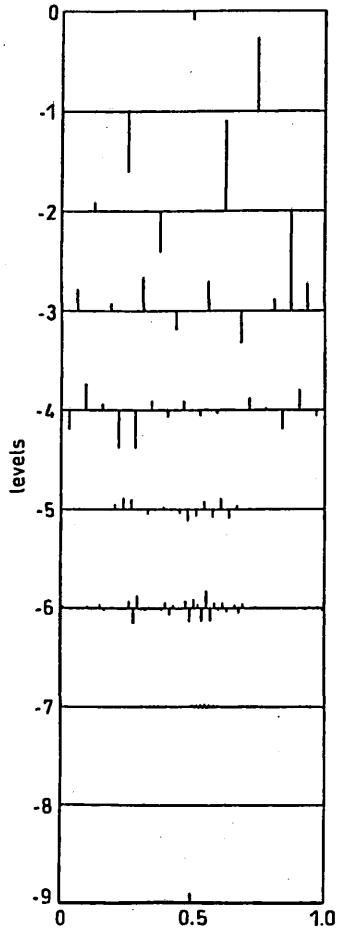

Fig. 18 *Spike plot of MRA coefficients for Fig. 15*

It is intended to use the developed EP recovery method to perform a detailed analysis of trial-to-trial variations in several types of EPs and in a number of brain related disorders in particular schizophrenia. The aim is to relate the information to the cognitive processes affected in the brain disorders considered. An analysis of trial-to-trial variations using different EPs may also provide further insight into the differences between EPs as well.

7 Conclusion

An adaptive multiresolution analysis based filtering algorithm was developed and was used for the single trial recovery of a cognitive cortical evoked potential (EP) known as the contingent negative variation (CNV). A method for evaluating its effectiveness was devised and was used to select best orthogonal filter for the process. It was demonstrated that the method can reduce the background EEG by a factor of 5 while preserving the main features of the CNV waveform. Although the CNV waveform was used in this study,

the technique is also applicable to other EPs. It is planned to use the method to study the trial-to-trial variations in a number of EPs and in specific brain related disorders, in particular schizophrenia. This may provide further insight into the cognitive processes affected in those disorders.

8 Acknowledgment

The authors are very grateful to all the volunteers who took part in the data recordings for their trust, time and patience. They appreciate the support of the organisations where they work. They are also grateful to Mr N. Hudson (Plymouth Hospital, Plymouth, UK) and Dr S. Oke (Mental Health Services, Barrow Hospital, Barrow Gurney, Bristol, UK) for their generous help and support in organising the data recordings and the valuable discussions.

9 References

1 CATON, R.: 'The electric currents of the brain', *Br. Med. J.*, 1875, **2**, pp. 278
2 BLACKWOOD, D.H.R., and MUIR, W.J.: 'Cognitive brain potentials and their application', *Br. J. Psychiat.*, 1990, **157**, pp. 96–101 (suppl. 9)
3 SAATCHI, M.R., OKE, S., ALLEN, E.M., JERVIS, B.W., and HUDSON, N.: 'Signal processing of the contingent negative variation in schizophrenia using multilayer perceptrons and predictive statistical diagnosis', *IEE Proc. Sci. Meas. Technol.*, 1995, **142**, (4), pp. 269–276
4 HENNERICI, M., HÖMBERG, V., and LANGE, H.W.: 'Evoked potentials in patients with Huntington's disease and their offspring. II. visual evoked potentials', *Electroencephalography Clin. Neurophysiol.*, 1985, **62**, pp. 176–176
5 DICK, J.P.R., ROTHWELL, J.C., DAY, B.L., CANTELLO, R., BURUMA, O., GIOUX, M., BENECKE, R., BERARDELLI, A., THOMPSON, P.D., and MARSDEN, C.D.: 'Bereitschaftspotential is abnormal in Parkinson's disease', *Brain*, 1989, **112**, pp. 233–244
6 McGILLEM, C.D., AUNON, J.J., and POMALAZA-RAEZ, C.A.: 'Improved waveform estimation procedures for event-related potentials', *IEEE Trans.*, 1985, **BME-32**, pp. 371–379
7 GASSER, T., MÖCKS, J., and VEREGER, R.: 'SELAVCO: a method to deal with trial-to-trial variability of evoked potentials', *Electroencephalography Clin. Neurophysiol.*, 1983, **55**, pp. 717–723
8 TECCE, J.J., and CATTANACH, L.: 'Contingent negative variation (CNV)' *in* NIEDERMEYER, E., and LOPES DA SILVA, F. (Eds.): 'Electroencephalography: basic priciples, clinical applications and related fields' (Urban and Schwartzenberg, 1987)
9 CERUTTI, S., CHIARENZA, G., LIBERATI, D., MASCELLANI, P., and PAVESI, G.: 'A parametric method of identification of signal-trial event related potentials in the brain', *IEEE Trans. Biomed. Eng.*, 1988, **35**, (9), pp. 701–711
10 KRIEGER, D., and LARIMORE, W.: 'Automatic enhancement of single evoked potentials', *Electroencephalography Clin. Neurophysiol.*, 1986, **64**, pp. 568–572
11 THAKOR, N.V.: 'Adaptive filtering of evoked potentials', *IEEE Trans.*, 1987, **BME-34**, (1), pp. 6–12
12 *Proc. IEEE*, 1996, **84**, (4), (special issue on wavelets)
13 ALDROUBI, A., and UNSER, M. (Eds): 'Wavelets in medicine and biology' (Boca Raton, Fl: CRC, 1996)
14 BARTNIK, E.A., BLINOWSKA, K.J., and DURKA, P.J.: 'Single evoked potential reconstruction by means of wavelet transform', *Biol. Cybernetics*, 1992, **67**, pp. 175–181
15 BERTRAND, O., BOHORQUEZ, J., and PERNIER, J.: 'Time-frequency digital filtering based on an inevitable wavelet transform: an application to evoked potentials', *IEEE Trans., Biomed. Eng.*, 1994, **41**, (1), pp. 77–88
16 MALLAT, S.: 'A theory for multiresolution signal decomposition: the wavelet representation', *IEEE Trans. Pattern Anal. Mach. Intell.*, 1989, **11**, (7), pp. 674–693
17 RIOUL, O.: 'A discrete-time multiresolution theory', *IEEE Trans. Signal Process.*, 1993, **41**, (8), pp. 2591–2606
18 AKANSU, A.N., and HADDAD, R.A.: 'Multiresolution signal decomposition: transforms, subbands, and wavelets' (Academic Press, 1992)
19 McCALLUM, W.C.: 'Potentials related to expectancy, preparation and motor activity' in PICTON, T.W. (Ed.): 'Human event related potentials', *Handbook of Electroencephalography and Clinical Neurophysiology*, (Elsevier, New York, 1988, revised), Chap. 3, pp. 427–534
20 WALTER, W.G.: 'The contingent negative variation; an electrocortical sign of sensori-motor reflex in man', *Prog. Brain Res.*, 1968, **22**, pp. 364–377
21 SAATCHI, M.R., and JERVIS, B.W.: 'PC-based integrated system developed to diagnose specific brain disorders', *Computing Control Eng. J.*, 1991, **2**, (2), pp. 61–68
22 VAIDYANATHAN, P.P.: 'Multirate systems and filter banks' (Prentice–Hall, 1993)
23 WICKERHAUSER, M.V.: 'Adapted wavelet analysis from theory to software' *in* PETERS, A.K.: '' (WELLESLEY, MA, 1994)

Bibliography

[1] Hillyard, S.A. and Woods, D.L.: Electrophysiological Analysis of Human Brain Function,
In Gazzaniga, M.S.:(Editor) Handbook of Behavioral Neurobiology, Vol. 2, (Plenum Publishing Corporation, 1979).

[2] Nuwer, M.R.: Fundamentals of evoked potentials and common clinical applications today, Electroencephalography and clinical Neurophysiology, 106 (1998) 142-148.

[3] Hillyard, S.A. and Kutas, M.: Electrophysiology of cognitive processing, Annual Review of Psychology, 34 (1983) 33-61.

[4] Brandeis, D. and Lehmann, D.: Event-related potentials of the brain and cognitive processes: Approaches and applications, Neuropsychologia, 24 (1986) 151-168.

[5] Pritchard, W.S.: Cognitive event-related potential correlates of schizophrenia, Psychological Bulletin, 100 (1986) 43-66.

[6] Challis, R.E. and Kitney, R.I.: Biomedical signal processing (in four parts) Part 1 time-domain methods, Medical and Biological Engineering and Computing, 28 (1990) 509-524.

[7] Hyde, M.L.: Signal processing and analysis,
In Jacobson, J.T.: (Editor) Principles and applications in evoked potentials, (Allyn and Bacon, 1994).

[8] Demiralp, T., Ademoglu, A., Istefanopulos, Y. and Gulcur, H.O.: Analysis of event-related potentials (ERP) by damped sinusoids, Biological Cybernetics, 78 (1998) 487-493.

[9] Melkonian, D., Gordon, E., Rennie, C. and Bahramali, H.: Dynamic spectral analysis of event-related potentials, Electroencephalography and clinical Neurophysiology, 108 (1998) 251-259.

[10] Graps, A.: An introduction to wavelets, IEEE Computational Science and Engineering, (1995) 50-61.

[11] Chan, Y.T.: Wavelet basics, (Kluwer Academic publishers, 1995).

[12] Unser, M. and Aldroubi, A.: A review of wavelets in biomedical applications, Proceedings of the IEEE, 84 (1996) 626-638.

[13] Aldroubi, A. and Unser, M.: Wavelets in medicine and biology, (Boca Raton, 1996).

[14] Samar, V.J.: Wavelet analysis of neuroelectric waveforms, Brain and Language, 66 (1999) 1-6.

[15] Daubechies, I.: The wavelet transform, time-frequency localization and signal analysis, IEEE Transactions on Information Theory, 36 (1990) 961-1005.

[16] Vetterli, M. and Kovacevic, J.: Wavelets and subband coding, (Prentice Hall, 1995).

[17] Basar, E.: Brain function and oscillations. Volume 1: Brain oscillations. Principles and approaches, (Springer Verlag, 1998).

[18] Bell, A.J. and Sejnowski, T.J.: An information maximisation approach to blind separation and blind deconvolution, Neural Computation, 7 (1995) 1129-1159.

[19] Sutton, S., Braren, M., Zubin, J. and John, E.R.: Evoked potential correlates of stimulus uncertainty, Science, 150 (1965) 1187-1188.

[20] Caton, R.: The electric currents of the brain, British Medical Journal, 2 (1875) 278.

[21] Goodin, D.S.: Event-related (endogenous) potentials, Electroencephalography and clinical Neurophysiology, (1993) 575-595.

[22] Picton, T.W., Hillyard, S.A., Krausz, H.J., and Galambos, R.: Human auditory evoked potentials. I. Evaluation of components, Electroencephalography and clinical Neurophysiology, 36 (1974) 179-190.

[23] Tecce, J.J.: Contingent negative variation (CNV) and psychological processes in man, Psychological Bulletin, 77 (1972) 73-108.

[24] Regan, D.M.: Human brain electrophysiology: Evoked potentials and evoked magnetic fields in science and medicine, (Elsevier, 1989).

[25] Vaughn Jr., H.G., Ritter, W. and Simson, R.: Neurophysiological considerations in event-related potential research,
In Gaillard, A.W.K. and Ritter, W.: (Editors) Tutorials in ERP research: Endogenous components, (North-Holland Publishing Company, 1983).

[26] Friston, K.J.: Imaging neuroscience: Principles or maps? Proceedings of the National Academy of Science, USA, 95 (1998) 796-802.

[27] Nunez, P.L.: The electrical fields of the brain, (Oxford University Press, 1981).

[28] Walter, W.G., Cooper, R., Aldridge, V.J., McCallum, W.C. and Winter, A.L.: Contingent negative variation: an electric sign of sensory motor association and expectancy in the human brain, Nature, 203 (1964) 380-484.

[29] Hillyard, S.A.: Relationships between the contingent negative variation (CNV) and the reaction time, Physiology and Behaviour, 4 (1969) 351-357.

[30] Low, M.D., Borda, R.P., Frost, J.D. and Kellaway, P.: Surface-negativity, slow-potential shift associated with conditioning in man, Neurology, 16 (1966) 771-782.

[31] Irwin, D.A., Knott, J.R., McAdam, C.S. and Rebert, C.S.: Motivational determinants of the contingent negative variation, Electroencephalography and clinical Neurophysiology, 21 (1966) 538-543.

[32] Tecce, J.J.: A CNV rebound effect, Electroencephalography and clinical Neurophysiology, 46 (1979) 546-551.

[33] Roth, W.T.: Late event-related potentials and psychopathology, Schizophrenia Bulletin, 3 (1977) 105-120.

[34] Saatchi, M.R., Oke, S., Allen, E.M., Jervis, B.W. and Hudson, N.: Signal processing of the contingent negative variation using multilayer perceptrons and predictive statistical diagnosis, IEE Proceedings of Science, Measurement and Technology, 142 (1995) 269-276.

[35] McGhie A., Chapman, J. and Lawson, J.S.: The effect of distraction on schizophrenic performance. I. Perception and immediate memory, British Journal of Psychiatry, 111 (1965) 383-390.

[36] Butcher, J.: Cognitive auditory responses,
In Jacobson, J.T.: (Editor) Principles and applications in evoked potentials, (Allyn and Bacon, 1994).

[37] Pritchard, W.S.: Psychphysiology of P300, Psychological Bulletin, 89 (1981) 506-540.

[38] Straumanis, J.J.: Event-related potentials in schizophrenia, Psychiatric medicine, 8 (1990) 53-72.

[39] Ruchkin, D.S., Johnson, R, Canoune, H.L.,Ritter, W. and Hammer, M.: Multiple Sources of P3b associated with different types of information, Psychophysiology, 27 (1990) 157-176.

[40] Chapin, J.K, Moxon, K.A., Markowitz, R.S. and Nicolelis, M.A.L.: Real-time control of a robot arm using simultaneously recorded neurons in the motor cortex, Nature Neuroscience, 2 (1999) 664-670.

[41] Rabiner, L.R. and Gold, B.: Theory and application of digital signal processing, (Prentice Hall, 1975).

[42] Mitra, S.K.: Digital signal processing, a computer based approach, (McGraw Hill, 1998).

[43] Burrus, C.S., Gopinath, R.A. and Guo, H.: Introduction to wavelets and wavelet transforms. A primer, (Prentice Hall, 1998).

[44] Bracewell, R.N.: The Fourier transform and its applications, (McGraw Hill, 1986).

[45] Challis, R.E. and Kitney, R.I.: Biomedical signal processing (in four parts). Part 3. The power spectrum and coherence function, Medical and Biological Engineering and Computing, 29 (1991) 225-241.

[46] Ifeachor, E.C. and Jervis, B.W.: Digital Signal Processing: a Practical Approach, (Addison Wesley, 1993).

[47] Ifeachor, E.C., Jervis, B.W., Morris, E.L., Allen, E.M. and Hudson, N.R.: A new microcomputer-based online occular artefact removal (OAR) system, IEE Proceedings, 133 (1986) 291-300.

[48] Matlab Signal Processing Toolbox, (Mathworks,1998).

[49] Cohen, L.: Time-frequency analysis, (Prentice Hall, 1994).

[50] Kaufman, L.: Cognition and local changes in brain oscillations,
In Pantev, C.: (Editor) Oscillatory event-related brain dynamics, (Plenum Press, 1994).

[51] Brandt, M.E.: Visual and auditory evoked phase resetting of the alpha EEG, International Journal of Psychophysiology, 26 (1997) 285-298.

[52] Gabor, D.: Theory of communication, IEEE Proceedings, 93 (1946) 429-441.

[53] Feichtinger, H.G. and Strohmer, T.: (Editors) Gabor analysis and algorithms, (Birkhauser, 1998).

[54] Makeig, S.: Auditory event-related dynamics of the EEG spectrum and effects of exposure to tones, Electronencephalography and clinical Neurophysiology, 86 (1993) 283-293.

[55] Pfurtscheller, G.: Event-related synchronization (ERS): an electrophysiological correlate of cortical areas at rest, Electroencephalography and clinical Neurophysiology, 83 (1992) 62-69.

[56] Pfurtscheller, G.: Event-related desynchronisation (ERD) and 40Hz oscillations in a simple movement task, In Pantev, C.: (Editor) Oscillatory event-related brain dynamics, (Plenum Press, 1994).

[57] Efron, B and Tibshirani, R.J.: An Introduction to the Bootstrap, (Chapman and Hall, 1993).

[58] Makeig, S., Elbert, T. and Braun, C.: Magnetic event-related spectral perturbations, Proceedings of the 9th International Conference on Biomagnetism, Vienna, 1993.

[59] Jung, T.P., Makeig, S., Westerfield, M., Townsend, J., Courchesne, E., Sejnowski, T.: Analysing and Visualising Single-Trial Event-Related Potentials, Advances in Neural Information Processing Systems, 11 (1999) 118-24.

[60] Daubechies, I.: Orthonormal bases of compactly supported bases, Communications on Pure and Applied Mathematics, 41 (1988) 909-996.

[61] Mallet, S,: Multiresolution approximations and wavelet orthonormal bases of L2(R), Transactions of the American Mathematical Society, 319 (1989) 69-87.

[62] Learned, R.E. and Willsky, A.S.: A wavelet packet approach to transient signal classification, Applied and Computational Harmonic analysis, 2 (1995) 265-278.

[63] Samar, V.J., Bopardikar, A., Rao, R. and Swartz, K.: Wavelet Analysis of Neuroelectric Waveforms: A conceptual Tutorial, Brain and Language 66 (1999) 7-60.

[64] Quiroga, R.Q., and Schurmann, M.: Functions and sources of event-related EEG alpha oscillations studied with the wavelet transform, Clinical Neurophysiology 110 (1999) 643-654.

[65] Demiralp, T., Ademoglu, A., Schurmann, M., Basar-Eroglu, C. and Basar, E.: Detection of P300 Waves in Single Trials by the wavelet Transform (WT), Brain and Language 66 (1999) 108-128.

[66] Dear, S.P. and Hart, C.B.: Synchronised Cortical Potentials and wavelet packets: A Potential Mechanism for perceptual binding and conveying information, Brain and Language 66 (1999) 201-231.

[67] Vaidyanathan, P.P.: Multirate systems and filter banks, (Prentice Hall, 1993).

[68] Grossman, A. and Morlet, J.: Decomposition of Hardy functions into square integrable wavelets of constant shape, SIAM Journal of Applied Mathematics, 15 (1984) 723-736.

[69] Rioul, O.: A discrete-time multiresolution theory, IEEE Transaction on Signal Processing, 41 (1993) 2591-2606.

[70] Goupillaud, P., Grossmann, A. and Morlet, J.: Cycle-octave and related transforms in seismic signal analysis, Geoexploration, 23 (1984) 85-102.

[71] Gramatikov, B. and Georgiev, I.: Wavelets as an alternative to short-time Fourier transform in signal averaged electrocardiography, Medical and Biological Engineering and Computing, 33 (1995) 482-487.

[72] Vaidyanathan, P.P.: Quadrature mirror filter banks, M-band extensions and perfect-reconstruction techniques, IEEE ASSP Magazine, 4 (1987) 4-20.

[73] Strang, G and Nguyen, T.: Wavelets and filter banks, (Wellesley-Cambridge Press, 1996).

[74] Vetterli, M. and Herley, C.: Wavelets and filter banks: Theory and design, IEEE Transactions on Signal Processing, 40 (1992) 2207-2232.

[75] Coifman, R.R., Meyer, Y., Quake, S., and Wickerhauser, M.V.: Signal processing and compression with wavelet packets, (Technical Report, Department of Mathematics, Yale University, 1991).

[76] Ramchandran, K., Vetterli, M. and Herley, C.: Wavelets, subband coding and best bases, Proceedings of the IEEE, 84 (1996) 541-560.

[77] Coifman, R.R. and Wickerhauser,M.V.: Entropy Based Algorithms for Best Basis Selection, IEEE Transactions on Information Theory, 38 (1992) 713-718.

[78] Wickerhauser,M.V.: Adapted wavelet analysis from theory to software, (Wellesley, 1994).

[79] Lee, T.: Independent Component Analysis: Theory and Applications, (Kluwer Academic Publishers, 1998).

[80] Makeig, S., Bell, A.J., Jung, T.P., Sejnowski, T.: Independent Component Analysis of Electronencephalographic Data, Advances in Neural Information Processing Systems 8 (1996) 145-151.

[81] Vigon, L., Saatchi, M.R., Mayhew, J.E.W. and Fernandes, R.: A Quantitative Evaluation of Techniques for Ocular Artefact Filtering of EEG Waveforms, IEE Proceedings in Science, Measurement and Technology (2000) in Press.

[82] Haykin, S.: Neural networks a comprehensive foundation, (Macmillan College Publishing, 1994).

[83] Kohonen, T.: Self-organisation and associative memory, 3rd Ed. (Springer Verlag, 1989).

[84] Rogers, J.: Object-oriented neural networks in C++, (Academic Press, 1997).

[85] Lin, C-T. and Lee, G.C.S.: Neural fuzzy systems. A neuro-fuzzy synergism to intelligent systems, (Prentice Hall, 1996).

[86] Sayers, B.McA., Beagley, H.A. and Henshall, W.R.: The mechanism of auditory evoked EEG responses, Nature, 247 (1974) 481-483.

[87] Basar, E., Basar-Eroglu, C., Roschke, J. and Schutt, A.: The EEG is a quasi-deterministic signal anticipating sensory-cognitive tasks,
In Basar, E. and Bullock, T.H.: (Editors) Brain dynamics, Progress and perspectives, (Springer, 1989).

[88] Woody, C.D.: Characterisation of an adaptive filter for the analysis of variable latency neuroelectric signals, Medical and Biological Engineering, 5 (1967) 539-553.

[89] Makeig, S., Westerfield, M., Jung,T-P., Covington, J., Townsend, J., Sejnowski, T.J. and Courchesne, E.: Functionally independent components of the late positive event-related potential during visual spatial attention, Journal of Neuroscience, 19 (1999) 2665-2680.

[90] Saatchi, R. Gibson, C, Allen, E.M. and Ghassemlooy, Z.: Application of Kohonen artificial network for identification of schizophrenic subjects based on the CNV waveforms trial-to-trial- variation trends, Proceedings of Fourth Annual International CSI Computer Conference, Tehran, Iran, (1999) 65-68.

[91] Chan, Y.H.F., Lam, F.K., Poon, P.W.F. and Qiu, W.: Detection of brainstem auditory evoked potentials by adaptive filtering, Medical and Biological Engineering and Computing, 33 (1995) 69-75.

[92] Thakor, N.V.: Adaptive filtering of evoked potentials, IEEE Transactions on Biomedical Engineering, 34 (1987) 6-12.

[93] Krieger, D. and Larimore, W.: Automatic enhancement of single evoked potentials, Electroencephalography and clinical Neurophysiology, 64 (1986) 568-572.

[94] Widrow, B., Glover Jr, J.R., McCool, J.M., Kaunitz, J., Williams, C.S., Hearn, R.H., Zeidler, J.R., Dong Jr, E. and Goodlin, R.C.: Adaptive noise cancelling: Principles and applications, Proceedings of the IEEE, 63 (1975) 1692-1717.

[95] deWeerd, J.P.C., Materns, W.L.J.: Theory and Practice of A Posteriori 'Weiner' Filtering of Average Evoked Potentials, Biological Cybernetics, 30 (1978) 81-94.

[96] deWeerd, J.P.C.: A Posteriori Time-varying Filtering of Averaged Evoked Potentials. I. Introduction and conceptual basis, Biological Cybernetics, 41 (1981) 211-222.

[97] deWeerd, J.P.C., and Kap, J.I.: A Posteriori Time-varying Filtering of Averaged Evoked Potentials. II. Mathematical and computational aspects, Biological Cybernetics, 41 (1981) 223-234.

[98] Samar, V.J., Swartz, K.P. and Raghuveer, M.R.: Multiresolution Analysis of Event-Related Potentials by Wavelet Decomposition, Brain and Cognition, 27 (1995) 398-438.

[99] Bartnik, E.A., Blinowska, K.J. and Durka, P.J.: Single evoked potential reconstruction by means of wavelet transform, Biological Cybernetics, 67 (1992) 175-181.

[100] Thakor, N., Xin-Rong, G., Yi-Chun, S. and Hanley D.F.: Multiresolution wavelet analysis of evoked potentials, IEEE Transactions on Biomedical Engineering, 40 (1993) 1085-1093.

[101] Bertrand, O., Bohorquez, J. and Pernier, J.: Time-frequency digital filtering based on an inevitable wavelet transform: an application to evoked potentials, IEEE Transactions on Biomedical Engineering, 41 (1994) 77-88.

[102] Carmona, R., and Hudgins, L.: Wavelet denoising of EEG signals and identification of evoked response potentials, Proceedings of SPIE Conference on Wavelet Applications in Signal and Image processing II, 2303 (1994) 91-104.

[103] Mallat, S. and Zhong, S.: Characterization of signals from multiscale edges, IEEE Transactions on Pattern Analysis and Machine Intelligence, 14 (1992) 710-732.

[104] Gibson, C., Saatchi, M.R. and Allen, E.M.: A comparative investigation of wavelet based EP estimation, Proceedings of the First International Symposium on Communication Systems and Digital Signal Processing, 2 (1998) 524-528.

[105] Saatchi, M.R., Gibson, C. Rowe, J.W.K. and Allen, E.M.: Adaptive multiresolution analysis based evoked potential filtering, IEE Proceedings Science, Measurement and Technology, 144 (1997) 149-155.

[106] Heinrich, H., Dickhaus, H., Rothenburger, A., Heinrich, V. and Moll, G.H.: Single-sweep analysis of event-related potentials by wavelet network. Methodological basis and clinical application, IEEE Transactions on Biomedical Engineering, 46 (1999) 867-879.

[107] Zhang, Q. and Benveniste, A.: Wavelet networks, IEEE Transactions on Neural Networks, 3 (1992) 889-898.

[108] Wavelab (1997) A library of Matlab routines for wavelet analysis and wavelet-packet analysis. It is freely available free on the internet. ftp://playfair.stanford.edu/pub/wavelab.

[109] Timsit-Berthier, M., Gerono, A., Rousseau, J.C., Mantanus, H., Abraham, P., Verhey, F.H.M., LAmers, T. and Emonds, P.: An international pilot study of CNV in mental illness, Annals of the New York Academy of Sciences, 425 (1984) 629-637.

[110] Teece, J.J. and Cattanach, L.: Contingent Negative Variation,
In Lopes de Silva, F.:(Editor) Electroencephalography basic principles, clinical applications and related fields, (Urban and Schwarzenberg, 1982).

[111] Cohen, J.: Cerebral psychophysiology: The contingent negative variation,
In Thompson, R.F. and Patterson, M.M.:(Editors) Bioelectric recording techniques Part B Electroencephalography and human brain potentials, (Academic Press, 1974).

[112] Hillyard, S.A.: Methodological issues in CNV research,
In Thompson, R.F. and Patterson, M.M.:(Editors) Bioelectric recording techniques Part B Electroencephalography and human brain potentials, (Academic Press, 1974).

[113] McGuffin, P., Owen, M.J. and Farmer, A.E.: Genetic basis of schizophrenia, Lancet, 346 (1995) 678-682.

[114] Andreasen, N.C.: Symptoms, signs and diagnosis of schizophrenia, Lancet, 346 (1995) 477-481.

[115] Heyman, I. and Murray, R.M.: Schizophrenia and neurodevelopment, Journal of the Royal College of Physicians of London, 26 (1992) 143-146.

[116] Ron, M.A. and Harvey, I.: The brain in schizophrenia, Journal of Neurology, Neurosurgery and Psychiatry, 53 (1990) 725-726.

[117] Timsit-Berthier, M.: Contingent negative variation and its relationships to arousal and stress in psychopathology,
In McCallum, W.C. and Curry, S.H.:(Editors) Slow potential changes in the human brain, (Plenum Press, 1993).

[118] Saatchi, R.: Developments in signal processing for computerised diagnosis in clinical neurophysiology, PhD Thesis, (Sheffield Hallam University, 1992).

[119] Basar, E., Yordanova, J., Kolev, V and Basar-Eroglu, C.: Is the alpha rhythm a control parameter for brain responses? Biological Cybernetics, 76 (1997) 471-480.

[120] Basar, E.: EEG-brain dynamics. Relation between EEG and brain evoked potentials, (Elsevier, 1980).

[121] Singer, W.: Neurobiology: Striving for coherence, Nature, 397 (1999) 391-393.

[122] Rodriguez, E., George, N., Lachaux, J-P., Martinerie, J., Renault, B. and Varela, F.J.: Perecption's shadow: Long-distance synchronisation of human brain activity, Nature, 397 (1999) 430-433.

[123] Miltner, W.H.R., Braun, C., Arnold, M.,Witte, H. and Taub, E.: Coherence of gamma-band EEG activity as a basisi for associative learning, Nature, 397 (1999) 434-436.

[illegible]

[illegible]

[illegible]

[illegible]

[illegible]

[illegible]

[illegible]

[illegible]

[124] Basar, E. and Bullock, T.H.: (Editors) Induced rhythms in the brain, (Birkhauser, 1992).

[125] Jervis, B.W., Nichols, M.J., Johnson, T.E., Allen, E. and Hudson, N.R.: A fundamental investigation of the composition of auditory evoked potentials, IEEE Transactions on Biomedical Engineering, 30 (1983) 43-49.

[126] Kolev, V and Yordanova, J.: Analysis of phase-locking is informative for studying event-related EEG activity, Biological Cybernetics, 76 (1997) 229-235.

[127] Yordanova, J and Kolev, V.: Event-related Alpha oscillations are functionally associated with P300 during information processing, Neuroreport, 9 (1998) 3159-3164.

[128] Sgro, J.A., Emerson, R.G. and Pedley, T.A.: Real-time construction of evoked potentials using a new two-dimensional filter method, Electronencephalography and clinical Neurophysiology, 62 (1985) 372-380.

[129] Paige, A.L., Ozdamar, O. and Delgado, R.E.: Two-dimensional spectral processing of sequential evoked potentials, Medical and Biological Engineering and Computing, 34 (1996) 239-243.

[130] Makeig, S., Westerfield, M., Townsend, J., Jung, T.P., Courchesne, E. and Sejnowski, T.: Functionally independent components of early event-related potentials in a visual spatial attention task, Philosophical Transactions of the Royal Society, London, 354 (1999) 1135-1144.

[131] Matlab version 5, (The Mathworks Inc, 1999).